KINETIC MECHANISM AND SUBSTRATE SPECIFICITY OF HEDGEHOG ACYLTRANSFERASE

by

Adina Schonbrun

A Dissertation

Presented to the Faculty of the Louis V. Gerstner, Jr.

Graduate School of Biomedical Sciences,

Memorial Sloan Kettering Cancer Center

in Partial Fulfillment of the Requirements for the Degree of Doctor of Philosophy

New York, NY

January, 2023

Marilyn D. Resh, PhD
Dissertation Mentor

Date

ABSTRACT

Sonic hedgehog (Shh) signaling is a key component of embryonic development and is a driving force in several cancers. Hedgehog acyltransferase (Hhat), a member of the membrane-bound *O*-acyltransferase (MBOAT) family of enzymes, catalyzes the attachment of palmitate to the N-terminal cysteine of Shh, a post-translation modification critical for Shh signaling. The activity of Hhat has been assayed in cells and *in vitro*, and cryogenic electron microscopy structures of Hhat have been reported, yet several unanswered questions remain regarding the enzyme's reaction mechanism, substrate specificity, and the impact of the latter on Shh signaling. In this work, I present an *in vitro* acylation assay with purified Hhat that directly monitors attachment of a fluorescently tagged fatty acyl chain to Shh. I employed this assay for extensive kinetic analyses not previously performed with Hhat, to identify the kinetic mechanism and investigate the fatty acyl-Coenzyme A (CoA) substrate specificity of Hhat. These kinetic analyses revealed that the reaction catalyzed by Hhat proceeds through a random sequential mechanism, and that Hhat can utilize multiple fatty acyl-CoA substrates for fatty acid transfer to Shh with varying preferences (affinity, turnover rate, and catalytic efficiency) for myristoyl-, palmitoyl-, palmitoleoyl-, and oleoyl-CoA. Furthermore, I investigated the functional consequence of differential fatty acylation of Shh in a luciferase-based Shh reporter system, and found that the potency of the signaling response in cells was higher for Shh acylated with saturated fatty acids compared to monounsaturated fatty acids. My findings demonstrate that Hhat can attach fatty acids other than palmitate to Shh and suggest that heterogeneous fatty acylation has the potential to impact Shh signaling in the developing embryo and/or cancer cells.

In a pursuit related to substrate specificity, I also explored potential interdependence of fatty acyltransferases in cells. Cellular fatty acyltransferases share a

pool of fatty acyl-CoA substrates, raising the possibility that the activities of fatty acyltransferases in cells are interdependent. Readout of enzymatic activity of diacylglycerol acyltransferases (DGATs) by cellular lipid droplet formation revealed that Hhat and the DGATs exhibit crosstalk to promote lipid droplet formation. qPCR analysis indicated that the crosstalk does not involve changes in mRNA expression levels of DGAT1 or 2 or related ACAT enzymes. While further experiments are needed to determine whether the observed crosstalk is related to substrate specificities of the fatty acyltransferases, the data suggest that MBOATs play an interdependent role in cells.

ACKNOWLEDGEMENTS

First and foremost, I would like to thank Dr. Marilyn Resh for being a fantastic mentor. I am so fortunate to have trained under your auspices. Your guidance, sensitivity, and encouragement toward matters within the lab as well as my need to balance life outside of the lab have made my graduate school experience smooth and outstanding.

To previous members of the Resh lab, I thank you for your direction and assistance. Thanks to our summer student, Rivka Shapiro, whom I had the pleasure of mentoring and who assisted me with some of the kinetic mechanism experiments. Raya and Debbie, I am grateful for your efforts in support of my lab work and for being great company. It was a pleasure to work with you both.

I am extremely appreciative to the graduate school and its administration for facilitating my success in so many ways. My peers at GSK – especially my classmates – have also been a tremendous source of support and encouragement, and I am fortunate to have had such comradery. I would also like to take this opportunity to mention and remember our classmate and friend, Jordan Aronowitz, who was an inspiring, hard-working, treasured member of our cohort.

Thank you to my committee members, Dr. Mary Baylies and Dr. Stephen Long, for keeping me on my toes throughout my years of graduate school. Your support and critical feedback during committee meetings have made me a better scientist.

I would like to express my appreciation to Heng Pan of the Memorial Sloan Kettering Microchemistry & Proteomics Core for demonstrating patience and persistence in helping me with challenging biochemical pursuits. I am also grateful to Dr. Vitaly

Boyko of the Memorial Sloan Kettering Molecular Cytology Core for confocal microscopy support.

I would like to thank my previous lab mentors who have remained mentors to me to this day: Dr. John Golin, Dr. Alyssa Schuck, and Dr. Josefa Steinhauer. I would also like to thank Mr. Max Rudmann and Dr. Harvey Babich. Each of you believed in me and encouraged me along this path to a PhD. Without your support, I would not have gotten to this point.

Finally, I would like to thank my incredible husband and our families. Your love and dedication to my success mean the world to me.

TABLE OF CONTENTS

LIST OF TABLES

LIST OF FIGURES

LIST OF ABBREVIATIONS

ACAT: Acyl-CoA:cholesterol acyltransferase

ACBP: acyl-CoA binding protein

CK1: Casein kinase 1

CoA: Coenzyme A

Cryo-EM: cryogenic electron microscopy

DAG: diacylglycerol

DDM: n-Dodecyl-β-D-maltopyranoside

DGAT: Diacylglycerol acyltransferase

Dhh: Desert hedgehog

Disp: Dispatched

EGF: Epidermal growth factor

ER: endoplasmic reticulum

Fzd: Frizzled

GOAT: Ghrelin *O*-acyltransferase

GSK3β: Glycogen synthase kinase 3β

Hh: Hedgehog

Hhat: Hedgehog acyltransferase

Ihh: Indian hedgehog

LPCAT: Lysophosphatidylcholine acyltransferase

LPEAT: Lysophosphatidylethanolamine acyltransferase

LPIAT: Lysophosphatidylinositol acyltransferase

LPLAT: Lysophospholipid acyltransferase

LRP: Lipoprotein receptor-related protein

MBOAT: membrane-bound *O*-acyltransferase

NBD: nitrobenzoxadiazole

NMT: N-myristoyltransferase

OG: n-Octyl-β-D-glucopyranoside

PCP: Planar cell polarity

Porcn: Porcupine

Ptch: Patched

Shh: Sonic hedgehog

Smo: Smoothened

SOAT: Sterol *O*-acyltransferase

SUFU: Suppressor of fused

TAG: triacylglycerol

Wg: Wingless

Wnt: Wingless/Integrated

Chapter One: Introduction

The Hedgehog (Hh) signaling pathway is one of a number of important cell signaling pathways that promote cell growth and differentiation during embryonic development. Following secretion from Hh-producing cells, Hh proteins act along a morphogen gradient, traveling to near and far cell distances to pattern tissues during embryonic development. In flies, Hh signaling is responsible for the patterning of multiple organs. In vertebrates, Hh signaling through three Hh family members drives formation of the skeletal system (Indian Hedgehog (Ihh)), gonads (Desert Hedgehog (Dhh)), neural tube, and limbs (Sonic Hedgehog (Shh)) (Sasai, Toriyama, and Kondo 2019). Hh proteins are secreted ligands that are post-translationally modified with one lipid at each terminus, resulting in a mature form that is secreted from cells. Binding of Hh ligand to its receptor, Patched (Ptch), on the surface of receiving cells results in inhibition of Ptch, and subsequent alleviation of Ptch-mediated inhibition of Smoothened (Smo). Activation of Smo ultimately enables Gli transcription factors to translocate from the cytoplasm into the nucleus, where they bind to and promote transcription of Hh target genes. Each of the steps of Hh processing and signaling will be described in detail below.

1) Hh processing

Hh proteins undergo several post-translational modifications to transform the 45 kDa precursor protein into the mature, dually lipidated, 19 kDa protein that proceeds

through the secretory pathway (Resh 2021) (Figure 1). Following synthesis, the Hh precursor protein is translocated into the endoplasmic reticulum (ER) lumen via recognition of its N-terminal signal sequence, which is subsequently cleaved. Hh then undergoes two independent lipid modifications inside the ER. The first modification occurs in tandem with an autocleavage reaction, in which a single cholesterol molecule displaces the C-terminal portion of Hh, resulting in a 19 kDa C-terminally cholesterol-modified Hh protein (Mann and Beachy 2004). The displaced portion of the precursor protein is degraded in the ER lumen. The second modification is the addition of palmitate, a 16-carbon, saturated fatty acid, to the N-terminus. This modification is catalyzed by the ER-transmembrane enzyme, Hedgehog acyltransferase (Hhat), a member of the membrane-bound O-acyltransferase (MBOAT) family of enzymes (Buglino and Resh 2008). These two lipid modifications are responsible for regulating key developmental and biochemical functions (Table 1), as will be discussed below. After the Hh protein is dually lipidated, it is packaged into vesicles and sent to the Golgi, and then to the plasma membrane, where it is secreted with the assistance of SCUBE2 and Dispatched (Disp) proteins (Tukachinsky et al. 2012).

Figure 1. Hh processing

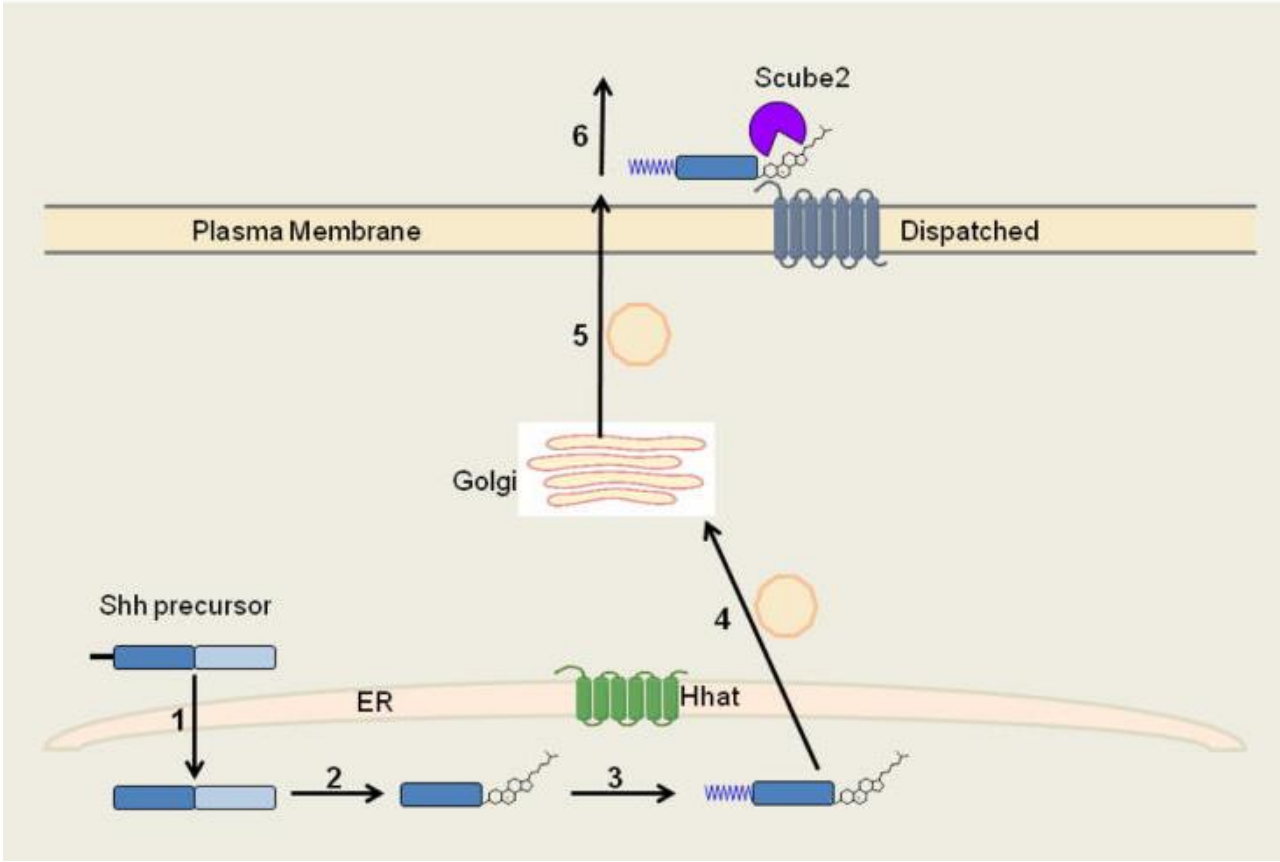

Hh undergoes multiple post-translational modifications in the ER lumen before it is secreted. (Image is from Resh, M. D. 2016. 'Fatty acylation of proteins: The long and the short of it', *Prog Lipid Res*, 63: 120-31 and reprinted with permission from Elsevier.)

Table 1. Developmental and biochemical roles of Hh cholesterol and fatty acid modifications

Hh Modification	Developmental Role(s) in Flies	Developmental Role(s) in Mice	Biochemical/Cellular Role(s)
C-terminal Cholesterol	• Restricts long-range signaling in wing discs (1)	• Promotes (2) or restricts (5) long-range signaling in limb buds • Responsible for proper brain, face, and limb formation during embryonic development (2)	• Targets Hh to Ptch1-enriched lipid rafts (2) • Contributes to inhibition of Ptch1 via direct binding within Ptch1 (3)
N-terminal Palmitate	• Responsible for proper cuticle segmentation and eye development (6-10)	• Promotes induction of ventral forebrain neurons (11) • Regulates signaling range in a tissue-dependent manner (12) • Maintains viability after birth (12) • Responsible for proper embryonic development (12) • Responsible for proper neural tube and limb bud patterning (12)	• Enhances Shh-mediated inhibition of Ptch1 (4) via direct binding within Ptch1 (3)

(1) (Burke et al. 1999)
(2) (Lewis et al. 2001)
(3) (Rudolf et al. 2019)
(4) (Tukachinsky et al. 2016)
(5) (Li et al. 2006)
(6) (Lee and Treisman 2001)
(7) (Lee et al. 2001)
(8) (Chamoun et al. 2001)
(9) (Micchelli et al. 2002)
(10) (Amanai and Jiang 2001)
(11) (Kohtz et al. 2001) Note: In this study, myristate (instead of palmitate) was used for *in vitro* analysis.
(12) (Chen et al. 2004)

Referred to as an anchor, the C-terminal cholesterol attached to Hh proteins is proposed to regulate the range of signaling by its insertion into the cell membrane. Release of cholesterol-modified Hh requires Disp (Burke et al. 1999). The mechanism by which the cholesterol anchor regulates the range of signaling in development is controversial. Mice expressing Shh protein lacking the C-terminal cholesterol demonstrated similar biological activity (i.e., development of Shh-dependent structures) to mice expressing the cholesterol-containing protein, but the signaling target field of the cholesterol-lacking construct was mostly localized to posterior, and not anterior, limbs (Lewis et al. 2001). These findings, supported by others in the study, suggested that cholesterol modification is dispensable for short-range signaling but essential for promoting long-range signaling in the mouse limb bud. In seeming contradiction to these results, a study in *Drosophila melanogaster* showed that expression of a cholesterol-lacking Hh transgene in the wing disc resulted in anterior compartment expansion, whereas the signaling range was five times lower and more restricted by the cholesterol-containing construct (Burke et al. 1999). Thus, the cholesterol adduct in the wing disc appeared to restrict the range of signaling and was essential for short-range signaling. Lewis *et al*. suggest that this apparent difference in cholesterol-mediated Hh signaling range might be due to the shorter overall range of signaling within the wing disc (8-10 diameters) compared to that in the vertebrate limb (30 cell diameters). An additional study on Hh signaling in mouse limb buds found that the cholesterol appendage restricted the range of signaling of Shh, in line with that found in flies (Li et al. 2006). On the individual cell level, the cholesterol modification might influence membrane trafficking and/or targeting of Shh to Ptch1-containing cholesterol-rich microdomains (lipid rafts) in the membrane (Lewis et al. 2001). Furthermore, a recent structure of dually lipidated Shh bound to Ptch1 suggests a role for the C-terminal cholesterol of Shh in mediating signaling by direct binding with Ptch1 (Rudolf et al. 2019). Biochemical evidence from

this study supports the authors' proposition that the cholesterol appendage, in tandem with palmitate but not by itself, inhibits intra-Ptch1 cholesterol transport, thereby enabling Smo activation.

Modification of the N-terminus of Hh proteins with palmitate was first discovered by mass spectrometry analysis of Shh in 1998 (Pepinsky et al. 1998). Subsequently, identification of the responsible palmitoyltransferase stemmed from genetic screens in *Drosophila melanogaster* that identified a gene required for proper embryonic segmentation (Micchelli et al. 2002; Chamoun et al. 2001; Amanai and Jiang 2001; Lee and Treisman 2001). The enzyme in flies has been referred to as Skinny Hedgehog, Sightless, Central Missing, and Rasp; denoted Rasp herein. The homology of Rasp to the MBOAT family, as well as abolishment of Hh palmitoylation by Rasp mutation or deletion, defined Rasp as an acyltransferase that was found to be required for Hh activity in Hh producing cells, yet dispensable for Hh gene expression, stability, and secretion (Micchelli et al. 2002; Chamoun et al. 2001; Amanai and Jiang 2001; Lee and Treisman 2001). A foundational study by our group provided direct biochemical evidence that Shh palmitoylation is mediated by Hhat in cells and by purified Hhat *in vitro* (Buglino and Resh 2008). Palmitoyl-Coenzyme A (CoA), and not another palmitate-containing lipid, was identified as the donor substrate for the reaction (Buglino and Resh 2008). As was shown for Rasp in flies (Amanai and Jiang 2001; Micchelli et al. 2002; Chamoun et al. 2001), N-terminal palmitate modification of Shh does not depend on prior cholesterol modification of the C-terminus (Buglino and Resh 2008). Additional experiments in this study established that transit of Shh through the secretory pathway is necessary for Shh palmitoylation (Buglino and Resh 2008).

The role of palmitate in development has been extensively characterized in flies and mice, primarily employing Hhat/Rasp mutant and Shh N-terminal cysteine-to-serine

mutant proteins for comparative analysis with WT Hh/Shh proteins and their signaling phenotypes. Palmitoylation of *Drosophila* Hh was shown to be required for proper cuticle segmentation, eye development, and wing formation (Amanai and Jiang 2001; Chamoun et al. 2001; Lee et al. 2001; Lee and Treisman 2001; Micchelli et al. 2002). In mice, fatty acylation of Shh is required to induce differentiation of ventral forebrain neurons (Kohtz et al. 2001), ensure proper (non-stunted) embryonic growth and limb formation, and maintain viability after birth (Chen et al. 2004). The latter study also proposed a role for palmitoylation in mediating the range of signaling, which was found to be different in different tissues (Chen et al. 2004).

In contrast to the developmental roles of palmitate modification on Shh, the biochemical mechanism of the palmitate adduct in the Shh pathway was not well understood until recent years. Given that the cell surface receptor for Shh is Ptch and that binding of palmitoylated Shh to Ptch initiates the downstream pathway cascade, it was initially puzzling that Shh lacking a fatty acyl attachment exhibited compromised signaling, yet was able to bind Ptch1 (Pepinsky et al. 1998; Tukachinsky et al. 2016). Equally surprising was the finding that differentially acylated forms of Shh yielded similar affinity for binding to Ptch in a cell-based assay, yet their signaling potency varied over a 1600-fold range (Taylor et al. 2001). These conundrums were resolved by recent structural studies which revealed that Ptch1 is a dimer (Ptch1-A,B) that binds Shh in a 2:1 ratio. The N-terminal palmitate of Shh binds within the Ptch1-A monomer, whereas the globular portion of Shh binds within the Ptch1-B monomer (Qian et al. 2019; Rudolf et al. 2019). Both Shh-Ptch1 interfaces independently contribute equally to the binding affinity of Shh to Ptch1 (Wierbowski et al. 2020). Thus, Shh can still bind Ptch1 via the Ptch1-B interface alone (i.e., even when palmitate is absent). However, the functional consequences of Shh binding to Ptch1 are most potent when palmitate is present and

bound within Ptch1-A (Tukachinsky et al. 2016). As alluded to earlier, the following mechanism has been proposed for Ptch1-mediated regulation of Smo activity (Kinnebrew et al. 2021): In the absence of Shh, Ptch1 sequesters cholesterol and prevents it from activating Smo. Interaction between the lipid moieties of Shh and a putative cholesterol transport tunnel in Ptch1-A either stabilizes Ptch1 in an inactive state or directly blocks Ptch1-mediated cholesterol transport. This inhibition of Ptch1 enables cholesterol in the plasma membrane to become accessible to activate Smo.

2) Hh signaling

After maturation, dually lipidated Shh is anchored into the cell membrane and requires other factors to release it into the extracellular milieu. These assistant proteins are SCUBE2 and Disp, which interact with the lipid moieties of Shh to free Shh from the membrane (Tukachinsky et al. 2012). How the dually lipidated, hydrophobic Hh protein then traverses the hydrophilic extracellular environment to signal from producing to receiving cells is a question that is not clearly resolved. Multiple modes of transport of hydrophobically modified Wingless/Integrated (Wnt) / Wingless (Wg) proteins to receiving cells have been identified, and include interaction with extracellular carrier proteins, heparan sulfate proteoglycans (HSPGs), lipoprotein particles, and exosomes (secreted vesicles), as well as cellular extension by cytonemes (specialized actin-rich filopodia-like cell protrusions) (Mehta, Hingole, and Chaudhary 2021). These transport methods shield the acyl appendage during transport to mediate transport through the hydrophilic extracellular environment. Several similar possibilities of transport have been suggested for Hh, including via exosomes and cytonemes (Gradilla et al. 2014; Bischoff et al. 2013; Sanders, Llagostera, and Barna 2013) and diffusible lipoprotein particles

(Steinhauer and Treisman 2009; Panakova et al. 2005). Several of these modes of transport have been found to overlap (e.g., cytoneme-mediated transport with exosomes (Gradilla et al. 2014)), and it is also possible that different modes of transport are operative in different organisms and tissues. Moreover, recent studies have found that dually lipidated Shh interacts with binding partners CDON/BOC and GAS1 in a handoff mechanism for delivery of the lipidated Hh protein to Ptch1 (Wierbowski et al. 2020; Huang et al. 2022). As above, these handoff proteins and the other suggested methods of transport are not necessarily mutually exclusive. In fact, a recent study identified cytoneme-mediated transport of Shh onto receiving cells which was dependent upon formation of a Disp-CDON/BOC complex in secreting cells (Hall et al. 2021).

Following handoff of dually lipidated Shh from GAS1 to Ptch1 (Wierbowski et al. 2020; Huang et al. 2022), Shh binds Ptch1 via three domains: the globular domain of Shh binds Ptch1-B, and the palmitate and cholesterol moieties of Shh insert into Ptch1-A. While none of these three interactions alone is absolutely necessary for Shh binding to Ptch1, the insertion of palmitate and cholesterol are proposed to inhibit Ptch1 in a joint fashion, whereby palmitate more robustly contributes to the inhibition mechanism (Rudolf et al. 2019). The current models for Shh-mediated inhibition of Ptch1 are based upon a central theory that Ptch normally functions to transport cholesterol within/through the plasma membrane (a finding confirmed in *C. elegans*, which lack Smo (Cadena Del Castillo et al. 2021)). When Ptch is bound by Shh, intra-Ptch cholesterol transport is obstructed, making cholesterol in the membrane accessible to directly activate Smo (Kinnebrew et al. 2021). Binding of the globular domain of Hh to Ptch1 is likely responsible for internalization of Ptch1 (Tukachinsky et al. 2016) and subsequent accumulation of Smo at the cell surface in *Drosophila* (Zhu et al. 2003) or ciliary

membrane in vertebrates (Corbit et al. 2005). These steps are necessary for canonical signal transduction of the Hh pathway via Smo.

Canonical Hh signaling occurs as follows (Pietrobono, Gagliardi, and Stecca 2019) (Figure 2): In the absence of Hh, Ptch is localized at the base of the primary cilium in vertebrate cells, and Smo activity is repressed. Gli-2 and Gli-3 are phosphorylated by Protein kinase A, Casein kinase 1 (CK1), and Glycogen synthase kinase 3β (GSK3β), and sequestered in the cytoplasm via interaction with Suppressor of Fused (SUFU). Subsequent proteolytic cleavage produces C-terminally truncated Gli forms that repress transcription of Hh target genes. Upon binding of Shh to Ptch, Ptch is displaced from the primary cilium, internalized, and degraded in the lysosome. This results in phosphorylation and translocation of Smo to the cilium. Activated Smo prevents Gli-2 and Gli-3 processing, and promotes their dissociation from SUFU. Full-length, active Gli is translocated into the nucleus and promotes transcription of Hh target genes. While Gli-2 and Gli-3 demonstrate both activator and repressor capabilities, Gli-1 serves only as a transcriptional activator (Niewiadomski et al. 2019).

Figure 2. The Hh signaling pathway

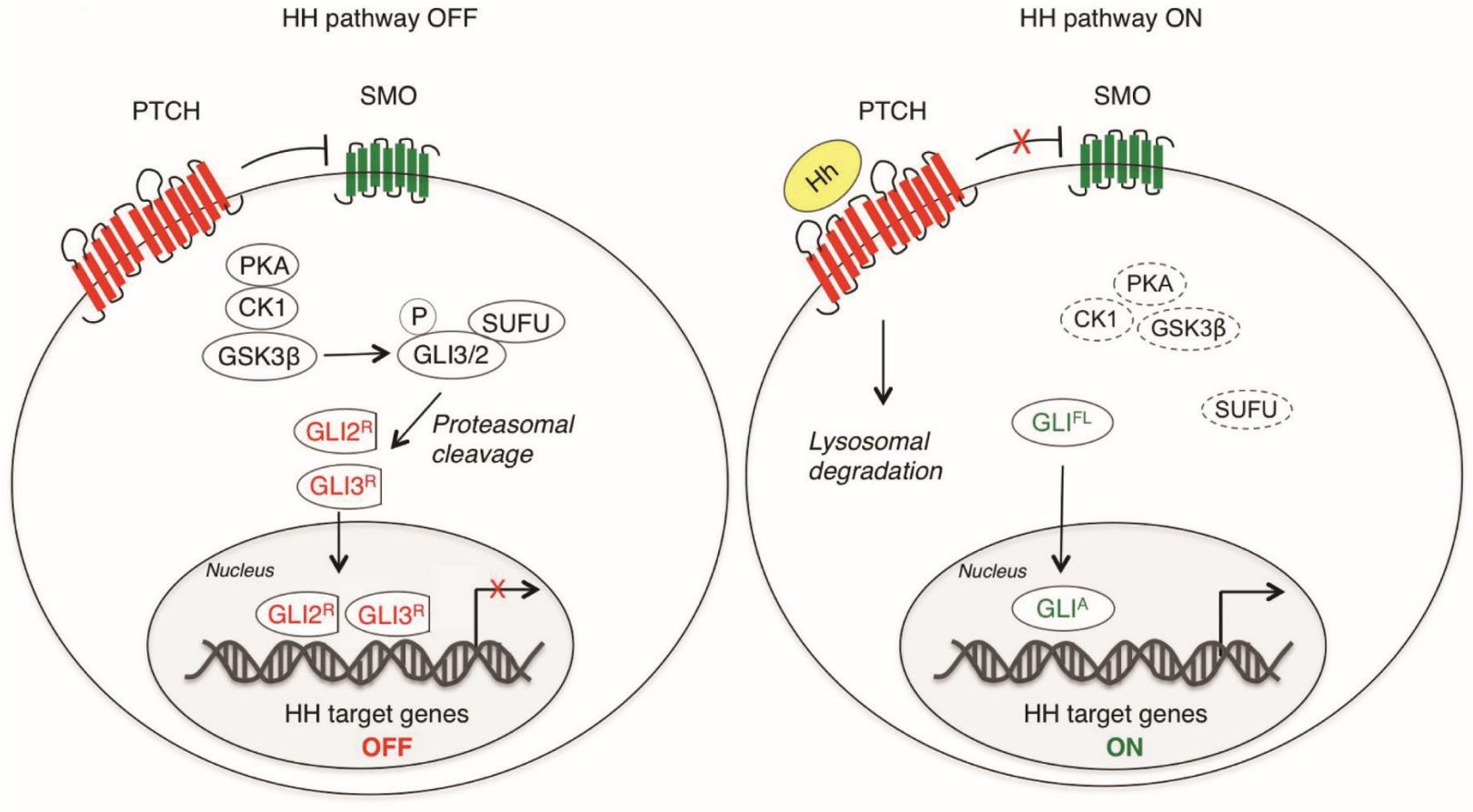

Canonical Hh signaling is activated by inhibition of Ptch through binding of Hh ligands. Subsequently, Smo is activated, causing Gli proteins to activate transcription of target genes. (Reprinted from Pietrobono, S., S. Gagliardi, and B. Stecca.

2019. 'Non-canonical Hedgehog Signaling Pathway in Cancer: Activation of GLI Transcription Factors Beyond Smoothened', *Frontiers in Genetics*, 10. Copyright © 2019 Pietrobono, Gagliardi and Stecca.)

Non-canonical Hh signaling can occur through mechanisms independent of Hh-Ptch1-Smo. For example, multiple cancers regulate Hh signaling by impacting Gli activity through crosstalk with other pathways and regulators (Pietrobono, Gagliardi, and Stecca 2019). Treating cancers driven by non-canonical Hh signaling is challenging, as targeting the typical upstream pathway members has been largely ineffective.

Multiple target genes of Hh signaling have been identified, including CCND2, CCNE1, BCL2, MYCN, ABCG2, FGF4, VEGFA, PAX6, PAX7, PAX9, FOXM1, and JAG1 (Skoda et al. 2018). Processes regulated through these factors include the cell cycle and apoptosis, and even Wnt signaling. Other gene targets of the Hh pathway include positive and negative regulators of Hh signaling, such as Hedgehog-interacting protein, Ptch1, Ptch2, and Gli-1.

3) The MBOAT family of enzymes

The MBOAT family of enzymes was identified in the year 2000, based on the identification of a shared region of primary sequence homology among several family members (Hofmann 2000). Conserved residues that are hallmarks of the MBOAT family include a histidine and asparagine or aspartic acid, whose mutation has been found to significantly reduce acyltransferase activity. The MBOAT family includes 11 enzymes in humans: Diacylglycerol acyltransferase 1 (DGAT1), Acyl-CoA:cholesterol acyltransferases (ACATs) (also known as sterol *O*-acyltransferases [SOATs]) 1 and 2, Lysophospholipid acyltransferases (LPLATs) 11-14 (also known as LPIAT1/MBOAT7, LPCAT3/MBOAT5, LPCAT4/MBOAT2, and LPEAT1/MBOAT1, respectively), Ghrelin *O*-acyltransferase (GOAT) (also known as MBOAT4), Porcupine (Porcn), Hhat, and Hhat-like (also known as GUP1/MBOAT3) (Valentine et al. 2022; Chang, Sun, and Chang

2011). Most MBOAT family members catalyze O-acylation, namely, linkage of a fatty acyl chain to an oxygen atom. With the protein substrates Ghrelin and Wnt, *O*-acylation occurs on an internal serine of the recipient substrate. In contrast, Hhat catalyzes amide linkage of palmitate to the amino group of the N-terminal cysteine of Hh proteins. Nonetheless, Hhat's homology to other members of the MBOAT family places Hhat in this category.

An anomaly to the MBOAT family in terms of homology is Hhat-like, the mammalian homolog of yeast GUP1. It is also the least studied mammalian MBOAT. In Hhat-like, the conserved histidine present in the other MBOATs is instead a leucine, and for this reason the enzyme is proposed to act as a negative regulator of Shh palmitoylation rather than an active acyltransferase (Abe, Kita, and Niikura 2008). Consistent with this hypothesis, a potential role for Hhat-like as a tumor suppressor has been identified (Zhang et al. 2005). However, the precise mechanisms underlying these possible roles for Hhat-like remain unidentified. GUP1 is proposed to function in a wide and diverse range of biological processes in yeast (Lucas et al. 2016), giving no specific clues as to the function of its ortholog in mammals. The differential expression of Hhat-like in very few tissues (heart, skeletal muscle, and brain) (compared to that of Hhat) further mystifies its function (Lucas et al. 2016).

i. Lipid-modifying MBOATs

Most enzymes in the human MBOAT family catalyze the transfer of a fatty acid from a fatty acyl-CoA donor substrate to a recipient lipid substrate. This group of enzymes includes DGAT1, which produces triacylglycerol (TAG) from diacylglycerol (DAG), and is critical for cellular fat storage (Yen et al. 2008). Other MBOAT enzymes important for lipid metabolism are ACATs 1 and 2, which convert cholesterol into cholesterol esters.

The largest known subfamily of MBOATs is that of the LPLATs, which includes multiple enzymes that generate a variety of phospholipids (Valentine et al. 2022). These enzymes attach saturated and unsaturated fatty acids, ranging from 16 to 22 carbons, to lysophosphatidic acid, lysophosphatidylcholine, lysophosphatidylethanolamine, lysophosphatidylserine, lysophosphatidylinositol, and lysophosphatidylglycerol (Valentine et al. 2022). LPLATs participate in the Kennedy and Lands pathways to generate phospholipid diversity (Valentine et al. 2022).

ii. Protein-modifying MBOATs

Porcn

Porcn is one of three known enzymes in the MBOAT family that catalyzes attachment of a fatty acid to a recipient protein substrate. Porcn transfers palmitoleate, a monounsaturated 16-carbon fatty acid, to Wnt proteins and plays a key role in the Wnt signaling pathway. First identified in flies as Wg in 1973, Wnt represents a mammalian family of 19 cysteine-rich proteins that mediate early cell development processes including proliferation, specification, and migration, as well as adult cell homeostasis (Li, Ortiz, and Kotula 2020). Like Hh proteins, Wnts are secreted proteins that are post-translationally modified in the ER. Wnt is glycosylated at several residues (Smolich et al. 1993) and fatty acylated by Porcn on an internal, conserved serine residue (Ser-209 in Wnt3a). These modifications are not inter-dependent (Gao and Hannoush 2014), and both are required for efficient cellular secretion of Wnt (Komekado et al. 2007). Acylation of Wnt is also necessary for binding of Wnt to its chaperone, Wntless (Takada et al. 2006; Barrott et al. 2011; Biechele, Cox, and Rossant 2011). Recent structural analysis revealed that Porcn directly hands off acylated Wnt proteins to Wntless (Nygaard et al. 2021), and this likely explains why unacylated Wnt accumulates in the ER. Wnt is then

transported from the ER to the Golgi via interaction with multiple proteins, and is ultimately released and secreted from the plasma membrane (Mehta, Hingole, and Chaudhary 2021).

Following secretion, Wnt proteins are transported to receiving cells through a variety of mechanisms including via interaction with extracellular carrier proteins, HSPGs, lipoprotein particles, and exosomes, as well as cellular extension by cytonemes (Mehta, Hingole, and Chaudhary 2021). Canonical Wnt signaling in receiving cells is induced by association of the palmitoleoylated Wnt ligand with its cell surface receptor Frizzled (Fzd) and co-receptor Lipoprotein receptor-related protein (LRP) 5/6. In the absence of Wnt ligands, this receptor complex remains inactive, and cytoplasmic β-catenin is phosphorylated by the β-catenin destruction complex (composed of Axin, APC, CK1, and GSK3β). Phosphorylation promotes ubiquitination of β-catenin, targeting it for proteasomal degradation. The absence of β-catenin in the nucleus enables binding of a transcriptional repressor complex (TCF, with the transcriptional repressor Groucho) to target genes, repressing their activity. In the presence of Wnt ligands, Fzd-LRP5/6 receptor complex activation leads to recruitment of Dishevelled proteins to the plasma membrane, where they inactivate the β-catenin destruction complex. β-catenin then accumulates in the cytoplasm and is translocated to the nucleus, where it forms a complex with TCF and promotes target gene transcription (Patel et al. 2019; Mehta, Hingole, and Chaudhary 2021). These targets include Cyclin D1, c-MYC, PDK, MTC-1, MMP7, Fibronectin, Cox-2, and Axin-2, which regulate critical cellular processes such as the cell cycle and energy metabolism (Lecarpentier et al. 2019). Non-canonical Wnt signaling, which is also mediated by the Fzd receptor (and/or ROR1/ROR2/RYK co-receptors) but does not involve β-catenin, occurs through several alternative signaling cascades. Typical examples include the planar cell polarity (PCP) and Wnt/Ca^{2+}

pathways, which regulate cell shape and directional migration, the orientation of primary cilia in the vertebrate inner ear, and directional organization of tissues (PCP pathway), as well as ventral fate in *Xenopus* embryos and axonal guidance in mammals (Wnt/Ca^{2+} pathway) (Patel et al. 2019; Mehta, Hingole, and Chaudhary 2021). Dysregulation of Wnt signaling results in multiple disorders. Specifically, the absence of functional Porcn has been implicated in developmental disorders including Goltz Syndrome (Barrott et al. 2011), and overactive Porcn has been implicated in human cancers (Polakis 2007).

Several fundamental components of Porcn activity have been established by our laboratory and others. Stearoyl-CoA Desaturase1 is needed to produce the monounsaturated palmitoleoyl-CoA donor substrate in cells, and conversion to the unsaturated fatty acyl form by Porcn occurs prior to its transfer to Wnt proteins (Rios-Esteves and Resh 2013). Additionally, a consensus sequence was identified in Wnt3a (CXCHGXSXXCXXKXC) containing residues that mediate Porcn binding, fatty acid transfer, and cellular signaling (Rios-Esteves, Haugen, and Resh 2014). Serine or threonine, but not cysteine, can serve as residues for Porcn-mediated fatty acylation (Rios-Esteves, Haugen, and Resh 2014; Miranda et al. 2014). The secondary structure and the cysteines surrounding Ser-209 are important for recognition of Wnt by Porcn. A peptide containing two disulfide bonds that form a Wnt hairpin surrounding Ser-209 serves as a Porcn substrate, whereas a linear peptide with the same primary sequence does not (Asciolla et al. 2017; Lee et al. 2019). Further insights into the molecular mechanism of Porcn have been elucidated in recent structural studies, as will be referenced below (Section 4).

GOAT

A second MBOAT whose recipient substrate is a protein is GOAT. GOAT was discovered in 2008 by two independent groups that used overexpression or silencing of MBOAT candidates to identify the Ghrelin acyltransferase (Gutierrez et al. 2008; Yang, Brown, et al. 2008). The discovery of GOAT came almost 10 years after the finding that Ser-3 of Proghrelin was acylated with octanoate, a saturated 8-carbon fatty acid, resulting in a mature peptide hormone that controls appetite (Kojima et al. 1999). Like Hh and Wnt, Ghrelin undergoes fatty acylation and additional processing through the secretory pathway. Preproghrelin is the immature form of Ghrelin that contains an N-terminal signal sequence. Following cleavage of the signal sequence in the ER lumen, Proghrelin is fatty acylated by GOAT, and then cleaved by Prohormone convertase 1/3 to produce the mature Ghrelin protein, which is secreted into the bloodstream (Zhu et al. 2006). On the cell surface, Ghrelin binds to its G-coupled protein receptor, GHS-R1a, resulting in subsequent downstream signaling through multiple pathways (Yin, Li, and Zhang 2014). The activated pathways are tissue-dependent and influence biological processes such as appetite stimulation, glucose homeostasis, and cardiovascular health (Davis et al. 2021). Unacylated Ghrelin cannot bind to GHS-R1a, but has been shown to modulate several other biological processes through an unidentified mechanism (Davis et al. 2021).

Proghrelin is the only known substrate for GOAT (Darling et al. 2015). Several studies have explored in detail the requirements within Proghrelin for fatty acylation by GOAT. The four N-terminal amino acids (Gly-Ser-Ser-Phe) underlie GOAT recognition with different chemical property requirements for each residue. Gly-1 is recognized by both its amino group and the absence of a side chain at the alpha carbon (Yang, Zhao, et al. 2008; Darling et al. 2015; Darling et al. 2013; Cleverdon, Davis, and Hougland 2018). The amino acid at position 2 need not strictly be serine; hydrogen bonding and

size of the side chain dictate its recognition by GOAT (Yang, Zhao, et al. 2008; Darling et al. 2015; Darling et al. 2013; Cleverdon, Davis, and Hougland 2018). Fatty acylation takes place on the side chain hydroxyl of Ser-3 and does not require stereochemical specificity (Taylor et al. 2015; Cleverdon, Davis, and Hougland 2018). Importantly, GOAT does not fatty acylate the neighboring Ser-2 even if Ser-3 is mutated to alanine (Darling et al. 2015; Darling et al. 2013; Yang, Zhao, et al. 2008; Yang, Brown, et al. 2008). The large, non-polar nature of Phe-4, along with its strict stereoselectivity, underlie its recognition by GOAT (Cleverdon, Davis, and Hougland 2018; Darling et al. 2015). Beyond these four N-terminal residues, it is possible that additional Ghrelin residues mediate GOAT binding to a smaller degree (Taylor et al. 2015; Darling et al. 2015).

Hhat

The third protein-modifying MBOAT is Hhat. Hhat's recipient substrates comprise the Hedgehog family of proteins (Hardy and Resh 2012). Vertebrates have three Hh family members, all of which are palmitoylated by Hhat: Desert hedgehog, Indian hedgehog, and Sonic hedgehog (Ingham and McMahon 2001). *Drosophila melanogaster* only has one Hh family member, termed Hh, which is palmitoylated by the Hhat ortholog, Rasp (Amanai and Jiang 2001; Chamoun et al. 2001; Lee and Treisman 2001; Micchelli et al. 2002). All four Hh family members have a high degree of primary sequence conservation, and importantly, contain the conserved N-terminal peptide sequence Cys-Gly-Pro-Gly-Arg that dictates palmitoylation (Hardy and Resh 2012). Interestingly, Rasp also palmitoylates Spitz, an Epidermal growth factor (EGF)-like ligand, and potentially two other EGF-like ligands, Keren and Gurken, which also contain an N-terminal cysteine following cleavage of the signal sequence (Miura et al. 2006). These EGF-like ligands do not have mammalian homologues. Our lab performed an *in silico* screen to

identify proteins in the human secretome that contain a cysteine following the predicted signal sequence cleavage site. Aside from Hh family members, none of the candidate proteins were found to be Hhat substrates (Hardy & Resh 2012). Thus, the only currently known substrates of Hhat in vertebrates are Hh family members.

Several molecular aspects of the Hhat-mediated palmitoylation reaction have been investigated by our group. A key mechanistic question is whether palmitoylation of the amide on the N-terminal cysteine occurs via S-acylation of the cysteine's sulfhydryl group, followed by an intramolecular S-to-N shift (Mann and Beachy 2004) (Figure 3A), or by direct linkage (Figure 3B). An N-acetylated Shh peptide did not serve as a substrate for palmitoylation, despite the presence of a free sulfhydryl group on the cysteine, suggesting that the proposed two-step mechanism is less likely (Buglino and Resh 2008). Structural analysis of Hhat (Jiang, Benz, and Long 2021) also favors a one-step mechanism (described below) (Figure 3C). Our group also determined that the first six N-terminal residues of Shh are sufficient for palmitoylation in cells, and that the chemical nature of these residues influences palmitoylation of the cysteine. Furthermore, at least one positively charged residue in the first seven amino acids is required for palmitoylation (Hardy and Resh 2012). This finding is supported by three dimensional structures of Hhat that revealed the presence of negatively charged residues lining the ER lumenal cavity where Shh enters (Jiang, Benz, and Long 2021; Coupland et al. 2021). Interestingly, cell-based experiments demonstrated that while a cysteine-to-alanine mutant (C24A) does not incorporate palmitate, a serine mutant (C24S) can be palmitoylated by Hhat (Hardy and Resh 2012), but not by Rasp (Lee and Treisman 2001; Hardy and Resh 2012). The ability of the serine to be palmitoylated by Hhat may explain why Shh-mediated skeletal patterning is retained to some degree in transgenic

mice expressing a C25S mutant Shh protein (Chen et al. 2004), compared to flies in which the C85S mutant abolishes Hh activity (Lee et al. 2001).

Figure 3. Molecular mechanism of Hhat catalysis

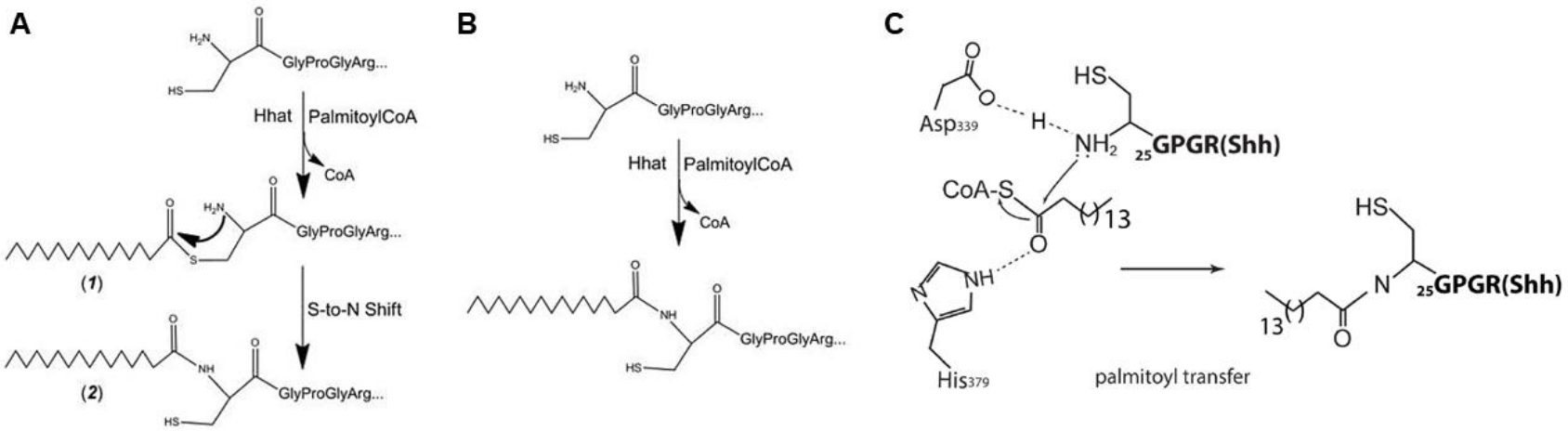

Hhat links palmitate to the N-terminal cysteine of Hh proteins via one of two possible mechanisms: ***A,*** an intramolecular S-to-N shift, or ***B*****,** direct amide linkage. (Images are from Buglino, J. A., and M. D. Resh. 2012. 'Palmitoylation of Hedgehog proteins', *Vitam Horm*, 88: 229-52 and reprinted with permission from Elsevier.) ***C,*** Direct amide linkage is supported by structural analysis. (Image is from Jiang, Y., T. L. Benz, and S. B. Long. 2021. 'Substrate and product complexes reveal mechanisms of Hedgehog acylation by HHAT', *Science*, 372: 1215-19 and reprinted with permission from AAAS.)

Transmembrane topology studies by our group and others (Matevossian and Resh 2015b; Konitsiotis et al. 2015) identified 10 transmembrane domains and two reentrant loops within Hhat. The N and C -termini of Hhat, as well as the conserved Asp-339 residue, were identified by both groups as localizing to the cytoplasmic side of the ER membrane. Overall, most of the enzyme's mass was predicted to be cytoplasmic or within the membrane, with only 4-5 loops predicted to be exposed to the ER lumen. The identification of multiple cytoplasmic loops within Hhat, and the fact that fatty acyl-CoAs have low membrane permeability due to their polarity, led to the hypothesis that Hhat may bind and transport the cytoplasmic palmitoyl-CoA substrate across the ER membrane itself. This hypothesis was tested and confirmed in *in vitro* and cell-based experiments (Asciolla and Resh 2019). Subsequent structural analyses of Hhat identified 12 transmembrane domains and found the majority of the mass of the protein to lie within the transmembrane region (Jiang, Benz, and Long 2021; Coupland et al. 2021). The analyses also confirmed the cytoplasmic localization of the N and C -termini as well as the notion that Hhat directly facilitates palmitoyl-CoA movement from the cytoplasmic opening of the enzyme into the ER membrane.

Identified in one of the Hhat topology studies was inaccessibility of cytosolic cysteines to chemical modification, as well as a lack of disulfide bonds (Konitsiotis et al. 2015). These findings led to the hypothesis that Hhat contains several sites for internal palmitoylation on cysteine residues by DHHC acyltransferase(s). Of note, Porcn has also been shown to be palmitoylated on at least one internal cysteine residue (Gao and Hannoush 2014). Konitsiotis and colleagues metabolically labeled cells expressing V5 epitope-tagged Hhat with an alkynyl palmitate analog, immunoprecipitated Hhat, and ligated palmitoylated protein to an azide-containing capture reagent. Palmitoylation of Hhat was detected by Western blot analysis. Treatment with hydroxylamine decreased

the signal from palmitoylated Hhat, consistent with S-acylation, and mutation of all four predicted cytoplasmic cysteine residues to alanine abolished Hhat palmitoylation entirely. Subsequent structural analysis of Hhat by the same laboratory proposed that one of these palmitoylation sites may play a role in preventing Hhat dimerization, and identified palmitoylation of another cysteine residue within Hhat (Coupland et al. 2021). Beyond internal palmitoylation, the Hhat structural analyses elucidated further important details of Hhat's biochemistry, which will be expounded upon below.

iii. Structural analyses of Hhat and other MBOATs

In the past four years, multiple structural studies on MBOATs have been published, shedding light on the membrane topology, molecular mechanism, and substrate specificity profiles of many of these acyltransferases. The first published 3D structure of an MBOAT was that of DltB (Ma et al. 2018), a bacterial enzyme that catalyzes the addition of D-alanine to cell wall teichoic acid in Gram-positive bacteria. Following suit quickly thereafter were computationally predicted and solved cryogenic electron microscopy (cryo-EM) structures of multiple mammalian MBOATs, including GOAT (Campana et al. 2019), DGAT1 (Wang et al. 2020; Sui et al. 2020), ACAT1 (Qian et al. 2020; Long et al. 2020; Guan et al. 2020), Porcn (Galli et al. 2021; Liu et al. 2022; Yu, Liao, et al. 2021), LPCAT3 (Zhang et al. 2021), and Hhat (Jiang, Benz, and Long 2021; Coupland et al. 2021).

DltB and the protein-modifying MBOATs (Porcn, Hhat, GOAT) share a common topology problem: their donor and recipient substrates are located on opposite sides of the membrane. Initial biochemical studies suggested that the enzymes themselves are responsible for transporting the donor substrate through the membrane (Perego et al. 1995; Asciolla and Resh 2019), a proposition that was confirmed by the structural

revelation of a tunnel within these enzymes that connects one side of the membrane to the other (Jiang, Benz, and Long 2021; Coupland et al. 2021; Ma et al. 2018; Campana et al. 2019; Yu, Liao, et al. 2021; Liu et al. 2022; Galli et al. 2021). Nearly all the recent structural studies of ER-resident MBOATs posit that the fatty acyl-CoA donor substrate enters the tunnel through the cytoplasmic opening, while the recipient substrate enters from either the lumenal opening (in the case of recipient substrates that are ER-lumenal proteins, e.g., Wnt, Ghrelin, Hh) (Figure 4A) or a lateral gate within the membrane (in the case of recipient substrates that are lipids, e.g., cholesterol, DAG) (Figure 4B) (Jiang, Benz, and Long 2021; Coupland et al. 2021; Wang et al. 2020; Sui et al. 2020; Qian et al. 2020; Yu, Liao, et al. 2021; Campana et al. 2019; Liu et al. 2022; Galli et al. 2021).

Figure 4. MBOAT structures

A

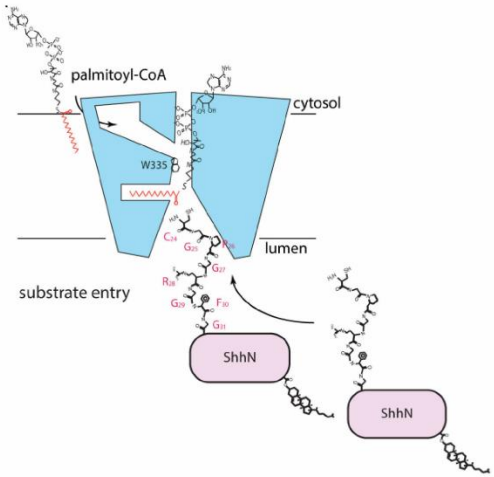

Hhat; Jiang *et al.* (2021) *Science*

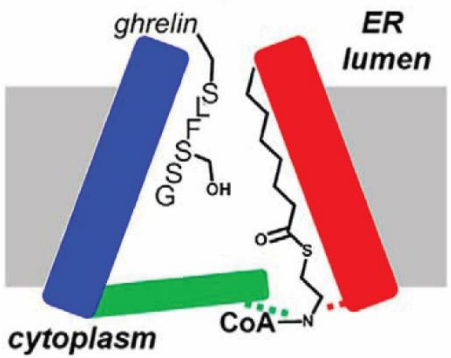

GOAT; Campaña *et al.* (2019) *Journal of Biological Chemistry*

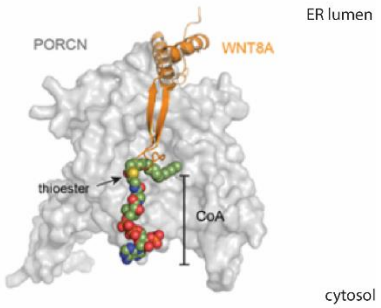

Porcn; Yu *et al.* (2021) *Journal of Cell Science*

B

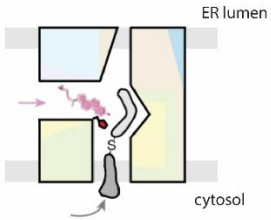

ACAT1; Qian *et al.* (2020) *Nature*

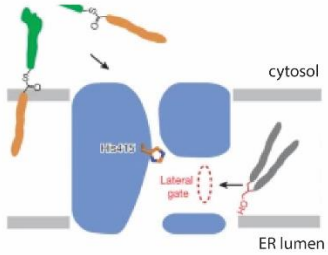

DGAT1; Sui *et al.* (2020) *Nature*

A, Protein-modifying MBOATs contain two ER tunnel openings: one to the cytoplasm (proposed for entry of the donor fatty acyl-CoA substrate and exit of the CoA byproduct), and one to the lumen (proposed for entry and exit of the recipient protein substrate). (Image of Hhat is from Jiang, Y., T. L. Benz, and S. B. Long. 2021. 'Substrate and product complexes reveal mechanisms of Hedgehog acylation by HHAT', *Science*, 372: 1215-19 and reprinted with permission from AAAS. Image of GOAT is from Campana, M. B., F. J. Irudayanathan, T. R. Davis, K. R. McGovern-Gooch, R. Loftus, M. Ashkar, N. Escoffery, M. Navarro, M. A. Sieburg, S. Nangia, and J. L. Hougland. 2019. 'The ghrelin O-acyltransferase structure reveals a catalytic channel for transmembrane hormone acylation', *J Biol Chem*, 294: 14166-74. Image of Porcn is from Yu, J., P. J. Liao, W. Xu, J. R. Jones, D. B. Everman, H. Flanagan-Steet, T. H. Keller, and D. M. Virshup. 2021. 'Structural model of human PORCN illuminates disease-associated variants and drug-binding sites', *J Cell Sci*, 134 and reprinted/adapted with permission from the *Journal of Cell Science*.) ***B***, Lipid-modifying MBOATs contain up to three ER tunnel openings: one to the cytoplasm (proposed for entry of the donor fatty acyl-CoA substrate and exit of the CoA byproduct), one within the membrane (proposed for entry and exit of the recipient lipid substrate), and one to the lumen (proposed for exit of the lipidated product in the ACAT1 structure shown). (Image of ACAT1 is from Qian, H., X. Zhao, R. Yan, X. Yao, S. Gao, X. Sun, X. Du, H. Yang, C. C. L. Wong, and N. Yan. 2020. 'Structural basis for catalysis and substrate specificity of human ACAT1', *Nature*, 581: 333-38 and reprinted with permission from Springer Nature. Image of DGAT1 is from Sui, X., K. Wang, N. L. Gluchowski, S. D. Elliott, M. Liao, T. C. Walther, and R. V. Farese, Jr. 2020. 'Structure and catalytic mechanism of a human triacylglycerol-synthesis enzyme', *Nature*, 581: 323-28 and reprinted with permission from Springer Nature.)

The MBOAT structural studies reveal that catalysis takes place within the ER membrane, and confirm earlier biochemical analyses that established that catalysis is mediated by conserved histidine and aspartate/asparagine residues (Jiang, Benz, and Long 2021; Coupland et al. 2021; Wang et al. 2020; Sui et al. 2020; Qian et al. 2020; Yu, Liao, et al. 2021; Zhang et al. 2021; Liu et al. 2022; Galli et al. 2021; Campana et al. 2019). Hhat catalysis occurs via linkage of the amino group of the Shh N-terminal cysteine to the carbonyl carbon of the fatty acyl-CoA's acyl chain (displacing CoA), either via direct amide linkage (Buglino and Resh 2008) or an intramolecular S-to-N shift (Mann and Beachy 2004). As proposed for the conserved asparagine residue in other MBOATs (Davis et al. 2021) and in support of direct amide linkage, Hhat Asp-339 may serve as a base to activate the N-terminal Shh cysteine for nucleophilic attack (Figure 3C) (Jiang, Benz, and Long 2021; Coupland et al. 2021). Hhat His-379 may act as a hydrogen-bond donor to activate the carbonyl carbon of palmitoyl-CoA for catalysis (Figure 3C) (Jiang, Benz, and Long 2021; Coupland et al. 2021). A common supposition among several of the structural studies is that the CoA byproduct is released from the enzyme into the cytosol, whereas the fatty acylated reaction product is released laterally into the ER membrane (Wang et al. 2020; Sui et al. 2020; Long et al. 2020; Coupland et al. 2021). In the case of Hhat, one study proposes that the lipidated Shh product is released into the ER lumen (Jiang, Benz, and Long 2021), while another study specifies that, due to the hydrophobicity of the lipidated product, Shh exit into the ER lumen cannot be direct. Instead, palmitoylated-Shh is proposed to occur by initial release into the ER membrane and/or by binding to membrane proteins (Coupland et al. 2021).

Structural studies have revealed several features that are unique to Hhat. Unlike DGAT1 (Wang et al. 2020; Sui et al. 2020) and ACAT1 (Qian et al. 2020; Long et al. 2020; Guan et al. 2020) which exist as a dimer or tetramer, Hhat is a monomer (Jiang,

Benz, and Long 2021; Coupland et al. 2021). Another aspect of Hhat that distinguishes it from the other MBOATs is the presence of a heme B prosthetic group (Jiang, Benz, and Long 2021; Coupland et al. 2021). While the heme does not make any contacts with Hhat residues involved in catalysis or palmitoyl-CoA binding, mutation of Cys-324, which coordinates the central iron, results in loss of enzymatic activity. It is likely that the heme group plays structural and/or regulatory roles in Hhat. One possibility is that the presence of the heme blocks Hhat dimerization (Coupland et al. 2021), as its location within Hhat corresponds to the site of dimerization in other MBOATs (Jiang, Benz, and Long 2021). Alternatively, the heme-Cys-324 binding site might compete with potential S-acylation that has been proposed to occur on cysteines within Hhat (Konitsiotis et al. 2015).

Another unique feature in the Hhat structure is the presence of a potential sterol binding site adjacent to the lumenal cavity that serves as the entry site for Shh (Coupland et al. 2021). The authors suggest that this site could belong to the C-terminal cholesterol of Shh, and they find reduced enzyme activity when certain mutations are introduced in this region. It should be noted that this mutational analysis was performed in the absence of a cholesterol appendage on the Shh ligand. It is possible that the sterol binding site, regardless of occupancy by the Shh C-terminal cholesterol, plays a role in maintaining structural stability of Hhat.

A final aspect of Hhat biology that has not been experimentally validated in other MBOATs is the novel finding of a transport function that is coordinated with, yet separate from, acyl transfer activity to Shh. Experiments by our group found that Hhat can transport nitrobenzoxadiazole (NBD)-labeled palmitoyl-CoA through a lipid bilayer *in vitro* and across the ER membrane in cells (Asciolla and Resh 2019). Uptake of NBD and [^{14}C] -labeled palmitoyl-CoA was detected in membrane vesicles containing Hhat, as

well as in liposomes reconstituted with purified Hhat, with an estimated stoichiometry of ~20 molecules of palmitoyl-CoA per molecule of Hhat. In the presence of a Shh peptide, this transport activity was slowed, likely due to obstruction of the Hhat tunnel by the Shh recipient substrate. Furthermore, mutation of Tyr-351, an Hhat acyl-CoA binding pocket residue (Jiang, Benz, and Long 2021; Coupland et al. 2021), to alanine had no effect on Shh palmitoylation activity, but decreased transport activity. Together, these findings led to the conclusion that transport of palmitoyl-CoA by Hhat can be functionally separated from palmitoylation of Shh. The cryo-EM structures of Hhat in their captured states do not support a transport function for Hhat, as the palmitoyl-CoA molecule would not fit through the enzyme's tunnel depicted in these studies (Jiang, Benz, and Long 2021; Coupland et al. 2021). However, it is possible that in the absence of the nanobodies/Fab fragments used to capture the Hhat structures, Hhat might be able to adopt an alternative conformation that would enable it to accommodate an elongated/flattened form of an acyl-CoA molecule which could potentially fit through the tunnel (Coupland et al. 2021). Such a flattened conformation of the CoA group is apparent in the DGAT1 structures (PDBs 6VP0 and 6VZ1) (Coupland et al. 2021).

Hhat mutations have been implicated in multiple diseases, and the structural relevance of these mutants has been illuminated by Coupland et al. (2021). A homozygous Hhat G287V missense mutation was identified in a patient with abnormal testicular development, and found to inhibit Hhat-mediated palmitoylation of Shh and Dhh *in vitro* (Callier et al. 2014). The loss of enzymatic activity is postulated to result from disruption of the heme and possibly palmitoyl-CoA binding sites and/or the catalytic center of Hhat. Hhat W386C is associated with intellectual disability (Agha et al. 2014), and demonstrates minor reduction in enzymatic activity, potentially due to palmitoylation of this cysteine residue. G448E is an Hhat mutation possibly involved in cancer

development (Kawakami et al. 2001). Its location at the edge of the ER lumenal cavity is hypothesized to obstruct access of the full-length Shh protein into the Shh binding site within Hhat. Hhat L257P was identified in two siblings with microcephaly and early infantile-onset seizures (Abdel-Salam et al. 2019), and is proposed to disrupt heme binding or cause protein misfolding. These findings highlight the functional importance of Hhat in development and human health.

4) Specificity and cellular consequences of fatty acyl-CoA substrate selectivity by fatty acyltransferases

i. DHHC acyltransferases

Protein lipidation in general is an important feature of cellular processes, regulating protein stability, localization, enzymatic activity, and interactions with membranes and other proteins (Jiang et al. 2018). There are multiple types of lipid modifications that occur on proteins, including fatty acylation and prenylation, as well as C-terminal cholesterol and glycosylphosphatidylinositol modification (Jiang et al. 2018). The major form of protein palmitoylation involves covalent attachment of palmitate to the sulfhydryl group of a cysteine residue. This modification, termed S-palmitoylation, is catalyzed by the DHHC family of acyltransferases and can be reversed by the activity of thioesterases (Malgapo and Linder 2021). There are currently 23 known members of the DHHC family of acyltransferases in humans (Malgapo and Linder 2021). S-palmitoylation is widespread in cells, occurring on signaling proteins, receptors, ion channels, and transcriptional regulators (Resh 2016). S-palmitoylated proteins make up at least 10% of the human proteome, and include the EGF receptor, Src-family tyrosine kinases Lck and

Fyn, and members of the Ras family of proteins, among many others (Blanc et al. 2015; Blanc, David, and van der Goot 2019).

DHHC palmitoyltransferases have been shown to recognize a multitude of fatty acyl-CoA substrates (Jennings and Linder 2012; Rana, Lee, and Banerjee 2019; Greaves et al. 2017). DHHC fatty acyl-CoA binding pockets have been referred to as “molecular rulers,” modulating binding and utilization of different chain length fatty acids when the binding cavity is altered by mutation (Rana, Lee, and Banerjee 2019) (a phenomenon reminiscent of that noted above for GOAT). *In vitro* competition assays with [^{3}H]-palmitoyl-CoA and unlabeled 2:0, 6:0, 10:0, 12:0, 14:0, 16:0, 16:1, 18:0, 18:1, 18:2, and 20:4 fatty acyl-CoAs found that fatty acyl-CoAs containing acyl chains of 12 or more carbons most effectively inhibited [^{3}H]-palmitoylation of different recipient protein substrates by DHHC2 and DHHC3 acyltransferases, although to different extents (Jennings and Linder 2012). Furthermore, direct analysis of 14:0, 16:0, 18:0, 18:1, and 20:4 acyl-CoA usage by these two acyltransferases via HPLC readout yielded different peak intensity profiles between the two enzymes, most notably among the 18:0, 18:1, and 20:4 acyl-CoAs. Interestingly, direct kinetic analysis revealed a higher apparent turnover rate for oleoyl-CoA compared to palmitoyl-CoA by DHHC2 but not DHHC3. Another study utilizing click chemistry to test multiple DHHC enzymes (DHHC- 2, 3, 4, 5, 7, 11, 15, 23) found marked differences in substrate preference among several of the enzymes when comparing 14:0, 16:0, and 18:0 fatty acid chains (Greaves et al. 2017). Differences in primary sequence lining the fatty acyl-CoA binding pocket of various DHHC family members are proposed to confer specific fatty acyl chain selectivity to individual DHHC enzymes (Stix et al. 2020). This has been demonstrated by the difference of even one amino acid in the fatty acyl-CoA binding pocket of DHHC3 and DHHC7, which otherwise have very similar primary sequences (Greaves et al. 2017).

The fatty acyl-CoA substrate promiscuity of DHHC acyltransferases is consistent with the identification of non-palmitate, thioester-linked fatty acids to proteins in platelets (Muszbek et al. 1999). Functionally, differential S-acylation of proteins by DHHC acyltransferases can influence the modified protein's ability to bind membranes and localize within the membranes, both of which can affect their subsequent trafficking and activities within the cell (Greaves et al. 2017).

ii. Lipid-modifying MBOATs

Biochemical studies have shown that MBOATs can utilize multiple fatty acyl-CoA substrates as the fatty acid donor. LPLATs demonstrate a range of fatty acyl-CoA substrate specificity, utilizing saturated and unsaturated fatty acyl-CoAs with acyl chains between 16 and 22 carbons long (Valentine et al. 2022). Interestingly, different LPLATs exhibit different specificity profiles that are also dependent upon the particular recipient lysophospholipid (Table 2) (Valentine et al. 2022). Other lipid-modifying MBOATs also demonstrate a range of fatty acyl-CoA substrate specificity. Although oleoyl-CoA is thought to be the primary fatty acyl-CoA substrate for DGAT1, *in vitro* kinetic analyses with purified hDGAT1 found that DGAT1 can transfer 16:0, 16:1, 18:0, and 18:1 fatty acids to DAG (Wang et al. 2020). While the apparent turnover rate is highest with oleoyl-CoA, DGAT1 demonstrates greatest apparent affinity for 16-carbon fatty acyl-CoAs among those tested (Wang et al. 2020). Similarly, *in vitro* kinetic analyses with purified hACAT1 showed that ACAT1 can transfer 16:0, 16:1 Δ9, 18:0, 18:1 Δ7, and 18:1 Δ11 fatty acids to cholesterol (Qian et al. 2020). ACAT1 exhibited the highest apparent turnover rate with oleoyl-CoA (18:1 Δ9), but greater apparent affinity for nearly all the other fatty acyl-CoAs tested (with the exception of stearoyl-CoA) (Qian et al. 2020).

Table 2. Substrate profiles of LPLATs 11, 12, 13, 14

		Fatty Acyl-CoA						
		16:0	**18:0**	**18:1**	**18:2**	**18:3**	**20:4**	**22:6**
Lysophospholipid	**Phosphatidic acid**			11, 12, 13, 14*	11, 12		11*	
	phosphatidylcholine	12	12	11*, 12, 13, 14*	11*, 12, 13	12	11, 12	12, 13
	phosphatidylethanolamine	12	11*	11*, 12, 13, 14*	11		11*, 12, 14*	13, 14
	phosphatidylserine	12	12, 14	11*, 12, 14	11*, 12, 14*		11*, 12	
	phosphatidylinositol				11*		11	
	phosphatidylglycerol			14*				

*Opposing reports

Adapted from Figure 4 of Valentine, W. J., K. Yanagida, H. Kawana, N. Kono, N. N. Noda, J. Aoki, and H. Shindou. 2022. 'Update and nomenclature proposal for mammalian lysophospholipid acyltransferases, which create membrane phospholipid diversity', *J Biol Chem*, 298: 101470.

Lipid substrate diversity is thought to be functionally significant in the regulation of multiple cellular processes. It is reasonable to speculate that an important functional consequence of acyl chain diversity in TAG and cholesterol esters is energy production, since TAG and cholesterol esters are stored in cellular LDs, and LD catabolism results in β-oxidation of the freed fatty acids via lipolysis or lipophagy (Kloska et al. 2020). Phospholipids are critical structural components of membranes, but the barrier function of membranes alone would not justify the need for substrate diversity of LPLATs (Dai, Tang, and Pang 2021). Indeed, saturated, monounsaturated, and polyunsaturated fatty acid-containing phospholipids have been shown to confer different properties to cellular membranes in the face of stress response, giving importance to the underlying molecular differences (Antonny et al. 2015). Phospholipids can also serve as signaling molecules. For example, phosphatidylinositol phosphates have varied fatty acid composition in whole cell membrane fractions vs. nuclear membrane fractions (Ogiso et al. 2010)), suggesting that different acyl chain-containing phospholipids might serve different functional roles (Hishikawa et al. 2014). Finally, since TAG and phospholipid synthesis both occur in the ER membrane, it has been suggested that the fatty acyl chain diversity of TAG conferred by DGAT fatty acyl-CoA substrate specificity may impact the availability of fatty acyl-CoAs for ER membrane lipid composition (Yu, Zhou, et al. 2021). The same proposal would apply for the opposite scenario, whereby the fatty acyl composition of the DGAT1-generated TAGs might be impacted by substrate usage by LPLATs for phospholipid synthesis. In fact, this concept would additionally apply to all other ER-resident MBOATs, since they share a cytosolic pool of fatty acyl-CoA substrates (see Chapter Four for further discussion of this idea).

iii. Protein-modifying MBOATs

Porcn

Several studies have shown that Porcn can transfer select saturated and unsaturated fatty acid analogs to Wnt in cells. These analogs include [^{125}I]-Iodinated 10, 12, 13, 15, 15:1, and 16:1 fatty acids (Rios-Esteves and Resh 2013), and alkyne-linked 10, 13, 14, 16, and 18 carbon saturated fatty acids, with preference for medium-chain alkyne-linked fatty acids (Gao and Hannoush 2014). Another study tested fatty acyl-CoA substrate preference for Porcn *in vitro*, and found that palmitoleoyl-CoA was the best substrate for Porcn. Increasing activity was observed with saturated 6-8 carbon fatty acyl-CoAs, and lowest activity was observed for saturated 12-16 carbon and monounsaturated 17-18 carbon fatty acyl-CoAs (Lee et al. 2019). Interestingly, Tuladhar and colleagues showed in a cell-based assay that the position of the double bond within the monounsaturated fatty acid affects incorporation into Wnt, with Δ7 and Δ11 fatty acids less efficiently transferred to Wnt compared to Δ9 (Tuladhar et al. 2019). The same study also showed that, although a fatty acid with a *trans*-double bond at Δ9 could serve as a weak substrate for Porcn, a *cis*-double bond was required for release of the fatty acylated Wnt from Porcn and for Wnt secretion from the cell.

Porcn-mediated fatty acylation of Wnt is required for multiple steps in the Wnt signaling pathway, including binding of Wnt to its intracellular chaperone, Wntless, secretion of Wnt, and binding of Wnt to its cell surface receptor, Fzd (Tuladhar and Lum 2015; Azbazdar et al. 2021). However, recent studies (Speer et al. 2019; Azbazdar et al. 2019) have indicated that the effect of fatty acylation on Wnt function varies with the particular Wnt protein and context in question.

The study of differential fatty acylation of Wnt proteins in cells is not well resolved. Mass spectrometry analysis of overexpressed Wnt3a protein isolated from cells determined that palmitoleate is the major species of fatty acyl attachment, with observation of myristoleate (14:1 Δ5) to a small degree (Takada et al. 2006). One recent

study employed computational modeling to determine the chemical identity of the fatty acyl group present in the crystal structure of xWnt8-mouse:Fz8-CRD (Azbazdar et al. 2019). The study found that the fatty acyl group in this structure was most likely palmitate rather than palmitoleate, and proposed that canonical Wnts are acylated with a saturated 16-carbon fatty acid rather than the monounsaturated form, consistent with preference for a saturated fatty acyl attachment to bind to membrane rafts and activate Wnt signaling in ordered membrane domains (Sezgin et al. 2017; Ozhan et al. 2013; Levental et al. 2010; Zhai, Chaturvedi, and Cumberledge 2004). Structural analyses have indicated that different Fzd receptors have conformational flexibility to accommodate Wnt fatty acid attachments of different chain lengths and degrees of unsaturation (Nile and Hannoush 2019), including a 24-carbon chain with an unidentified degree of unsaturation in the human Fzd7 CRD structure (Nile et al. 2017). Importantly, the presence of *cis*-unsaturated (and not saturated) fatty acids in the latter structure promoted Fzd dimerization. That and other structural observations led to the proposition that the dimer-mediated, U-shaped binding mode for fatty acyl chains within Fzd is the biologically functional conformation, and forms the basis for Fzd selectivity of Wnt ligands with *cis*-monounsaturated fatty acids (Nile et al. 2017). Beyond a requirement for *cis* vs. *trans* unsaturated fatty acylation in Wnt secretion (Tuladhar et al. 2019), the impact of differential fatty acylation of Wnt proteins on cellular signaling has not been experimentally explored.

GOAT

The fatty acyl-CoA substrate specificity of GOAT has been investigated in several studies. In one cell-based study, GOAT and Ghrelin were co-transfected in HEK293 cells, and the media was supplemented with saturated 2, 4, 5, 6, 7, 8, 9, 10, 12, 13, and 16 -carbon fatty acids (Gutierrez et al. 2008). Mass spectrometry analysis identified

Ghrelin peptides containing each of the above fatty acid modifications, with 4, 7, 8, 9, 10, and 12 -carbon fatty acylated forms demonstrating the greatest peak intensity. Another study utilized an *in vitro* assay with HPLC readout and tested the ability of membrane-embedded GOAT to utilize saturated 6, 8, 10, 14, and 16 -carbon acyl-CoAs. Only 6, 8, and 10 -carbon fatty acylated Ghrelin products were detected, with more robust activity (determined by kinetic analysis) for the 6-carbon over the 8-carbon acyl-CoA, and very low output of decanoylated Ghrelin (Ohgusu et al. 2009). Interestingly, the short fatty acyl-CoA binding pocket in GOAT is capped by large aromatic residues whose mutation to alanine enables accommodation of longer chain (12 and 14 -carbon) fatty acyl-CoA substrates (Campana et al. 2019).

The functional significance of differential Ghrelin fatty acylation has been analyzed utilizing synthetic Ghrelin analogs. One study measuring *in vitro* binding and activation of the human Ghrelin receptor GHSR1a by differentially acylated Ghrelin found that increasing hydrophobicity of the acyl attachment, regardless of size or flexibility, conferred greater interaction than hydrophilic acyl attachments (Bednarek et al. 2000). Another study compared the activities of saturated 8 and 10 -carbon acylated Ghrelin forms in a cell-based assay and in rats, finding their activities to be similar (Hosoda et al. 2003). In the latter study, purification of Ghrelin from human stomach tissue extracts coupled with biochemical analyses identified 8:0, 10:0, and 10:1 -modified forms of Ghrelin, with 8:0-modified Ghrelin in highest abundance. Manipulating the diet of mice with various fatty acids resulted in detection of ingested medium chain (6, 8, and 10, but not 4 or 16 -carbon) saturated fatty acids in the stomachs of these mice (Nishi et al. 2005). Thus, it is likely that, in addition to GOAT's fatty acyl-CoA substrate specificity profile, the fatty acyl attachment to Ghrelin is also dependent upon *in vitro* and *in vivo* availability and concentrations of different fatty acyl-CoAs.

Hhat

In contrast to the acyltransferases discussed above, the fatty acyl-CoA substrate specificity of Hhat has not been thoroughly investigated. Differences in cryo-EM structures observed between the fatty acyl-CoA binding cavity of Hhat and other MBOATs – namely, a more defined and slender cavity in the Hhat structure compared to DGAT1 and ACAT1, and an unidentified lipid inserting into the acyl-CoA binding cavity in one of the Hhat structures – led to the proposition that the configuration of the fatty acyl-CoA binding pocket in Hhat is selective for palmitoyl-CoA (Jiang, Benz, and Long 2021) and is restricted to a maximum of 16 carbons (Coupland et al. 2021). However, previous biochemical evidence suggests that Hhat is able to bind a variety of fatty acyl-CoAs. Addition of unlabeled 10, 12, and 14, and to a lesser extent 16:1 and 18:0 fatty acyl-CoAs inhibited incorporation of [^{125}I]-Iodopalmitate into Shh by purified Hhat, likely acting as substrate competitors (Buglino and Resh 2008). However, until this thesis research was performed, direct analyses demonstrating that Hhat can transfer fatty acids other than palmitate to Shh had not been reported.

The question of Hhat's substrate specificity profile is important because it is one of several factors that may dictate the fatty acid that is ultimately attached to Shh in cells. Another likely influential factor, as noted above for GOAT and should likewise apply to all fatty acyltransferases, is the availability and abundance of particular fatty acyl-CoAs within the cell. Indeed, as demonstrated with Ghrelin (Nishi et al. 2005), the specificity of fatty acylation of proteins in cells and *in vivo* can be manipulated by exogenous supplementation of particular fatty acids (Muszbek et al. 1999; Liang et al. 2001; Webb, Hermida-Matsumoto, and Resh 2000; Lindwasser and Resh 2002). This was exemplified with Shh by increased modification of Shh with myristate when the growth medium was supplemented specifically with myristate (Long et al. 2015). Mammalian cells and tissues

contain multiple fatty acids and fatty acyl-CoAs with variation in relative abundance depending on cell/tissue type and context; consistently, 16:0, 18:0, 18:1, and 18:2 fatty acids/acyl-CoAs are among the most abundant (Spector and Yorek 1985; Greaves et al. 2017; Woldegiorgis et al. 1985; Hama et al. 2020; Palladino et al. 2012; Haynes et al. 2008). Thus, *in vivo*, Hhat (and other acyltransferases) would have access to multiple fatty acyl-CoAs.

Although palmitoyl-CoA has been proposed as Hhat's preferred fatty acyl-CoA substrate (Jiang, Benz, and Long 2021), fatty acids other than palmitate have been detected on Shh purified from mammalian cells. These N-terminal acyl attachments were detected by mass spectrometry and include 14:0, 14:1, 16:1, 18:0, 18:1, and 20:4 fatty acids (Long et al. 2015; Pepinsky et al. 1998). Importantly, the prevalence of various fatty acyl attachments on Shh was found to be dependent upon cellular context, e.g., metabolic state and Shh expression level. In some cases, other fatty acyl attachments to Shh were detected at even higher proportions than palmitate (Long et al. 2015). Specifically, while palmitoylated Shh was the dominant species in SHH-I cells cultured in media containing 10% FBS and in which Shh was not overexpressed, oleoylated Shh was the dominant form when Shh was overexpressed (Long et al. 2015). In cells overexpressing Shh and grown in serum-free media, monounsaturated fatty acylated (16:1 and to a lesser extent 14:1) Shh comprised the most abundant species of Shh (Long et al. 2015).

Differential fatty acylation has been shown to impart differences in signaling potency to the Shh protein. One study characterized the signaling potency of modified N-terminal forms of Shh in a C3H10T1/2 cell-based assay that measures the production of alkaline phosphatase in response to Shh signaling (Taylor et al. 2001). Various fatty acids and hydrophobic groups were artificially attached to Shh by non-enzymatic, *in vitro*

acylation, and equal amounts of purified protein were added to cells. The strength of Shh signaling output was found to generally increase with increasing hydrophobicity of the N-terminus. Specifically, Shh fatty acylated with saturated 8, 10, 12, and 14 -carbon fatty acids demonstrated increasing signaling potency with increasing chain length. Interestingly, signaling conferred by myristoylated Shh was found to be four times more potent compared to palmitoylated Shh, a finding that the authors attribute to possible stability or solubility issues in their assay. Another related, notable finding in this study was the increased signaling potency conferred by mutation of the N-terminal cysteine to increasingly hydrophobic amino acids. One such construct, the C24ii (N-terminal cysteine replaced with two isoleucine residues) construct, has since been widely used in signaling experiments as an analog to palmitoylated Shh. To date, only one other study has examined signaling activity mediated by differential fatty acylation of Shh. There it was shown that Shh isolated from chick limb buds exhibited reduced signaling activity when the explants were incubated with palmitoleate compared to palmitate (Long et al. 2015). Despite being limited by indirect analysis, this finding establishes precedent that unsaturation of the fatty acid attachment may impact Shh signaling. Since unsaturated fatty acyl-CoAs are used by multiple MBOATs (e.g., Porcn, DGAT1, ACAT1) and fatty acyl-CoA species such as oleoyl-CoA exist in cells in equal abundance to palmitoyl-CoA, further analysis of the ability of Shh to be modified and mediate signaling with monounsaturated fatty acids is of great interest and was therefore explored in this work.

5) Hh signaling in disease and cancer

Understanding the Hh pathway is critical for clinical purposes. At different stages of embryogenesis, Shh is expressed in the axial mesoderm in the head and caudal areas,

the ventral region of the neural tube including the floor plate domain, and in the zone of polarizing activity of the fore and hind -limbs (Sasai, Toriyama, and Kondo 2019). Ihh is primarily expressed in the developing skeletal system, and Dhh in Sertoli cells to control gonad formation (Sasai, Toriyama, and Kondo 2019). Mutations in Hh genes underlie developmental defects and disorders, including holoprosencephaly (small head; Shh) (Roessler et al. 1996), cleft lip and palate (mouth malformation) and brachydactyly type A-1 (short fingers) (Ihh) (Gao et al. 2001), and gonadal dysgenesis (Dhh) (Canto et al. 2004). As described earlier (Section 3), Hhat mutations have also been implicated in disease, including holoprosencephaly as noted above with Shh mutation. Mutations in downstream pathway members are responsible for numerous other syndromes, including Curry-Jones (multi-system disorder; Smo), Greig cephalopolysyndactyly (abnormalities in limbs, head, and face; Gli-3), Joubert, Meckel, and Acrocallosal (kidney, liver, skeletal, and facial abnormalities; Kif7) (Sasai, Toriyama, and Kondo 2019).

Following embryonic development and birth, the Hh pathway remains active in stem cells and certain tissues to maintain homeostasis (Petrova and Joyner 2014). Aberrant reactivation of the pathway in tissues in which it is otherwise silenced, or constitutive activation of the pathway in tissues in which the Hh pathway is operative, is conferred by mutations associated with negative (Ptch1, Ptch2, SUFU) and positive (Gli-2, Smo) Shh pathway regulators, and has been implicated in numerous cancers (Raleigh and Reiter 2019). These cancers can be categorized by several underlying mechanisms (Niyaz, Khan, and Mudassar 2019; Skoda et al. 2018). (1) Ligand-independent cancers represent constitutive activation of Hh pathway members downstream of Shh itself, and include basal cell carcinoma, medulloblastoma, and rhabdomyosarcoma. (2) Cancers driven by ligand-dependent, autocrine signaling constitute Hh overexpression in a Shh-

producing cell that acts on itself to proliferate excessively. These cancers have been identified in the stomach, esophagus, pancreas, colon, ovaries, endometrium, breast, prostate, lung, blood, and brain. (3) Cancers driven by ligand-dependent, paracrine signaling stem from Hh overexpression in a producing cell that activates growth factor responses in surrounding stromal cells. These cancers include prostate, pancreatic, and colorectal. The reverse model for this mechanism has also been identified in hematological cancers, whereby bone marrow or lymph node stromal cells secrete Hh to tumor cells. (4) Cancer stem cells have also been found to demonstrate aberrant Shh pathway activation, triggering stem cell renewal and tumor spread via ligand-dependent, autocrine or paracrine signaling. These cancers include chronic myelogenous leukemia, glioma, multiple myeloma, gastrointestinal, and pancreatic. It has been estimated that aberrant Hh pathway activation is associated with about one quarter of all cancer-related deaths (Iovine et al. 2016). Thus, pharmacological pursuits to specifically target Hh pathway components have been extensive. Several pathway components have been targeted with generation of multiple drugs per target; many of these agents have progressed to clinical trials (Wu et al. 2017).

Beginning with cyclopamine, Smo antagonists such as Vismodegib and Sonidegib represent a major class of Hh pathway cancer drugs developed between 2002 and 2013 (Wu et al. 2017). However, resistance and relapse have posed obstacles to the long-term success of these drugs (Chahal, Parle, and Abagyan 2018). Because of this and the fact that many Hh pathway cancers are ligand-dependent (Chahal, Parle, and Abagyan 2018), targeting the pathway at the level of the ligand is an appealing approach. To date, several pharmacological agents have been developed for this purpose, including inhibitors of cilia biogenesis and the activities of Hhat and Shh (Wu et al. 2017). *In vitro,* cell-based, and *in vivo* studies from our lab and others set the stage

for the targeting of Hhat, implementing Hhat knockdown and pharmacological inhibition with RU-SKI 43 to identify Hhat as a specific target in pancreatic, breast, and lung cancers (Petrova, Matevossian, and Resh 2015; Matevossian and Resh 2015a; Konitsiotis et al. 2014; Rodriguez-Blanco et al. 2013). Another member of the RU-SKI series (Resh et al. 2016), RU-SKI 201, continues to be investigated and modified to generate potent Hhat inhibitors that can be promising for the clinic (Rodgers et al. 2016; Lanyon-Hogg et al. 2021; Coupland et al. 2021).

6) Major unanswered questions addressed by this thesis work

i. Kinetic mechanism of the Hhat reaction

While much of Hhat enzymology has been elucidated in recent years, some unanswered questions remain regarding Hhat's substrate binding and product release. It is not known whether Hhat catalysis proceeds as a two-step reaction, as reported for DHHC acyltransferases (Jennings and Linder 2012), or a one-step reaction, which can be random or ordered. To determine the kinetic mechanism of Hhat, we implemented a classical biochemistry approach utilizing *in vitro* kinetic analysis with purified Hhat in a novel, fluorescence-based Hhat activity assay that we developed. We found that Hhat catalyzes a random sequential reaction, binding either of its substrates in no obligate order to form a ternary complex, and generating both its CoA byproduct and fatty acylated Shh products in a single step of catalysis.

ii. Substrate specificity of Hhat and consequences on Shh signaling

A) Hhat fatty acyl-CoA substrate specificity

Palmitoyl-CoA is thought to be the major acyl-CoA substrate for Hhat, but differential fatty acyl modification of Shh proteins has been shown to occur in different contexts. The

possibility that Hhat can utilize fatty acyl-CoAs other than palmitoyl-CoA to modify Shh has not yet been reported. To this end, we implemented our novel *in vitro* activity assay to investigate fatty acyl-CoA substrate specificity of purified Hhat, utilizing both saturated and unsaturated fatty acyl-CoAs, and found that Hhat can transfer fluorescently labeled 14:0, 16:0, 16:1, and 18:1 fatty acids to Shh, with some comparable preferences.

B) Consequences of differential fatty acylation on Shh signaling

The consequences of differential fatty acylation, especially unsaturation, of Shh on cellular signaling have not been fully explored. We utilized a direct, cell-based assay to explore the signaling consequences of differential fatty acylation of Shh. We compared the signaling potency of two unsaturated fatty acylated Shh species to that of two saturated fatty acylated Shh species, and found that signaling potency conferred by both unsaturated fatty acylated Shh species was lower than that of the saturated fatty acylated species.

iii. Fatty acyltransferase crosstalk

MBOATs and other acyltransferases share a pool of cytosolic fatty acyl-CoAs, prompting the question of whether these acyltransferases crosstalk. Whether the activity of one acyltransferase can impact the activity of another has been postulated (Yu, Zhou, et al. 2021) but unexplored. To probe this question for Hhat and other fatty acyltransferases in cells, we utilized cellular lipid droplet formation stimulated by exogenous addition of oleic acid as a readout of DGAT activity. We found that lack of functional Hhat resulted in an increase in lipid droplet formation in a DGAT1/2-repressed background, and that this increase was not due to increased mRNA expression levels of DGAT or ACAT enzymes.

Chapter Two: Kinetic mechanism of Hhat

Data and text from this chapter have been previously published in Schonbrun, A.R., and M.D. Resh. 2022. 'Hedgehog acyltransferase catalyzes a random sequential reaction and utilizes multiple fatty acyl-CoA substrates', *Journal of Biological Chemistry,* 298(10): 102422 and Schonbrun, A. R. and Resh, M. D. (2022). A Direct in vitro Fatty Acylation Assay for Hedgehog Acyltransferase. Bio-protocol 12 (24): e4573. DOI:10.21769/BioProtoc.4573.

I. Introduction

Two recent cryo-EM studies provide major insights into the structure of the active site and the transmembrane topology of Hhat, and propose a molecular mechanism for Hhat-mediated Shh palmitoylation (Coupland et al. 2021; Jiang, Benz, and Long 2021). However, the kinetic mechanism of Hhat catalysis – the sequence of substrate binding and product formation – remains unknown, not only for Hhat but for other MBOAT enzymes, such as DGAT1, ACAT1, GOAT, and Porcn. Unlike for DHHC acyltransferases (Jennings and Linder 2012), no study has reported whether Hhat catalysis involves an acyl-enzyme intermediate, or instead proceeds via formation of a ternary complex. Utilizing a classical biochemical approach that entails comprehensive kinetic analysis, I determined the kinetic mechanism of Hhat. To carry out the analysis, I developed a novel assay that directly monitors the activity of purified Hhat *in vitro*.

To date, several assays have been reported to measure the catalytic activity of Hhat (Table 3). However, these assays employ radioactive substrates (Jiang, Benz, and Long 2021; Buglino and Resh 2008), specialized equipment (Lanyon-Hogg et al. 2017), or require multiple steps for product readout (Lanyon-Hogg et al. 2015). While this thesis work was in progress, an *in vitro* Hhat assay that avoids these issues was developed, using Hhat in solubilized membranes, and fluorescence anisotropy of an acylated Shh peptide for assay readout (Lanyon-Hogg et al. 2019; Andrei, Tate, and Lanyon-Hogg 2022). However, the assay presented in this work is the first direct, fluorescent assay that tracks the fatty acyl group attached to Shh to measure catalytic activity of purified Hhat.

Table 3. Previously reported Hhat acylation assays

Assay Name	Reference	Assay Method and Output	Limitation (relative to our current assay)
n/a	(Buglino and Resh 2008)	1) Shh and Hhat -expressing cells labeled with [^{125}I]-iodopalmitate 2) *In vitro* assay with [^{125}I]-iodopalmitoyl-CoA and biotinylated Shh peptide • Measure [^{125}I]-iodopalmitate incorporation into Shh	Uses radioactive materials
Click chemistry–armed enzyme-linked immunosorbent assay (Click-ELISA)	(Lanyon-Hogg et al. 2015)	• *In vitro* assay employing click chemistry (alkyne-tagged palmitoyl-CoA analog and azido-FLAG Shh peptide) and ELISA • Measure colorimetric readout (FLAG-HRP) of immobilized Shh peptide consisting of a FLAG-tagged palmitate analog	Requires multiple steps to achieve product readout
Microfluidic mobility shift assay (MSA)	(Lanyon-Hogg et al. 2017)	• *In vitro* assay with palmitoyl-CoA and fluorescent Shh peptide • Separation of palmitoylated Shh peptide from non-palmitoylated peptide by chemical properties • Measure conversion % (Shh peptide detected by fluorescence)	Requires specialized equipment
Acylation-coupled lipophilic induction of polarisation (Acyl-cLIP)	(Lanyon-Hogg et al. 2019)	• *In vitro* assay with palmitoyl-CoA and fluorescent Shh peptide • Measure fluorescence anisotropy change upon palmitoylation of detergent micelle-bound, fluorescent Shh peptide	Does not allow for fatty acyl-CoA competition analysis
n/a	(Jiang, Benz, and Long 2021)	• *In vitro* assay with [^{3}H]-palmitoyl-CoA and biotinylated Shh peptide • Measure [^{3}H]-palmitate transfer to Shh	Uses radioactive materials

II. Materials and Methods

Reagents

n-Dodecyl-β-D-maltopyranoside (DDM) was purchased from Anatrace (catalog # D310). n-Octyl-β-D-glucopyranoside (OG) was purchased from EMD Millipore (catalog # 494459). Triton X-100 was purchased from Fisher Scientific (catalog # BP151-500). MES was purchased from Fisher Scientific (catalog # BP300-100). DTT was purchased from Promega (catalog # V3151). Anti-FLAG® M2 Affinity Gel (catalog # A2220), and 3X FLAG® peptide (catalog # F4799) were purchased from Millipore Sigma. Pierce High Capacity Streptavidin Beads were purchased from Thermo Scientific (catalog # 20361). NBD-palmitoyl-CoA and NBD-palmitic acid were obtained from Avanti Polar Lipids. Biotinylated Shh peptides (CGPGRGFGKR-(PEG2)-K(Biotin)-NH2) and (AGPGRGFGKR-(PEG2)-K(Biotin)-NH2) were synthesized by Anaspec and Peptide 2.0.

Hhat Purification

Hhat was purified as reported previously (Buglino and Resh 2008; Asciolla, Rajanala, and Resh 2019), with a few modifications. 100mm plates of 85% confluent HEK293FT cells were transfected with triple tagged (HA-FLAG-His) WT Hhat in pcDNA3.1 or an empty pcDNA3.1 vector (6µg DNA, 15µL Lipofectamine 2000 Transfection Reagent [Invitrogen catalog # 11668019], and 1mL Opti-MEM media [Gibco catalog # 31985070] per plate). 18-24 hours post-transfection, cells were split 1:2, then incubated for an additional 24 hours. Cells were collected in ice-cold STE buffer by gentle scraping, pelleted by centrifugation at 1000 × *g* for 10 minutes, then washed with ice-cold STE buffer. Cell pellets were resuspended in ice-cold hypotonic lysis buffer (10mM HEPES, pH 7.3 and 0.2mM MgCl2) and incubated on ice for 15 minutes. Cells were lysed by 30 up/down strokes in a Dounce homogenizer on ice, sucrose was added to a final

concentration of 0.25mM, and membranes were pelleted by ultracentrifugation at 100,000 × *g* for 45 minutes (4°C) in a Beckman Ti-70.1 fixed angle rotor. After centrifugation, the supernatant was discarded, and the membrane pellets were resuspended by Dounce homogenization in hypotonic lysis buffer supplemented with 0.25mM sucrose on ice and pelleted by ultracentrifugation as above. Membrane pellets were resuspended in ice-cold solubilization buffer (20 mM HEPES, pH 7.5, 350 mM NaCl, 1% [v/v] glycerol, and 1% [w/v] DDM) in a Dounce homogenizer on ice and solubilized by rocking for 1 hour at 4˚C. Ultracentrifugation as above was repeated to pellet the insoluble material, which was subsequently discarded. Anti-FLAG® M2 Affinity Gel, which had been washed twice and resuspended in solubilization buffer, was added to the detergent-solubilized membranes, and the mixture was rocked overnight at 4°C. The next morning, the FLAG® M2 beads were pelleted by centrifugation at 1000 × *g* for two minutes and washed four times with solubilization buffer. Elution buffer (solubilization buffer supplemented with 150µg/mL 3X FLAG® peptide) was added and tubes were rocked at 4˚C for two hours. Beads were pelleted by centrifugation at 1000 × *g* for two minutes, and eluate was collected from each tube. This elution process was repeated twice with decreasing volumes of elution buffer, and repeated eluates were combined. Protein concentrations were calculated using an extinction coefficient for Hhat of 187,085 $cm^{-1}M^{-1}$ and absorbance read at 280nm (empty vector eluate was used as the blank).

In Vitro *Hhat Assay*

NBD-palmitoyl-CoA, biotinylated Shh peptide, purified Hhat (typically 130nM), and reaction buffer (final concentrations of 142mM MES, pH 6.5, 0.07% [w/v] OG, and 850µM DTT) in a volume of 100µL were added at the indicated concentrations to 0.5mL tubes at room temperature. Reactions were initiated by addition of Hhat, and tubes were

incubated in the dark at 37°C for the indicated amount of time. Reactions were quenched by placement of tubes on ice, followed by addition of a 60µL cold suspension of Pierce High Capacity Streptavidin Beads in wash buffer (167mM MES, pH 6.5 and 0.083% [v/v] Triton X-100). Tubes were rocked in the dark at 4°C for 1 hour. Beads were centrifuged at 2700 × *g*, 4°C in a microcentrifuge for 1 minute, then washed three times with 100µL wash buffer. After the final wash, beads were transferred in 60µL wash buffer to wells of a black side, clear bottom 96-well plate (Thermo Scientific catalog # 265301), and fluorescence was read in a BioTek Synergy H1 plate reader at emission/excitation wavelengths of 465/535 nm using Gen5 2.09 software. All assays were performed at least twice in duplicate. For determination of the stoichiometry of palmitoylation, reactions contained 10µM Shh peptide and 10µM NBD-palmitoyl-CoA, and were incubated at 37°C for 90 minutes. This experiment was performed twice in duplicate, and the reported error is SD.

Hhat Kinetic Analysis

Kinetic analysis was carried out by *in vitro* fatty acylation assays performed as described above, with a 10-minute reaction incubation period. Background RFU values from matched reactions containing elution buffer instead of Hhat were subtracted for each assay condition. The initial rate of Hhat-mediated NBD-acylation of Shh was quantified as pmol NBD-acylated Shh per minute per pmol Hhat and reported in (min^{-1}). Assays were performed at least twice in duplicate. Titration data were graphed in GraphPad Prism 9 software. Data from substrate titrations performed in the presence of various fixed concentrations of co-substrate were fit to the Michaelis-Menten model ($V = V_{max}[S]/(K_m + [S])$), from which apparent K_m and k_{cat} values were derived. Lineweaver-Burk plots ($1/V = K_m/V_{max}[S] + 1/V_{max}$) were generated via transformation of titration data to double-reciprocal values and simple linear regression analysis.

III. Results

Development of a direct, fluorescent assay to measure Hhat activity

I sought to develop a direct, fluorescent assay to measure the acyltransferase activity of Hhat (Figure 5a). The assay utilizes a reaction mix containing purified Hhat (Buglino and Resh 2008; Asciolla, Rajanala, and Resh 2019), a biotinylated Shh peptide containing 10 N-terminal amino acids sufficient for fatty acylation (Petrova et al. 2013), and NBD-palmitoyl-CoA, a fluorescent analog of palmitoyl-CoA that serves as a substrate for other fatty acyltransferases (Asciolla and Resh 2019; Rojas et al. 2016; McFie et al. 2011; Rana et al. 2018; Verardi et al. 2017). Following incubation, the biotinylated Shh peptide was captured on streptavidin-coated agarose beads, and fluorescence intensity of the NBD-palmitoylated Shh product was quantified. Palmitoylation of Shh occurred in a time, temperature, and enzyme -dependent manner (Figure 5b,c), and a stoichiometry of 0.99 ± 0.05 mol palmitate/mol Shh peptide was achieved. Substitution of the N-terminal cysteine on the Shh peptide with alanine, or blockage with N-acetylation, reduced the fluorescent signal to background, as did use of a free fatty acid (NBD-palmitic acid) instead of NBD-palmitoyl-CoA (Figure 5d). Hhat activity was also strongly reduced when the enzyme was heat-inactivated (Figure 5d), or when a small molecule Hhat inhibitor, RU-SKI 201 (Figure 6d) (Resh et al. 2016), was included in the reaction (Figure 6e,f). Hhat-mediated Shh palmitoylation obeyed Michaelis-Menten kinetics (Figure 5e,f), with apparent kinetic values similar to those reported previously (Jiang, Benz, and Long 2021).

Figure 5. *In vitro* assay for Hhat-mediated Shh fatty acylation

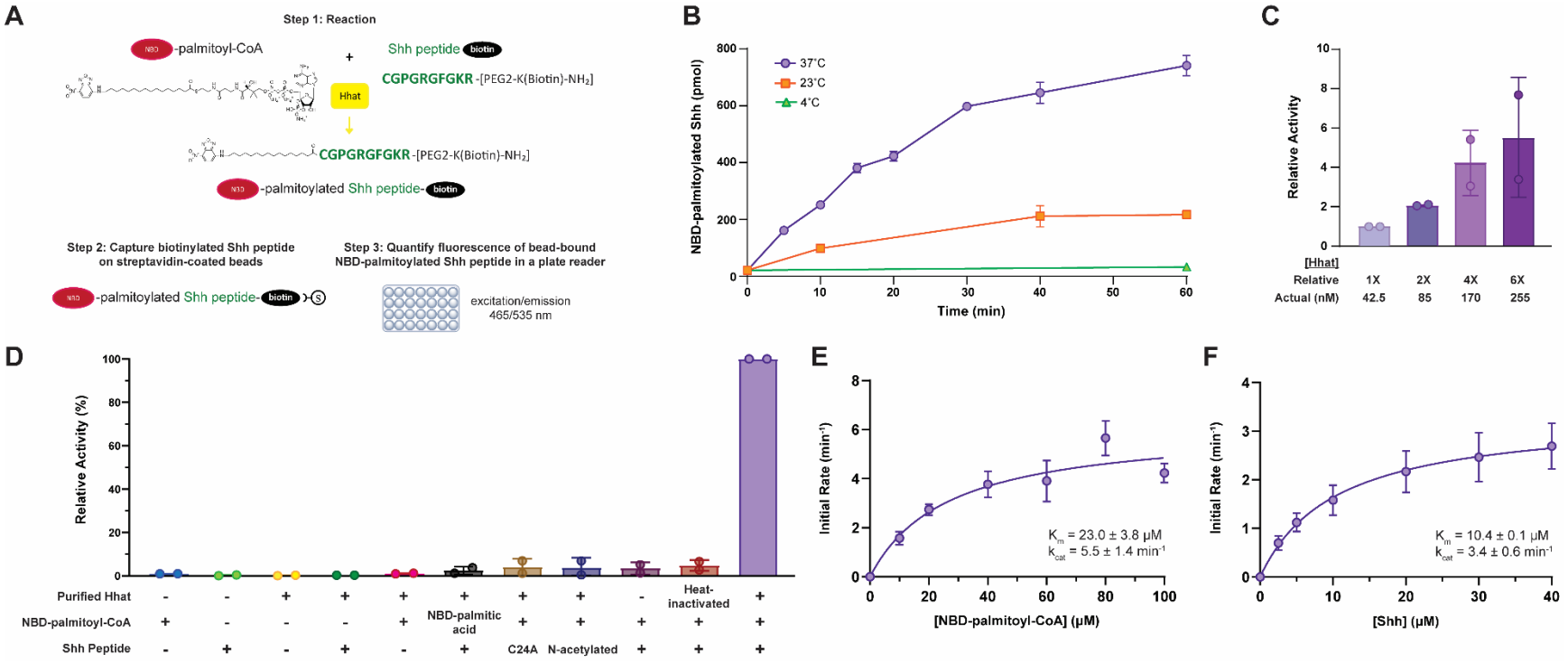

A, Assay schematic. ***B***, 25μM NBD-palmitoyl-CoA and 25μM WT Shh peptide were incubated with purified Hhat as indicated. NBD-palmitoylated Shh was quantified, with subtraction of background fluorescence from the average of duplicate 60-minute reactions containing elution buffer instead of Hhat. This experiment was performed at least twice (n≥2) in duplicate. A representative graph is shown. Data points represent the average of duplicate reactions ± SD. ***C***, 25μM NBD-palmitoyl-CoA and 25μM WT Shh peptide were

incubated with the indicated concentrations of purified Hhat at 37°C for 10 minutes. NBD-palmitoylated Shh was quantified, with subtraction of background fluorescence from the average of duplicate reactions containing elution buffer instead of 255nM Hhat. Data were normalized to that of the reactions with 42.5nM Hhat. This experiment was performed at least twice (n≥2) in duplicate. Data represent the average of two experiments ± SD. ***D***, Reactions containing elution buffer or purified Hhat (untreated or heat-inactivated at 95°C for 10 minutes), 10μM NBD-palmitoyl-CoA or NBD-palmitic acid, and/or 10μM WT, C24A, or N-acetylated Shh peptide were incubated for 40 minutes at 37°C. NBD-palmitoylated Shh was quantified, and data were normalized to that of the standard reaction. Each reaction condition was assayed at least twice (n≥2) in duplicate. Data represent the average of two assays ± SD. ***E***, Increasing concentrations of NBD-palmitoyl-CoA were incubated with 25μM WT Shh peptide and purified Hhat or elution buffer for 10 minutes at 37°C. The initial rate of Hhat-mediated NBD-palmitoylation of Shh was quantified; Michaelis-Menten fit of the data is shown with apparent kinetic parameters as insets. Data points represent the average of at least two experiments (n≥2) performed in duplicate, ± SD. ***F***, As in *E,* except WT Shh peptide was titrated in the presence of 25μM NBD-palmitoyl-CoA.

Kinetic mechanism of Hhat catalysis

Bi-substrate enzyme reactions typically proceed through one of two mechanisms (Segel 1975). In a non-sequential (ping-pong) reaction, one substrate binds, an enzyme-intermediate is formed, and the first product is simultaneously released. The second substrate then binds, and the second product is formed and released. Alternatively, in a sequential reaction, both substrates need to be bound to the enzyme in a ternary complex in order for catalysis to occur, resulting in simultaneous generation of both products. In both cases, the enzyme's affinity for its substrates and/or maximal turnover rate can change with increasing concentrations of one fixed substrate, until saturating concentrations of the fixed substrate are reached. Sequential vs. non-sequential kinetic mechanisms can be distinguished by titrating one substrate in the presence of increasing, non-saturating concentrations of the second substrate. In Lineweaver-Burk plots of 1/V vs. 1/[S], intersecting lines indicate a sequential reaction, whereas parallel lines indicate a non-sequential reaction (Table 4). As depicted in Figure 6a,b, intersecting lines were observed when Shh was titrated in the presence of increasing concentrations of NBD-palmitoyl-CoA, and vice versa. These findings rule out a ping-pong mechanism, and suggest that the kinetic mechanism of Hhat-mediated acylation of Shh is sequential and involves the formation of a ternary complex.

Table 4. Differentiating features of Lineweaver-Burk plots for Hhat kinetic mechanism

<table>
<tr><th></th><th>Non-sequential</th><th>Random sequential</th><th>Ordered sequential: Palmitoyl-CoA binds before Shh</th><th>Ordered sequential: Shh binds before palmitoyl-CoA</th></tr>
<tr><td colspan="5">Differentiating a non-sequential vs. random or ordered sequential reaction</td></tr>
<tr><td>Titrating palmitoyl-CoA in the presence of various [fixed Shh]</td><td>Parallel lines</td><td>Intersecting lines to the left of the Y-axis</td><td>Intersecting lines to the left of the Y-axis, above or below the X-axis</td><td>Intersecting lines on the Y-axis</td></tr>
<tr><td>Titrating Shh in the presence of various [fixed palm-CoA]</td><td>Parallel lines</td><td>Intersecting lines to the left of the Y-axis</td><td>Intersecting lines on the Y-axis</td><td>Intersecting lines to the left of the Y-axis, above or below the X-axis</td></tr>
<tr><td colspan="5">Differentiating a random vs. ordered sequential reaction using an Hhat inhibitor competitive with palmitoyl-CoA</td></tr>
<tr><td>Titrating palmitoyl-CoA in the presence of various [fixed inhibitor]</td><td rowspan="2"></td><td colspan="3">Intersecting lines on the Y-axis</td></tr>
<tr><td>Titrating Shh in the presence of various [fixed inhibitor]</td><td>Intersecting lines to the left of the Y-axis</td><td>Intersecting lines on the Y-axis</td><td>Parallel lines</td></tr>
</table>

Adapted from Table VI-1 of Segel, Irwin H. 1975. Enzyme kinetics: behavior and analysis of rapid equilibrium and steady state enzyme systems (Wiley: New York).

Figure 6. Kinetic mechanism of Hhat

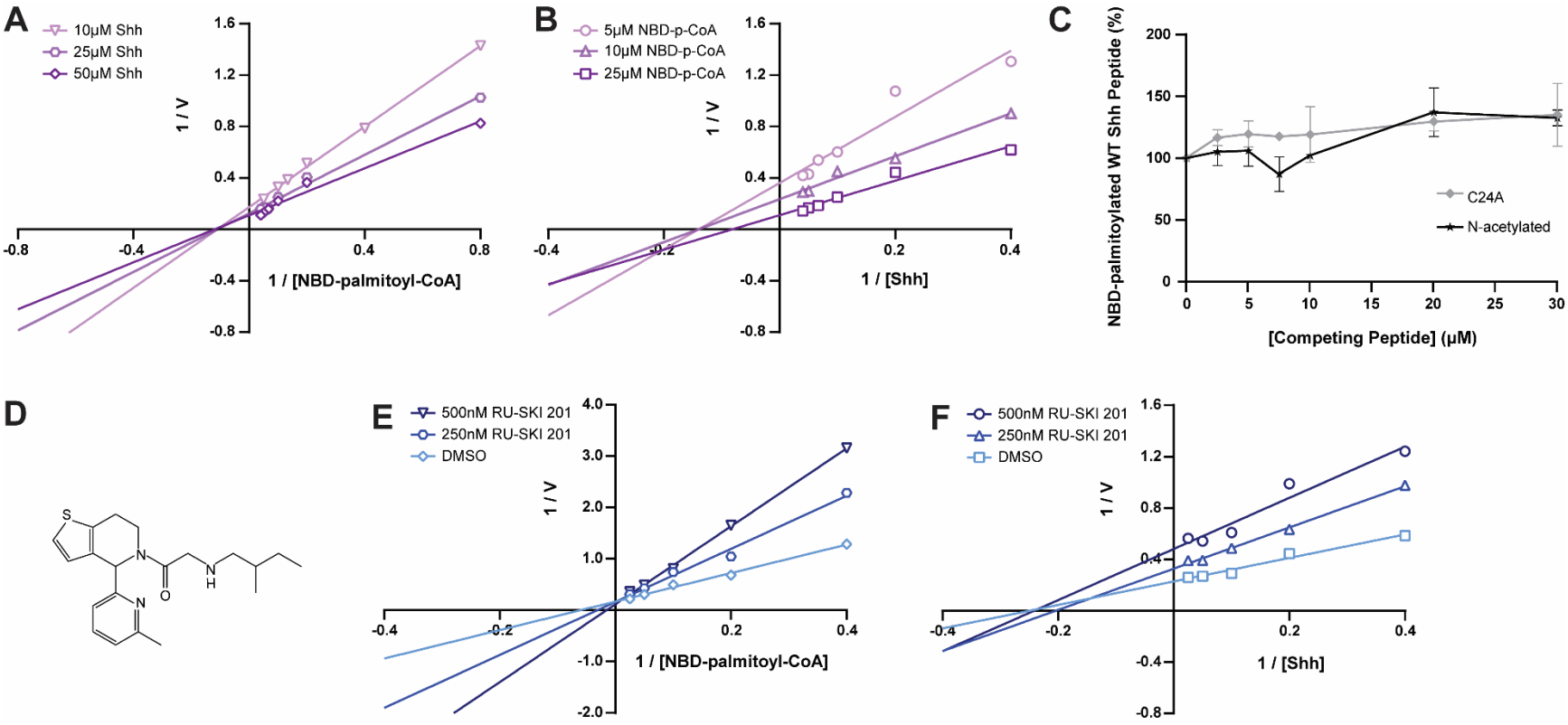

A, Increasing concentrations of NBD-palmitoyl-CoA were incubated with purified Hhat or elution buffer and the indicated concentrations of WT Shh peptide for 10 minutes at 37°C. The initial rate of Hhat-mediated NBD-palmitoylation of Shh was quantified; a Lineweaver-Burk plot of the data is shown. Each line contains the average data points from at least two titrations (n≥2)

performed in duplicate. ***B***, As in *A*, except WT Shh peptide was titrated in the presence of the indicated concentrations of NBD-palmitoyl-CoA. ***C***, Purified Hhat, 10μM NBD-palmitoyl-CoA, and 10μM WT Shh peptide were incubated with increasing concentrations of N-acetylated and C24A Shh peptides for 10 minutes at 37°C. NBD-palmitoylated Shh was quantified, and data were normalized to the amount of NBD-palmitoylated Shh when no competing peptide was present. This experiment was performed twice (n=2) in duplicate. Data points represent the average of two experiments ± SD. ***D***, Chemical structure of RU-SKI 201. ***E***, Increasing concentrations of NBD-palmitoyl-CoA were incubated with 10μM WT Shh peptide, purified Hhat or elution buffer, and 0 (DMSO), 250, and 500nM RU-SKI 201 for 10 minutes at 37°C. The initial rate of Hhat-mediated NBD-palmitoylation of Shh was quantified; a Lineweaver-Burk plot of the data is shown. Each titration was performed at least twice (n≥2) in duplicate. A representative graph is shown. ***F***, As in *E*, except WT Shh peptide was titrated in the presence of 0 (DMSO), 250, and 500nM RU-SKI 201. Each line contains the average data points from two titrations (n=2) performed in duplicate.

Sequential reactions can occur in a random fashion, in which either substrate can bind before the other, or in an ordered fashion, in which one substrate is required to bind first in order for the second substrate to bind. Random vs. ordered sequential reactions can be differentiated with Lineweaver-Burk plots from the substrate titrations performed above (Figure 6a,b, Table 4). In a random reaction, the Lineweaver-Burk plots for both titrations will yield intersecting lines to the left of the Y-axis. In an ordered reaction, the Lineweaver-Burk plot for titration of the second substrate in the presence of increasing concentrations of the obligate first substrate will yield intersecting lines along the Y-axis. Lineweaver-Burk plots titrating NBD-palmitoyl-CoA or Shh in the presence of increasing concentrations of the other yielded intersecting lines to the left of the Y-axis (Figure 6a,b), indicative of a random sequential reaction (Table 4).

To confirm this finding, I implemented an additional approach. Titration of one substrate with various fixed concentrations of a dead-end inhibitor competitive with the other substrate will yield patterns of lines in Lineweaver-Burk plots that indicate whether the reaction is random or ordered (Segel 1975). To identify a competitive, dead-end Hhat inhibitor, I first investigated potential inhibitory properties of the N-acetylated and C24A Shh peptides. However, these peptides were neither substrates (Figure 5d) nor inhibitors (Figure 6c) of Hhat. I then tested RU-SKI 201 (Figure 6d) for potential competition with palmitoyl-CoA. Titration of palmitoyl-CoA in the presence of various fixed concentrations of RU-SKI 201 produced intersecting lines on the Y-axis of a Lineweaver-Burk plot (Figure 6e), indicative of a competitive inhibition profile. Of note, a derivative of RU-SKI 201, IMP-1575, was found to inhibit Hhat by competing with palmitoyl-CoA binding (Lanyon-Hogg et al. 2021; Coupland et al. 2021). When Shh was titrated in the presence of various fixed concentrations of RU-SKI 201, intersecting lines to the left of the Y-axis were observed (Figure 6f), ruling out a mechanism whereby

either substrate is required to bind first, and confirming a random sequential kinetic mechanism (Table 4).

IV. Discussion

Development of a direct, fluorescent assay to measure Hhat activity

In this study, I used a fluorescence-based assay to perform extensive and previously unpursued kinetic analyses with purified Hhat. For many years, the Resh laboratory relied on the use of radioactive palmitoyl-CoA analogs to assay Hhat, but safety considerations, cost effectiveness, and the nuisance of radioactive waste disposal prompted a switch to an alternative, less hazardous assay. NBD-palmitoyl-CoA has been used as a substrate in studies by the Resh laboratory and others for fatty acyltransferases including Hhat, DHHC17, DHHC20, and DGAT1 (Asciolla and Resh 2019; Rojas et al. 2016; McFie et al. 2011; Rana et al. 2018; Verardi et al. 2017; Zhang et al. 2022). The NBD fluorophore is located at the end of the fatty acyl tail (Figure 7a), farthest away from Hhat residues that have been shown to mediate catalysis at the CoA-acyl chain junction (Coupland et al. 2021; Jiang, Benz, and Long 2021). An N-terminal Shh peptide containing a C-terminal biotin served as the Shh recipient substrate, and has also been used previously by the Resh laboratory and others in Hhat activity assays (Buglino and Resh 2008; Lanyon-Hogg et al. 2015; Jiang, Benz, and Long 2021; Petrova et al. 2013). Incubation of these two substrates with purified Hhat resulted in a robust and reproducible assay. Moreover, kinetic data obtained with NBD-palmitoyl-CoA and the Shh peptide (Figure 5e,f) were in good agreement with those obtained with [^{3}H]-palmitoyl-CoA and a similar Shh peptide (Jiang, Benz, and Long 2021). Importantly, the

presence of an NBD group did not shield apparent kinetic differences for Hhat among fatty acyl-CoAs with differing acyl chains (Figure 7a, 8, Table 5).

Kinetic mechanism of Hhat catalysis

To my knowledge, the kinetic mechanism of any MBOAT, including Hhat, has not been determined to date. Hhat binds Shh in the lumenal leaflet of the ER membrane, and palmitoyl-CoA in the cytoplasmic leaflet (Jiang, Benz, and Long 2021; Coupland et al. 2021), suggesting that binding of the two substrates might be independent. Here I show that Hhat palmitoylates Shh via a random sequential mechanism, in which Shh and palmitoyl-CoA bind in no obligate order to form a ternary complex with Hhat. This is consistent with evidence in the literature that Hhat can bind palmitoyl-CoA in the absence of Shh (Asciolla and Resh 2019), and that Hhat can bind Shh in the absence of palmitoyl-CoA (Coupland et al. 2021). In binding assays, the latter study also found that binding of Shh to Hhat was three times higher in the presence of palmitoyl-CoA, indicating that palmitoyl-CoA binding enhances Shh binding. However, under my assay conditions, the observed patterns in Lineweaver-Burk plots (namely, the intersection point of the lines was not above the X-axis (Figure 6a,b)) were indicative of lack of positive cooperativity (Segel 1975), suggesting that neither substrate enhanced the binding of the other.

It is interesting to compare the mechanism of Hhat-mediated palmitoylation with that of DHHC acyltransferases, the other major family of palmitoyl transferases, for which the kinetic mechanism is known. DHHC acyltransferases are broadly thought to catalyze a two-step, ping-pong reaction, involving the formation of an acyl-enzyme intermediate. Incubation of DHHC2, DHHC3, and Erf2 with palmitoyl-CoA but no protein

substrate results in autoacylation of the enzymes (Jennings and Linder 2012; Mitchell et al. 2010), and single turnover assays demonstrate transfer of a radiolabeled fatty acyl group from DHHC2 and DHHC3 to a protein substrate (Jennings and Linder 2012). However, not all DHHC enzymes necessarily employ this kinetic mechanism (Gottlieb and Linder 2017; Gonzalez Montoro, Chumpen Ramirez, and Valdez Taubas 2015). Swf1 and Pfa4 are two yeast DHHC proteins that are not autoacylated, and retain at least partial palmitoyltransferase activity when the DHHC cysteine is mutated to alanine or arginine (Gonzalez Montoro, Chumpen Ramirez, and Valdez Taubas 2015). One possibility to explain these results is that in some DHHCs, a sequential reaction might occur, involving direct nucleophilic attack of the sulfhydryl group of the protein substrate's cysteine acceptor on palmitoyl-CoA, promoted by the first histidine of the DHHC motif (Gonzalez Montoro, Chumpen Ramirez, and Valdez Taubas 2015).

An important, unresolved question regarding Shh acylation is whether Hhat directly N-acylates the N-terminal cysteine, or whether catalysis proceeds via initial S-acylation of the cysteine sulfhydryl, followed by an intramolecular S-to-N shift. Direct amide linkage is favored by Hhat structural analysis, whereby Asp-339 is proposed to serve as a base to activate the N-terminal amine for nucleophilic attack of the carbonyl carbon of the palmitoyl-CoA molecule (Jiang, Benz, and Long 2021). To investigate this question biochemically, I tested the ability of Hhat to transfer NBD-palmitate to a Shh peptide with a blocked, N-acetylated N-terminus. The peptide does not serve as an Hhat substrate (Figure 5d), despite the presence of a free sulfhydryl group on the N-terminal cysteine. This confirms results previously obtained using a radioactivity-based Hhat assay (Buglino and Resh 2008). However, the N-acetylated Shh peptide does not inhibit Hhat-mediated catalysis with the WT peptide (Figure 6c), implying that the N-acetylated

peptide does not bind to the enzyme. Thus, this peptide cannot necessarily distinguish between a direct, one-step mechanism for N-acylation and a two-step, S-to-N shift.

Chapter Three: Differential fatty acylation of Shh

Data and text from this chapter have been previously published in Schonbrun, A.R., and M.D. Resh. 2022. 'Hedgehog acyltransferase catalyzes a random sequential reaction and utilizes multiple fatty acyl-CoA substrates', *Journal of Biological Chemistry,* 298(10): 102422.

I. Introduction

An unresolved aspect of Hhat biology concerns fatty acyl-CoA substrate specificity. Palmitoyl-CoA is thought to be the primary acyl-CoA substrate for Hhat, yet fatty acids other than palmitate have been detected on Shh purified from mammalian cells, in some cases at even higher proportions than palmitate (Long et al. 2015; Pepinsky et al. 1998). The ability of Hhat to directly transfer fatty acids other than palmitate to Shh has not been reported. The fatty acid selectivity of Hhat is important because it has the potential to play a critical role in Shh signaling. When different fatty acids and hydrophobic groups are artificially attached to Shh by non-enzymatic, *in vitro* acylation, the strength of Shh signaling output increases with increasing hydrophobicity and fatty acid chain length (Taylor et al. 2001; Baker, Taylor, and Pepinsky 2007). However, investigation of the effect of unsaturation on signaling through fatty acylated Shh has been limited and indirect; only one study showed that Shh isolated from chick limb buds exhibits reduced signaling activity when the explants are incubated with palmitoleate compared to palmitate (Long et al. 2015). To address these issues, I used my *in vitro* Shh palmitoylation assay to investigate Hhat's substrate specificity, and I also

explored the consequences of differential fatty acylation on Shh signaling directly in cells.

II. Materials and methods

Reagents

DDM was purchased from Anatrace (catalog # D310). OG was purchased from EMD Millipore (catalog # 494459). Triton X-100 was purchased from Fisher Scientific (catalog # BP151-500). MES was purchased from Fisher Scientific (catalog # BP300-100). DTT was purchased from Promega (catalog # V3151). Anti-FLAG® M2 Affinity Gel (catalog # A2220), and 3X FLAG® peptide (catalog # F4799) were purchased from Millipore Sigma. Pierce™ High Capacity Streptavidin Beads were purchased from Thermo Scientific (catalog # 20361). Antibodies were purchased as follows: rabbit α-HA (Sigma, catalog #H6908), mouse α-Shh E-1 (Santa Cruz, catalog # sc-365112), ECL™ donkey anti-rabbit IgG, horseradish peroxidase linked whole antibody (Cytiva, catalog # NA934), ECL™ sheep anti-mouse IgG, horseradish peroxidase linked whole antibody (Cytiva, catalog # NA931). NBD-palmitoyl-CoA, NBD-oleoyl-CoA, and NBD-palmitic acid were obtained from Avanti Polar Lipids. NBD-myristoyl-CoA and NBD-palmitoleoyl-CoA were synthesized by the Memorial Sloan Kettering Organic Synthesis Core Lab. Biotinylated Shh peptides (CGPGRGFGKR-(PEG2)-K(Biotin)-NH_2) and (AGPGRGFGKR-(PEG2)-K(Biotin)-NH_2) were synthesized by Anaspec and Peptide 2.0.

Cell Culture

HEK293FT cells were cultured at 37˚C in Dulbecco's Modified Eagle Medium (4500 g/L glucose, 1% Penicillin, 1% Streptomycin) containing 1X Glutamax, 1mM sodium

pyruvate, 1X MEM Non-Essential Amino Acids Solution, 10% fetal bovine serum, 0.5g/L geneticin (G418). Shh Light II cells were cultured at 37˚C in Dulbecco's Modified Eagle Medium (as above) with 10% calf serum, 1X Glutamax, 0.4 g/L G418, and 0.15 g/L zeocin. Glutamax (catalog # 35050061), sodium pyruvate (catalog # 11360070), and 1X MEM Non-Essential Amino Acids Solution (catalog # 11140050) were purchased from Gibco.

Hhat Purification

Hhat was purified as reported previously (Buglino and Resh 2008; Asciolla, Rajanala, and Resh 2019), with a few modifications. 100mm plates of 85% confluent HEK293FT cells were transfected with triple tagged (HA-FLAG-His) WT Hhat in pcDNA3.1 or an empty pcDNA3.1 vector (6µg DNA, 15µL Lipofectamine 2000 Transfection Reagent [Invitrogen catalog # 11668019], and 1mL Opti-MEM media [Gibco catalog # 31985070] per plate). 18-24 hours post-transfection, cells were split 1:2, then incubated for an additional 24 hours. Cells were collected in ice-cold STE buffer by gentle scraping, pelleted by centrifugation at 1000 × *g* for 10 minutes, then washed with ice-cold STE buffer. Cell pellets were resuspended in ice-cold hypotonic lysis buffer (10mM HEPES, pH 7.3 and 0.2mM $MgCl_2$) and incubated on ice for 15 minutes. Cells were lysed by 30 up/down strokes in a Dounce homogenizer on ice, sucrose was added to a final concentration of 0.25mM, and membranes were pelleted by ultracentrifugation at 100,000 × *g* for 45 minutes (4°C) in a Beckman Ti-70.1 fixed angle rotor. After centrifugation, the supernatant was discarded, and the membrane pellets were resuspended by Dounce homogenization in hypotonic lysis buffer supplemented with 0.25mM sucrose on ice and pelleted by ultracentrifugation as above. Membrane pellets were resuspended in ice-cold solubilization buffer (20 mM HEPES, pH 7.5, 350 mM NaCl, 1% [v/v] glycerol, and 1% [w/v] DDM) in a Dounce homogenizer on ice and

solubilized by rocking for 1 hour at 4˚C. Ultracentrifugation as above was repeated to pellet the insoluble material, which was subsequently discarded. Anti-FLAG® M2 Affinity Gel, which had been washed twice and resuspended in solubilization buffer, was added to the detergent-solubilized membranes, and the mixture was rocked overnight at 4°C. The next morning, the FLAG® M2 beads were pelleted by centrifugation at 1000 × *g* for two minutes and washed four times with solubilization buffer. Elution buffer (solubilization buffer supplemented with 150µg/mL 3X FLAG® peptide) was added and tubes were rocked at 4˚C for two hours. Beads were pelleted by centrifugation at 1000 × *g* for two minutes, and eluate was collected from each tube. This elution process was repeated twice with decreasing volumes of elution buffer, and repeated eluates were combined. Protein concentrations were calculated using an extinction coefficient for Hhat of 187,085 $cm^{-1}M^{-1}$ and absorbance read at 280nm (empty vector eluate was used as the blank).

In Vitro Hhat Assay

NBD-acyl-CoA, biotinylated Shh peptide, purified Hhat (typically 130nM), and reaction buffer (final concentrations of 142mM MES, pH 6.5, 0.07% [w/v] OG, and 850µM DTT) in a volume of 100µL were added at the indicated concentrations to 0.5mL tubes at room temperature. Reactions were initiated by addition of Hhat, and tubes were incubated in the dark at 37°C for the indicated amount of time. Reactions were quenched by placement of tubes on ice, followed by addition of a 60µL cold suspension of Pierce™ High Capacity Streptavidin Beads in wash buffer (167mM MES, pH 6.5 and 0.083% [v/v] Triton X-100). Tubes were rocked in the dark at 4°C for 1 hour. Beads were centrifuged at 2700 × *g*, 4°C in a microcentrifuge for 1 minute, then washed three times with 100µL wash buffer. After the final wash, beads were transferred in 60µL wash buffer to wells of a black side, clear bottom 96-well plate (Thermo Scientific catalog # 265301), and

fluorescence was read in a BioTek Synergy H1 plate reader at emission/excitation wavelengths of 465/535 nm using Gen5 2.09 software. All assays were performed at least twice in duplicate.

NBD-Fatty Acylation of Shh Protein

Recombinant, 19 kDa Shh protein (Cys24-Gly197), purified from *E. coli* as described previously (Asciolla, Rajanala, and Resh 2019; Buglino and Resh 2008), was incubated for 1 hour with reaction buffer, purified Hhat, and individual NBD-acyl-CoAs in the reaction conditions described above. Immediately following the reaction, sample buffer was added, samples were boiled at 95˚C for five minutes, and 32% (volume) of each sample was subjected to electrophoresis in 15% polyacrylamide gels. In-gel NBD fluorescence was detected on a Typhoon™ FLA 9500 Imager using a 473nm laser and excitation/emission settings of 495/519 nm. For subsequent Western blotting analyses, proteins were transferred from the gel to PVDF, the membrane was blocked with 5% [w/v] non-fat, dry milk in TBST (20 mM Tris, 150 mM NaCl, 0.1% [v/v] Tween-20) for 10 minutes, then incubated overnight at 4°C with primary antibodies (for Hhat, 1:1000 rabbit α-HA; for Shh, 1:200 mouse α-Shh E-1) in TBST, 5% [w/v] non-fat, dry milk. The next day, blots were washed three times for five minutes with TBST, then incubated at room temperature for 1.5 hours with a 1:2500 dilution of the appropriate (anti-rabbit or anti-mouse) horseradish peroxidase-conjugated secondary antibody in TBST, 5% [w/v] non-fat, dry milk. Blots were washed three times for five minutes with TBST, developed with Pierce ECL Western Blotting Substrate (ThermoFisher catalog #32209), and imaged on a ChemiDoc Gel Imaging System (BioRad). Relative band intensities were quantified using ImageJ software. NBD-fatty acylated Shh band intensities were normalized to Shh band intensities on the Western blot. This experiment was performed four times.

Hhat Kinetic Analysis

Kinetic analysis was carried out by *in vitro* fatty acylation assays performed as described above, with a 10-minute reaction incubation period. Background RFU values from matched reactions containing elution buffer instead of Hhat were subtracted for each assay condition. The initial rate of Hhat-mediated NBD-acylation of Shh was quantified as pmol NBD-acylated Shh per minute per pmol Hhat and reported in min^{-1}. Assays were performed at least twice in duplicate. Titration data were graphed in GraphPad Prism 9 software. Data from substrate titrations performed in the presence of various fixed concentrations of co-substrate were fit to the Michaelis-Menten model ($V = V_{max}[S]/(K_m + [S])$), from which apparent K_m and k_{cat} values were derived.

Shh Signaling Assays

Approximately 100,000 Shh Light II cells per well were seeded in white side, transparent bottom 96-well tissue culture plates (Corning Costar catalog # 3610) and cultured until confluent. 40µM recombinant, 19 kDa Shh protein (Cys24-Gly197) purified from *E. coli* (Asciolla, Rajanala, and Resh 2019; Buglino and Resh 2008) was incubated with reaction buffer (final concentrations of 108mM MES, pH 6.5, 0.05% [w/v] OG, 645µM DTT), 200µM NBD-fatty acyl-CoA, and 170nM purified Hhat (or equal volume of elution buffer in Hhat-lacking reactions), in a total volume of 100µL at 37˚C for 2 hours. Reactions were quenched on ice. To quantify the relative amount of NBD-fatty acylated Shh in each sample, 30% (volume) of each reaction was mixed with sample buffer, incubated at 95˚C for 5 minutes, then subjected to electrophoresis in 12% polyacrylamide gels (BioRad catalog # 4561044). Relative in-gel NBD fluorescence was detected and quantified as above, using average values from two gels/quantifications. Dilutions containing equal amounts of Shh protein from each reaction were prepared in

low-serum media (Dulbecco's Modified Eagle Medium, 4500 g/L glucose, 1% Penicillin, 1% Streptomycin, with 0.5% calf serum, 1X Glutamax, 0.4 g/L G418, and 0.15g/L zeocin). For control reactions lacking Shh protein, dilutions were prepared using the equivalent dilution factor to Shh-containing reactions. Media in the wells was replaced with 100µL of prepared reaction dilutions, and plates were incubated at 37˚C for ~42 hours. Cells were then lysed, and Firefly and *Renilla* luciferase activities were measured using the Promega Dual-Luciferase® Reporter Assay System (Promega catalog # E1980), according to the manufacturer's instructions. Titrations were performed two or three times (as indicated in the figure legend) in duplicate (two wells of cells per reaction dilution). The Firefly/*Renilla* luciferase ratio for each well was calculated, and data were normalized as indicated in the figure legend. Titration data were graphed using GraphPad Prism 9 software and fit to the curve [Agonist] vs. response (three parameters) ($Y = Bottom + X(Top - Bottom)/(EC_{50} + X)$), from which EC_{50} values were derived. This entire experiment was repeated and resulted in the same outcome.

III. Results

Fatty acyl-CoA substrate specificity of Hhat

The ability of Hhat to catalyze transfer of different fatty acids to Shh was investigated. Four NBD-labeled fatty acyl-CoAs were chosen: NBD-myristoyl-CoA (14:0), NBD-palmitoyl-CoA (16:0), NBD-palmitoleoyl-CoA (16:1 *cis*-Δ9), and NBD-oleoyl-CoA (18:1 *cis*-Δ9) (Figure 7a), the primary substrates of the fatty acyltransferases N-myristoyltransferase (NMT), DHHC acyltransferases, Porcn, and DGAT1/2 and ACAT1/2, respectively. I first examined fatty acid incorporation into Shh as the reaction approached completion. Similar overall amounts of myristate, palmitate, and

palmitoleate were transferred to the Shh peptide, but the amount of oleate transferred was significantly lower compared to myristate and palmitoleate (Figure 7b). Incorporation of all four NBD-labeled fatty acids was strongly and equally inhibited by RU-SKI 201 (Figure 7c). Hhat-mediated transfer of fatty acids to the recombinant, 19 kDa Shh protein was then examined by analyzing the reaction products via SDS-PAGE. The pattern of NBD-fatty acid incorporated into Shh protein was similar to that observed for the Shh peptide, with lowest incorporation of oleate into Shh and no other significant differences observed (Figure 7d).

Figure 7. Fatty acyl-CoA substrate specificity of Hhat

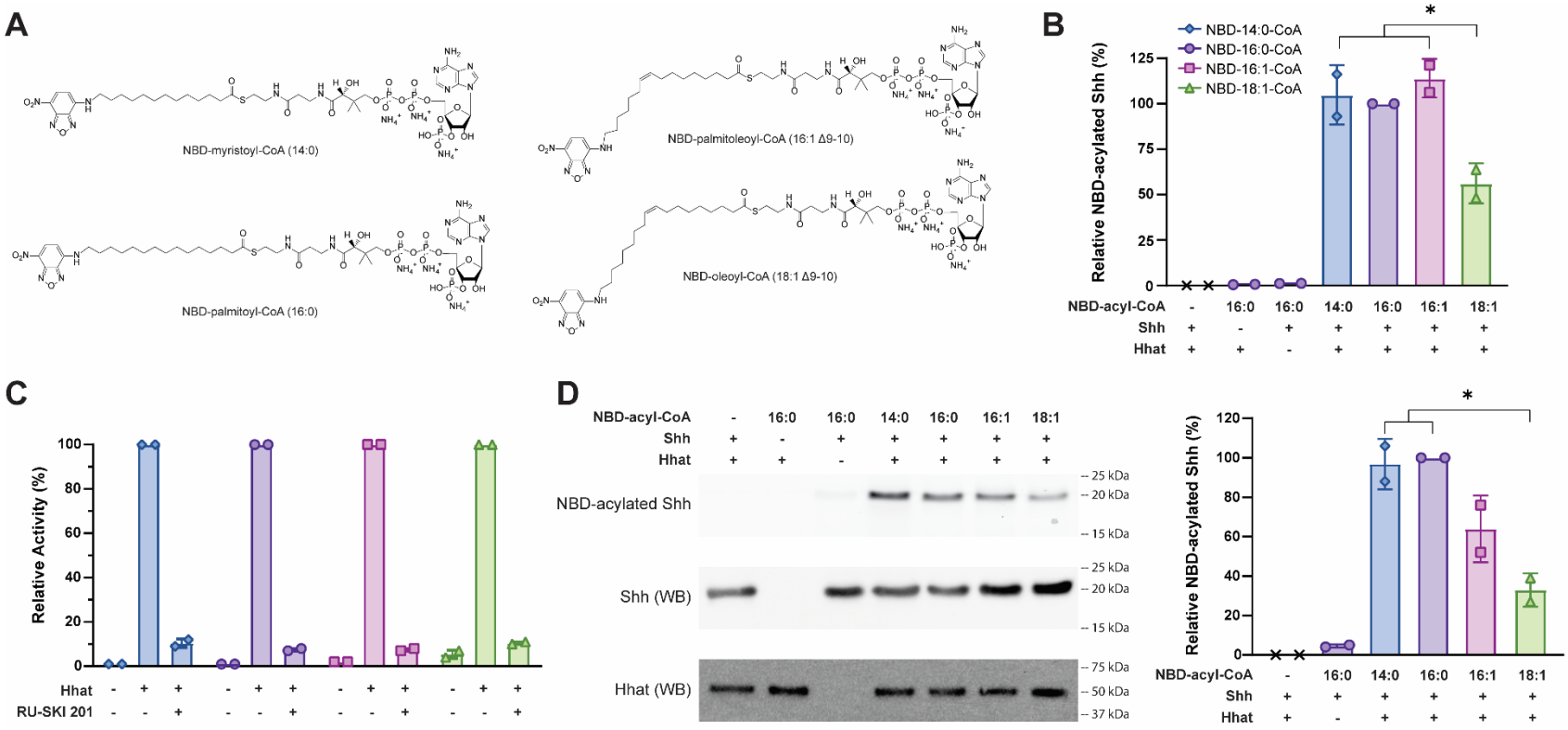

***A*,** Chemical structures of NBD-labeled fatty acyl-CoAs. ***B*,** Purified Hhat or elution buffer, 10µM NBD-fatty acyl-CoA, and/or 10µM WT Shh peptide were incubated for 1 hour at 37°C. NBD-fatty acylated Shh was quantified, and data were normalized to that of the NBD-palmitoyl-CoA reaction. Data represent the average of two experiments (n=2) performed in duplicate ± SD. Significant

differences are noted with an asterisk (* $p \leq 0.05$) and were determined via ordinary one-way ANOVA with Tukey's multiple comparisons test. ***C*****,** Purified Hhat or elution buffer, 10µM NBD-fatty acyl-CoA, and 10µM WT Shh peptide were incubated with or without 10µM RU-SKI 201 for 40 minutes at 37°C. NBD-fatty acylated Shh was quantified, and data were normalized to that of the untreated reaction for each NBD-fatty acyl-CoA. Data represent the average of two experiments (n=2) performed in duplicate ± SD. ***D*****,** Purified Hhat or elution buffer, 10µM NBD-acyl-CoA, and/or 10µM recombinant, 19 kDa Shh protein were incubated for 1 hour at 37°C, and samples were subjected to PAGE. NBD fluorescence was detected by fluorescent imaging, and Shh and Hhat proteins were detected by Western blot. This experiment was performed four times. NBD-fluorescence intensity values were normalized for levels of Shh in each sample. Data were normalized to that of the NBD-palmitoyl-CoA reaction. Data represent the average of two experiments ± SD. Significant differences are noted with an asterisk (* $p \leq 0.05$) and were determined via ordinary one-way ANOVA with Tukey's multiple comparisons test.

To further explore potential differences in fatty acyl-CoA substrate specificity, I employed initial rate studies for kinetic analysis of Hhat. Each of the four NBD-acyl-CoAs was titrated individually in the presence of the same fixed concentration of Shh peptide (Figure 8a), and vice versa (Figure 8e), and apparent K_m and k_{cat} values were determined (Figure 8b,c,f,g, Table 5). Titration of the NBD-acyl-CoAs yielded similar kinetic values for Hhat with all four fatty acyl-CoAs, with the exception of a higher turnover rate (k_{cat}) with myristoyl-CoA compared to palmitoleoyl-CoA and oleoyl-CoA (Figure 8b,c,d, Table 5). The catalytic efficiency (k_{cat}/K_m) of Hhat with each of the four NBD-acyl-CoAs was similar (Figure 8d, Table 5). Titration of Shh in the presence of the same fixed concentration of each NBD-acyl-CoA revealed similar turnover rates among all four NBD-acyl-CoAs (Figure 8f, Table 5). Hhat exhibited lower affinity (higher K_m) for Shh in the presence of oleoyl-CoA compared to the other three acyl-CoAs, but exhibited no significant differences in affinity for Shh among the other acyl-CoAs (Figure 8g, Table 5). The catalytic efficiency of Hhat with Shh was highest using palmitoleoyl-CoA, and higher using myristoyl-CoA compared to oleoyl-CoA (Figure 8h, Table 5). My data demonstrate that Hhat can transfer multiple types of fatty acids, both saturated and monounsaturated, to Shh with some varying preferences.

Figure 8. Kinetic analysis of Hhat fatty acyl-CoA substrate specificity

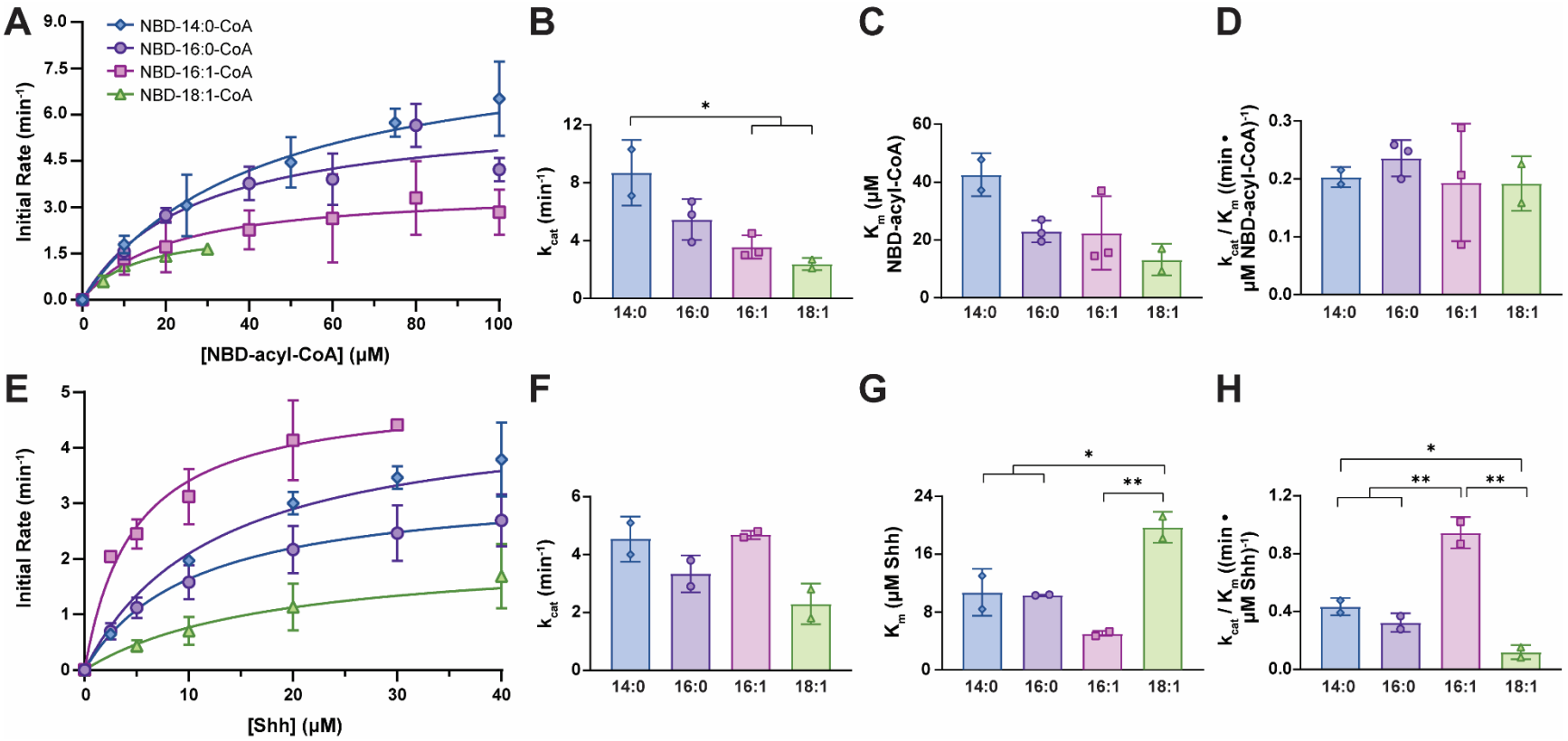

A, NBD-fatty acyl-CoAs were incubated with 25μM WT Shh peptide and purified Hhat or elution buffer for 10 minutes at 37°C. The initial rate of Hhat-mediated NBD-fatty acylation of Shh was quantified; Michaelis-Menten fit of the data is shown. Data obtained when NBD-oleoyl-CoA was titrated above 30μM did not continue to fit the Michaelis-Menten model, possibly due to alteration in

substrate accessibility conferred by a monomer-to-micelle transition (the critical micelle concentration of oleoyl-CoA is 32-33μM in phosphate buffer (Smith and Powell 1986; Constantinides and Steim 1985)). Data points from each curve represent the average of at least two titrations (n≥2) performed in duplicate, ± SD. ***B, C***, ***D***, Apparent kinetic values (*B*, k_{cat}; *C*, K_m; *D*, k_{cat}/K_m) for Hhat with the four NBD-acyl-CoAs were derived from the Michaelis-Menten fit of the data, and represent the averages (± SD) from at least two titrations (n≥2) performed in duplicate (per NBD-acyl-CoA). Significant differences are noted with asterisks (* $p \leq 0.05$, ** $p \leq 0.01$) and were determined via ordinary one-way ANOVA with Tukey's multiple comparisons test. ***E*****,** As in *A*, except WT Shh peptide was titrated in the presence of 25μM NBD-acyl-CoA. ***F, G, H***, As in *B, C*, *D*, respectively, except for titration with Shh.

Table 5. Hhat apparent kinetic parameters

Titrating NBD-acyl-CoA in the presence of 25μM Shh			
NBD-acyl-CoA	**k_{cat} (min^{-1})**	**K_m (μM NBD-acyl-CoA)**	**k_{cat}/K_m ($(min \cdot \mu M \text{ NBD-acyl-CoA})^{-1}$)**
Myristoyl (14:0)	8.7 ± 2.3	42.5 ± 7.5	0.20 ± 0.02
Palmitoyl (16:0)	5.5 ± 1.4	23.0 ± 3.8	0.24 ± 0.03
Palmitoleoyl (16:1)	3.6 ± 0.8	22.4 ± 12.7	0.19 ± 0.10
Oleoyl (18:1)	2.4 ± 0.4	13.2 ± 5.4	0.19 ± 0.05
Titrating Shh in the presence of 25μM NBD-acyl-CoA			
NBD-acyl-CoA	**k_{cat} (min^{-1})**	**K_m (μM Shh)**	**k_{cat}/K_m ($(min \cdot \mu M \text{ Shh})^{-1}$)**
Myristoyl (14:0)	4.6 ± 0.8	10.7 ± 3.3	0.43 ± 0.06
Palmitoyl (16:0)	3.4 ± 0.6	10.4 ± 0.1	0.32 ± 0.06
Palmitoleoyl (16:1)	4.7 ± 0.1	5.0 ± 0.4	0.95 ± 0.11
Oleoyl (18:1)	2.3 ± 0.7	19.7 ± 2.1	0.12 ± 0.05

Reported apparent kinetic values represent the averages (± SD) of at least two titrations (n≥2) performed in duplicate (per NBD-acyl-CoA).

Consequences of differential fatty acylation of Shh on cellular signaling

Palmitoylation of Shh plays a key role in propagation of Shh signaling through Ptch (Tukachinsky et al. 2016; Pepinsky et al. 1998). Recent structural studies of Ptch1 have revealed that the palmitate moiety of Shh binds within a hydrophobic pocket of Ptch1 (Qian et al. 2019; Rudolf et al. 2019). Since unsaturation changes the geometry of the fatty acyl chain, and the number of carbon atoms determines fatty acid chain length, I hypothesized that differential fatty acylation of Shh with monounsaturated fatty acids could impact Shh signaling output. To investigate this at the cellular level, I used Shh Light II cells, which stably express a Gli-1 responsive Firefly luciferase reporter along with constitutively expressed *Renilla* luciferase. Different fatty acylated forms of Shh were generated by incubating the recombinant, 19 kDa Shh protein with Hhat and a saturating concentration of individual NBD-labeled fatty acyl-CoAs (14:0, 16:0, 16:1 Δ9, 18:1 Δ9). Relative amounts of NBD-fatty acid incorporation were quantified, equal amounts of Shh protein were added to the cells, and EC_{50} curves were generated. Each of the four fatty acylated Shh species conferred more potent signaling compared to unmodified Shh from a mock reaction performed in the absence of NBD-acyl-CoA (Figure 9a). The signaling potency of Shh modified with 14:0 and 16:0 fatty acids was ~10 times higher than that of Shh modified with 16:1 and 18:1 fatty acids (Figure 9a, Table 6). In the absence of Hhat, addition of NBD-acyl-CoAs to the reactions did not result in a shift of the dose response curves beyond that of unacylated Shh (Figure 9b). As expected, background levels of luciferase activity were obtained when Shh was omitted from the reaction (Figure 9c). I conclude that Hhat-mediated differential fatty acylation regulates Shh signaling, with attachment of saturated fatty acids (myristate or palmitate) conferring higher signaling potency compared to monounsaturated fatty acids (palmitoleate or oleate).

Figure 9. Differential fatty acylation of Shh regulates Shh signaling activity

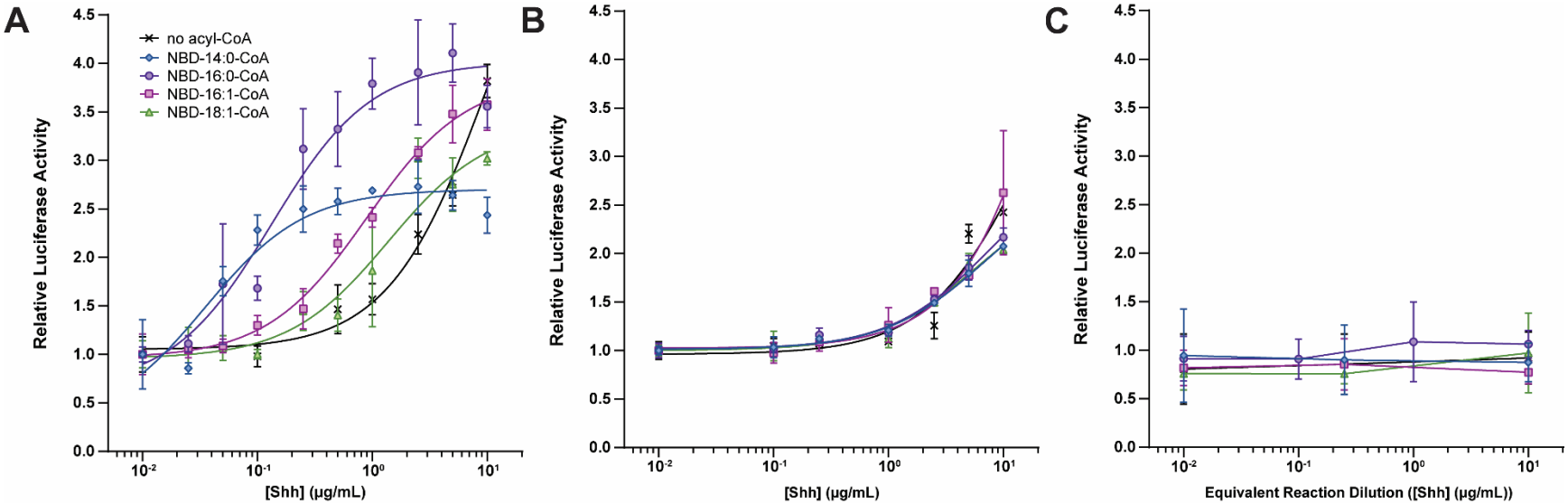

A*,** Shh Light II cells were treated with increasing amounts of NBD-fatty acylated Shh protein (19kDa) from Hhat, NBD-acyl-CoA, and Shh -containing reactions, and relative signaling output was quantified. Data for each reaction were normalized to the average Firefly/*Renilla* luciferase value at 0.01 µg/mL Shh. Data points represent the average of three titrations (n=3) performed in duplicate ± SD. ***B, As in *A*, except cells were incubated with equivalent dilution preparations from reactions lacking Hhat. Data points represent the average of two titrations (n=2) performed in duplicate ± SD. ***C,*** As in *A*, except cells were incubated with equivalent dilution preparations from reactions lacking Shh protein. Data were normalized to the average Firefly/*Renilla* luciferase value of untreated wells. Data points represent the average of two titrations (n=2) performed in duplicate, ± SD.

Table 6. Signaling potency of NBD-fatty acylated Shh proteins

NBD-acyl-Shh	EC_{50} (µg/mL Shh)	Potency relative to NBD-16:0-Shh
Myristoyl (14:0)	0.04 ± 0.01	3.57x
Palmitoyl (16:0)	0.13 ± 0.02	1.00x
Palmitoleoyl (16:1)	0.89 ± 0.07	0.15x
Oleoyl (18:1)	1.80 ± 1.04	0.07x

Reported EC_{50} values represent the averages (± SD) of three titrations (n=3) performed in duplicate (per fatty acylated Shh species).

IV. Discussion

Fatty acyl-CoA substrate specificity of Hhat

Several lines of evidence indicate that the fatty acyl-CoA substrate specificity of Hhat is not limited to palmitoyl-CoA. Addition of unlabeled fatty acyl-CoAs ranging in chain length from 10 to 18 carbons inhibited incorporation of [^{125}I]-Iodopalmitate into Shh by purified Hhat (Buglino and Resh 2008), implying that Hhat might be able to bind to a variety of fatty acyl-CoAs. Furthermore, when Shh was purified from mammalian cells, N-terminal acyl attachments to Shh other than palmitate (16:0) were detected by mass spectrometry, including 14:0, 14:1, 16:1, 18:0, 18:1, and 20:4 fatty acids (Long et al. 2015; Pepinsky et al. 1998). The prevalence of various fatty acyl attachments on Shh was found to be dependent upon the metabolic state and Shh expression level within cells (Long et al. 2015). Mammalian cells and tissues contain multiple fatty acids and acyl-CoAs, with 16:0, 18:0, 18:1, and 18:2 being the most abundant (Spector and Yorek 1985; Greaves et al. 2017; Woldegiorgis et al. 1985; Hama et al. 2020; Palladino et al. 2012). Thus, Hhat would have access to multiple fatty acyl-CoAs in potentially equal abundance *in vivo*. Hhat is the only known acyltransferase for Shh, and autoacylation of Shh in cells is highly unlikely given that Shh and fatty acyl-CoAs are compartmentalized on opposite sides of the ER membrane and that permeability of fatty acyl-CoAs across lipid bilayers is restricted (Polokoff and Bell 1978). Therefore, I hypothesized that Hhat is able to utilize multiple fatty acyl-CoA substrates, a supposition confirmed by the experiments depicted in Figures 7 and 8.

Other fatty acyltransferases have been shown to utilize more than one fatty acyl-CoA as a substrate. For example, members of the DHHC acyltransferase family have substrate binding pockets that function as “molecular rulers,” allowing binding and

utilization of different length fatty acyl chains (Jennings and Linder 2012; Rana, Lee, and Banerjee 2019; Greaves et al. 2017). Additionally, while oleoyl-CoA serves as the primary acyl-CoA substrate for DGAT1 and ACAT1 with the highest apparent turnover rate, *in vitro* kinetic analyses with purified human DGAT1 and ACAT1 revealed that the enzymes demonstrate greatest apparent affinity for other (non-oleoyl) fatty acyl-CoAs (Wang et al. 2020; Qian et al. 2020). Moreover, saturated and monounsaturated fatty acids ranging from 10-16 carbons, with a *cis*- but not *trans*- double bond at Δ9, can serve (in fatty acyl-CoA form) as substrates for Porcn-mediated fatty acylation of Wnt proteins in cells (Rios-Esteves and Resh 2013; Tuladhar et al. 2019).

Differences in cryo-EM structures observed between the fatty acyl-CoA binding cavity of Hhat and other MBOATs led to the proposition that the fatty acyl-CoA binding pocket of Hhat is more confined, with a preference for palmitoyl-CoA (Jiang, Benz, and Long 2021) and restriction of the pocket to a maximum of 16 carbons (Coupland et al. 2021). However, my biochemical analyses of purified Hhat reveal not only a substrate range wider than palmitoyl-CoA, but also that the enzyme can accommodate an iodine (Buglino and Resh 2008; Petrova et al. 2013) or an NBD group (this study) on the end of the fatty acyl chain and transfer the labeled acyl chain to Shh. It is possible that the use of antibodies (Fab fragments in (Jiang, Benz, and Long 2021) or megabodies in (Coupland et al. 2021)) to generate the Hhat structures conferred additional rigidity to the enzyme that is not otherwise present when the enzyme is not subjected to cryo-EM conditions. Alternatively, the use of different detergents may allow Hhat to adopt different conformations, enabling flexibility to bind different fatty acyl-CoAs. Other studies have demonstrated that MBOATs, including Hhat, can be differentially active (Lanyon-Hogg et al. 2015) and adopt different oligomeric states (Wang et al. 2020) in different detergents.

Indeed, the two Hhat structures themselves were determined via purification of Hhat with different detergents, and there are a few small but notable differences in the structures.

Our data indicate that palmitoleoyl and oleoyl -CoA are substrates for Hhat. This is consistent with the findings that these unsaturated fatty acids are attached to Shh in cells, and are even the major species of fatty acylated Shh under certain cellular conditions (Tuladhar et al. 2019; Long et al. 2015). A previous study found that, when assayed in microsomal membranes, Hhat did not utilize [^{125}I]-Iodo-pentadecenoyl-CoA, a CoA with a 15-carbon *cis*-Δ9, iodinated fatty acid, as a substrate (Asciolla et al. 2017). It is possible that the use of different detergents and enzyme environments may account for the result in the latter study. Overall, my data indicate that Hhat can attach a spectrum of fatty acids to Shh. Given this finding and that differential fatty acylation of Shh is dependent upon cell context (Long et al. 2015), it is possible that Shh signaling in cells which have altered metabolic states and/or high levels of Shh expression (e.g., cancer cells) might be mediated by Shh proteins modified with fatty acids other than palmitate.

Consequences of differential fatty acylation Shh on cellular signaling

My findings, and those of others, indicate that heterogeneous fatty acylation impacts Shh signaling (Taylor et al. 2001; Baker, Taylor, and Pepinsky 2007). My results are consistent with a previous report that hydrophobic modifications to Shh confer greater signaling potency compared to unmodified Shh, and that signaling conferred by myristoylated Shh is ~four times more potent compared to palmitoylated Shh (Table 6) (Taylor et al. 2001). Here I show that the potency of signaling output was stronger when Shh was modified with saturated compared to monounsaturated fatty acids. Only one

other study examined the effect of monounsaturation on cellular signaling, where it was shown that Shh isolated from chick limb buds exhibits reduced signaling activity when the explants are incubated with palmitoleate compared to palmitate (Long et al. 2015). I have shown in a direct Gli-1 reporter system with two unsaturated fatty acyl-CoAs that the degree of saturation of the fatty acid chain regulates Shh signaling.

I attempted to further investigate the cellular consequences of differential Shh acylation using non-NBD labeled fatty acyl-CoAs to acylate Shh. This approach provides the flexibility of using a wide range of fatty acyl-CoAs. However, I was unable to achieve robust and reliable separation and quantification of acylated and unacylated proteins using DOC-PAGE (a method that incorporates deoxycholate into the gel and has been used to separate lipidated from non-lipidated proteins (Shirakawa et al. 2020)), TritonX-114 phase separation, or reverse phase HPLC analysis. I also tested signaling activity of custom-synthesized, differentially acylated Shh effector peptides, based on the report that a palmitoylated 22 amino acid Shh peptide could induce Shh signaling in Shh Light II cells (Tukachinsky et al. 2016). However, I was unable to detect signaling activity above background levels using this Shh peptide acylated with 14:0, 16:0, 16:1, 18:0, or 18:1 fatty acids. (A C24A mutant version of this peptide was included as a negative control.)

Multiple stages of the Shh signaling pathway in cells are likely to be impacted by differential fatty acylation. Dually lipidated Shh associates with the cell membrane, and is then secreted from the cell in a process mediated by SCUBE2 and Disp (Tukachinsky et al. 2012). At this level, differential fatty acylation of Shh has been shown to alter lipid raft association and secretion of Shh (Long et al. 2015). Specifically, 16:1-modified Shh conferred lower lipid raft association and secretion compared to the saturated fatty acylated Shh forms 14:0, 16:0, and 18:0. This is consistent with the preference of

saturated over unsaturated fatty acids for membrane raft partitioning (Almeida 2009). Disp is thought to interact with the cholesterol moiety of Shh, while SCUBE2 is thought to interact with both the palmitate and cholesterol moieties (Hall, Cleverdon, and Ogden 2019; Wierbowski et al. 2020). While interaction of SCUBE2 with the palmitate moiety is not absolutely required for Shh binding and secretion from cells, the presence of palmitate enhances these activities (Creanga et al. 2012).

After secretion, Shh has been shown to travel to Ptch on receiving cells via carrier proteins (Wierbowski et al. 2020; Hall et al. 2021). In a recently proposed mechanism, GAS1 acts as the final agent in the carrier protein sequence to deliver dually lipidated Shh to Ptch1 on the receiving cell surface (Wierbowski et al. 2020; Huang et al. 2022). Although not absolutely required for binding of Shh to Ptch1 and subsequent signaling, GAS1-mediated handoff of Shh greatly enhances these activities, and interaction between GAS1 (but not CDON/BOC) and Shh requires a Shh N-terminal fatty acid (Huang et al. 2022; Wierbowski et al. 2020). Importantly, the affinity of GAS1 for Shh is ~10-fold higher when palmitate is the N-terminal modification compared to octanoate (8:0) (Huang et al. 2022). Additional studies that compare the binding of differentially acylated Shh proteins with GAS1 as well as SCUBE2 would help further elucidate the importance of differential Shh acylation in the signaling pathway.

The final Shh binding partner in the signaling pathway is Ptch. Inhibition of Ptch and subsequent activation of Smo are robustly induced by binding of palmitoylated Shh (Pepinsky et al. 1998; Tukachinsky et al. 2016). Structural studies reveal that Ptch1-A is inhibited by insertion of the palmitate moiety of Shh into the protein core of Ptch1-A (Qian et al. 2019; Rudolf et al. 2019). Whether and how differential fatty acylation might impact Shh binding to Ptch was explored in limited capacity in one study, using cells overexpressing a truncated murine Ptch1 protein and two different N-terminally modified

forms of Shh (C24ii and myristoylated; both lacking C-terminal cholesterol) (Taylor et al. 2001). No difference in binding affinity of the two modified Shh species to Ptch1 was detected. Moreover, no differences were detected between these modified and the unmodified and C24S forms of Shh tested in the same assay. The authors posited that high levels of receptor overexpression may have masked potential differences. It is interesting to note that these results are consistent with those of Pepinsky and colleagues (1998), who showed with the same assay that binding affinities of dually lipidated and non-lipidated Shh to mPtch1 were not significantly different. Both studies' findings might be explained by the revelation of the Ptch1 structure as a dimer that interfaces with the mature Shh protein at three sites (Shh globular domain-Ptch1-B, Shh cholesterol-Ptch1-A, Shh palmitate-Ptch1-A) (Rudolf et al. 2019; Kowatsch et al. 2019). (As previously alluded to, the cholesterol moiety was shown to bind within Ptch1-A at a distinct site above the palmitate moiety (Kowatsch et al. 2019; Rudolf et al. 2019). Indeed, recent experiments confirmed that each interface alone is not absolutely necessary to mediate Shh-Ptch1 binding (Wierbowski et al. 2020). Thus, it is possible that potential differences in binding affinity of differentially lipidated forms of Shh to Ptch1 were masked in the earlier studies (Taylor et al. 2001; Pepinsky et al. 1998) via compensation in binding by the interaction of the globular domain of Shh with Ptch1-B. However, in contrast to earlier findings, Wierbowski and colleagues (2020) showed that Shh proteins lacking the cholesterol modification demonstrated significantly (~30 times) greater binding of N-terminally palmitoylated Shh to Ptch1 compared to an unpalmitoylated form. Here, both Shh proteins were able to interface with Ptch1B. Overall, it would be informative . to further investigate the potential compensation of Shh-Ptch1 binding by the Shh-Ptch1B interaction in the presence of differentially fatty acylated forms of Shh. To this end, *in vitro* binding assays with purified components would be useful.

The C-terminal cholesterol moiety on Shh has been proposed to play a role in inhibiting Ptch1 by blocking intra-Ptch1 cholesterol transport (Kowatsch et al. 2019; Rudolf et al. 2019). Interestingly, Pepinsky and colleagues (1998) found similar signaling potency conferred by either dually lipidated or only cholesterol-modified Shh, implying that the palmitate appendage was dispensable for signaling in the presence of the cholesterol appendage. However, in this study, the Shh protein samples were not fully pure (and were contaminated with up to 30% of the other) (Pepinsky et al. 1998). The ability of each of the Shh lipid appendages to promote cell signaling was later more specifically investigated in a cell-based assay using Shh constructs containing neither, one, or both lipid modifications (Rudolf et al. 2019). The cell signaling potency of a C-terminally cholesterol-modified Shh protein (C24S-G197) was significantly greater than that of the unlipidated form. Moreover, the potency of an N-terminally palmitoylated (15 amino acid) Shh peptide was significantly enhanced with the addition of a C-terminally cholesterol-modified (seven amino acid) Shh peptide (that was not responsible on its own for activating Smo). Importantly, the cholesterol-modified peptide was unable to inactivate Ptch1 on its own. These findings suggest a mechanism whereby the two Shh lipid appendages cooperate to achieve robust Ptch1 inactivation. It is interesting to contemplate the possibility and extent to which Ptch1 inactivation might be compensated for by binding of the cholesterol in the presence of less potent Shh N-terminal fatty acyl attachments.

Chapter Four: Intracellular crosstalk among fatty acyltransferases

I. Introduction

Hhat and other cellular fatty acyltransferases utilize a variety of fatty acyl-CoA substrates. These fatty acyl-CoAs are generated in the cytoplasm by fatty acyl-CoA synthetases. The cellular abundance of different fatty acyl-CoAs is likely dependent upon dietary intake of fatty acids, and differs between cells and tissues of different types. The metabolic state of the cell also influences fatty acyl-CoA composition (Faergeman and Knudsen 1997). Multiple studies investigating different cell and tissue types found 16:0, 18:0, 18:1, and 18:2 fatty acids and fatty acyl-CoAs to be the common, most abundant species (Spector and Yorek 1985; Greaves et al. 2017; Woldegiorgis et al. 1985; Hama et al. 2020; Palladino et al. 2012). The existence of multiple cellular fatty acyltransferases and the overlap of many of these enzymes' fatty acyl-CoA substrate profiles, including palmitoyl-CoA and oleoyl-CoA, raises an important question: Are fatty acyltransferase activities interdependent? If fatty acyl-CoA substrate availability is influenced by the extent to which other fatty acyltransferases in the cell utilize a shared pool of fatty acyl-CoAs, then the activities of fatty acyltransferases in cells could be interdependent. This concept has not been experimentally investigated with Hhat or any other fatty acyltransferases. To explore this question, the potential influence of Hhat on DGAT and ACAT enzyme activity and expression was examined.

II. Materials and Methods

Cell Culture

Control and Hhat knockout HepG2 cells, generated by a previous graduate student using the HHAT Human Gene Knockout Kit (CRISPR) (Origene KN208447LP), were cultured at 37˚C in MEM (with non-essential amino acids, 1mM sodium pyruvate, 1.5 g/L sodium bicarbonate, 100 units/mL penicillin, 100 µg/mL streptomycin sulfate) containing 1X Glutamax (Gibco catalog # 35050061), 10% fetal bovine serum, and 1 µg/mL puromycin. Non-CRISPR-modified HepG2 cells were cultured the same way except without puromycin.

Lipid Droplet Analysis

4.5×10^4 HepG2 cells were seeded in 6-well tissue culture plates (Greiner Bio-One catalog # 657160) containing a glass cover slip. The following day, cells were treated with one or more of the following reagents in fresh media (as indicated in the figure legends): DMSO, 7µM T863 (DGAT1 inhibitor, Sigma catalog # SML0539) and 3µM PF-06424439 (DGAT2 inhibitor, Sigma catalog # PZ0233), and 2µM TDI-3410 (Hhat inhibitor). After incubation at 37°C for 21 hours, oleic acid (Sigma catalog # O1008) at a final concentration of 200µM was added, and cells were incubated for an additional three hours. Cells on the cover slip were rinsed once with Assay Buffer (prepared from Cell-Based Assay Buffer Tablet (Cayman Chemical catalog # 10009322) per the manufacturer's instructions) and fixed for 20 minutes with 3.7% formaldehyde in Assay Buffer. Cells were rinsed with Assay Buffer, then stained for 15 minutes as follows: Lipid droplets were stained with Cell-Based Assay Nile Red Solution (Cayman Chemical catalog # 600055) at a 1:4000 dilution, and nuclei were stained with Hoechst

(Invitrogen catalog # 33258) at a 1:1000 dilution. Cells were rinsed with Assay Buffer, and cover slips were mounted on slides using one drop of SlowFade Diamond Antifade Mountant (Invitrogen catalog # S36967). Fluorescence was monitored using an Axio Imager.A1 microscope (Carl Zeiss) on the green (lipid droplets) and blue (nuclei) channels with a 100X oil objective. 8-15 cells per sample per experiment were imaged using an AxioCam MRm (Carl Zeiss) camera and AxioVision Release 4.8.2 SP2 (Carl Zeiss) software. Experiments were performed at least twice. To generate well resolved images, confocal microscopy was implemented. A Leica SP8 confocal microscope was used with a HyD SMD 2 detector. 2-5 confocal images/cells per sample were imaged on the green and blue channels with a 63X oil objective, Imaris software was used to analyze the images, and representative images from this analysis are displayed in the figures. Confocal microscopy was performed by Vitaly Boyko of the Memorial Sloan Kettering Molecular Cytology Core.

qPCR Analysis

2×10^5 HepG2 cells were seeded in 35mm tissue culture dishes (Greiner Bio-One catalog # 627160). The following day, cells were treated with inhibitors as indicated in the figure legend, followed by addition of 200µM oleic acid 21 hours later, as performed for the lipid droplet experiments described above. Three hours after oleic acid addition, RNA was extracted from cells using the Aurum™ Total RNA Mini Kit (BioRad catalog # 7326820) according to the manufacturer's instructions. Purity and concentrations of samples were determined via nanodrop, and cDNA was prepared from each sample by reverse transcription PCR in a thermal cycler (BioRad C1000 Touch) using the iScript cDNA Synthesis Kit (BioRad catalog # 1708891) with 500-600 ng RNA template, according to the manufacturer's instructions. cDNA was then mixed with qPCR probes and SsoAdvanced Universal SYBR Green Supermix (BioRad catalog #

1725271). Reaction mixtures were aliquoted into at least duplicate wells (20µL reaction mixture per well) of a 96-well PCR plate (BioRad catalog # MLL9601), and analyzed in a real-time thermal cycler (BioRad CFX Connect). Experiments were performed at least three times. Data were analyzed in Microsoft Excel. mRNA expression was normalized to that of GAPDH within each sample and reported as $(2^{-\Delta CT}) \times 100$, where ΔCT = [CT of gene of interest] - [CT of GAPDH]. Data were graphed in GraphPad Prism 9 software and analyzed with the statistical test indicated in the figure legend. qPCR probes were obtained from Eurofins Genomics US: GAPDH forward (CTTCACCACCATGGAGGAGGC) and reverse (GGCATGGACTGTGGTCATGAG), DGAT1 forward (5' TCGCCTGCAGGATTCTTTAT 3') and reverse (5' GCATCACCACACACCAGTTC 3'), DGAT2 forward (5' AGTGGCAATGCTATCATCAT 3') and reverse (5' GAGGCCTCGACCATGGAAGAT 3'), ACAT1 forward (5' ATGCCAGTACACTGAATGATGG 3') and reverse (5' GATGCAGCATATACAGGAGCAA 3'), ACAT2 forward (5' CATGCTGCTGCTCATCTTCT 3') and reverse (5' ACTGCGGAGACCAGGAACA 3').

III. Results

To pursue the question of fatty acyltransferase interdependence, the effect of the presence of functional Hhat on DGAT1/2 activity was investigated. DGAT1/2 activity was monitored using lipid droplet formation in cells. Lipid droplets are cytoplasmic storage units for lipids, composed of a phospholipid monolayer with TAG and cholesterol esters in the interior (Onal et al. 2017). Lipid droplet formation is dependent upon DGATs 1 and 2, which catalyze the formation of TAG from DAG (Harris et al. 2011; Yen et al. 2008). HepG2 cells, hepatocytes which express high endogenous

levels of DGAT 1 and 2 (www.proteinatlas.org), were preincubated for 24 hours in the presence or absence of pharmacological inhibitors of both DGATs. Oleic acid, a potent inducer of lipid droplet formation (Nakajima et al. 2019; Fujimoto et al. 2006), was subsequently added to cells, and cells were fixed and stained with Nile Red, a fluorescent dye (excitation/emission wavelengths 529/576 nm) that stains neutral lipids, e.g., TAG and cholesterol esters, which comprise lipid droplets (Greenspan, Mayer, and Fowler 1985). Lipid droplet formation was observed by fluorescent microscopy. Cells in which either DGAT1 or DGAT2 alone was inhibited demonstrated no apparent qualitative difference in lipid droplet formation compared to untreated cells and each other (data not shown), consistent with reports that the two DGAT enzymes compensate for one another (Stone et al. 2004; van Rijn et al. 2019). However, compared to untreated cells (Figure 10a), cells in which DGAT1 and 2 were simultaneously inhibited exhibited very few lipid droplets (Figure 10b).

Figure 10. Lipid droplet biogenesis in HepG2 cells

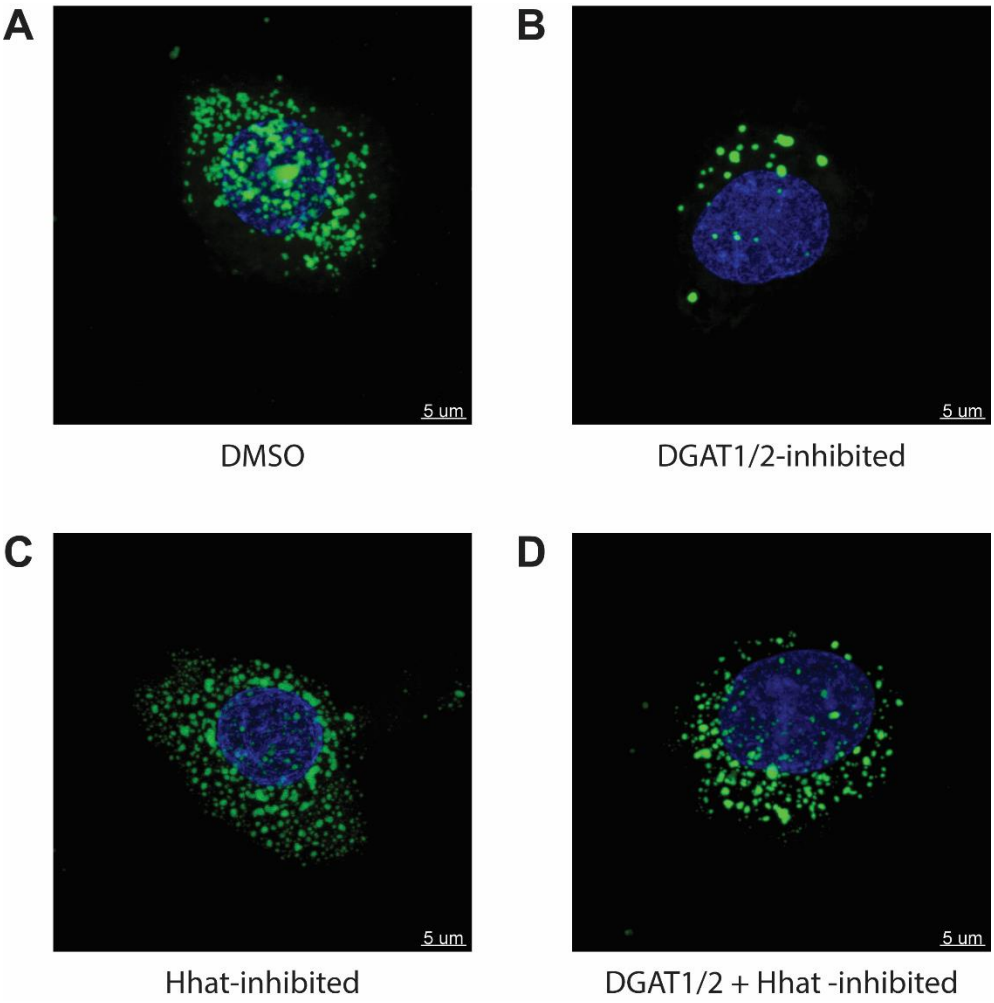

Lipid droplet formation in HepG2 cells was monitored following treatment with 200µM oleic acid and pre-treatment with ***A*****,** DMSO, ***B*****,** 7µM T863 (DGAT1 inhibitor) + 3µM PF-06424439 (DGAT2 inhibitor), ***C*****,** 2µM TDI-3410 (Hhat inhibitor), and ***D*****,** 7µM T863 + 3µM PF-06424439 + 2µM TDI-3410. Experiments were performed at least twice, and representative confocal microscopy images are shown. Blue, Hoechst; Green, Nile Red.

To determine whether the presence of Hhat has an impact on DGAT activity, cells were treated with TDI-3410, a small molecule Hhat inhibitor developed by the Resh laboratory. Compared to untreated cells, inhibition of Hhat alone had no definitive, observable effect on lipid droplet formation (Figure 10c). However, when inhibition of Hhat was coupled with inhibition of DGAT1 and 2, lipid droplet biogenesis was rescued, with an appearance of increased lipid droplet formation (Figure 10d), compared to cells in which only DGAT1 and 2 were inhibited. To ensure that this observation was not a result of a toxic or off-target effect of TDI-3410, Hhat knockout HepG2 cells were tested, and the above results were recapitulated (Figure 11).

Figure 11. Lipid droplet biogenesis in control and Hhat knockout HepG2 cells

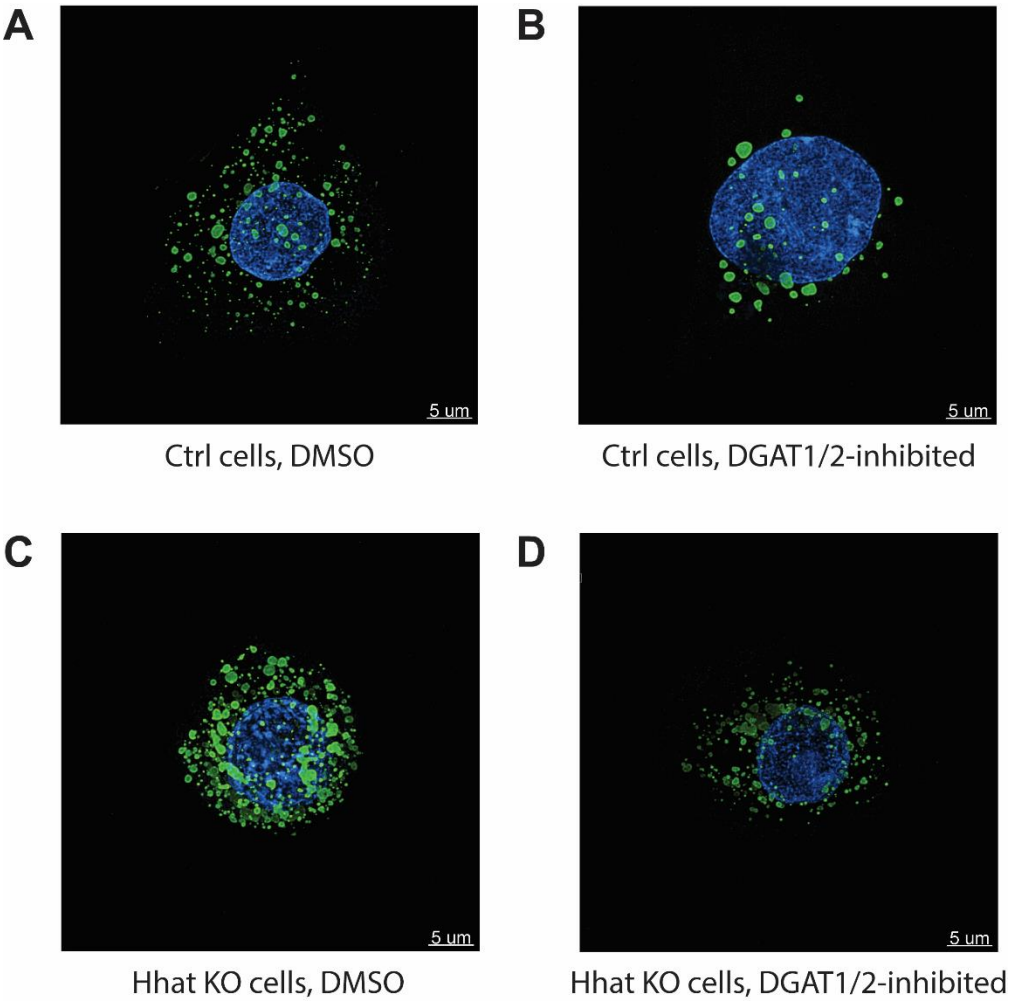

Lipid droplet formation was observed following treatment with 200µM oleic acid and pre-treatment with ***A*****,** DMSO in control HepG2 cells, ***B*****,** 7µM T863 (DGAT1 inhibitor) + 3µM PF-06424439 (DGAT2 inhibitor) in control HepG2 cells, ***C*****,** DMSO in Hhat knockout HepG2 cells, and ***D*****,** 7µM T863 + 3µM PF-06424439 in Hhat knockout HepG2 cells. Experiments were performed at least twice, and representative confocal microscopy images are shown. Blue, Hoechst; Green, Nile Red.

The rescue of lipid droplet formation observed in DGAT1/2-inhibited cells by inhibition or knockout of Hhat was mysterious, given that lipid droplet formation is dependent upon the DGAT enzymes (Yen et al. 2008; Harris et al. 2011). One possible explanation is that the two DGAT enzymes were not fully inhibited, thus allowing for an increase in DGAT-mediated lipid droplet formation by residual, active DGATs. A second possibility is that the additional lipid droplets were being formed by ACATs 1 and 2, which generate cholesterol esters that also comprise lipid droplets (Onal et al. 2017). In either case, Hhat inhibition might stimulate lipid droplet formation by increasing availability of fatty acyl-CoA substrates (i.e., oleoyl-CoA, formed from the exogenously supplied oleic acid, or buildup of other fatty acyl-CoAs not being used by Hhat) to the available DGAT or ACAT enzymes. I hypothesized that upregulated expression levels of the DGATs or ACATs could result in order to accommodate the increased fatty acyl-CoA substrate load and maintain cell viability by protecting the cell from harmful levels of free fatty acyl-CoAs. This was a reasonable possibility given that expression levels of some lipid-utilizing enzymes have been reported to increase in response to increased lipid substrate presentation (Black, Faergeman, and DiRusso 2000). To this end, mRNA expression levels of DGATs and ACATs 1 and 2 were probed by qPCR in HepG2 cells subjected to various treatments as above. Compared to untreated cells, no significant changes in DGAT1 or 2 mRNA expression levels were observed when Hhat was inhibited (Figure 12a,b) or knocked out (Figure 12c,d). Additionally, no consistent, significant differences in ACAT1 or 2 mRNA expression levels were observed among untreated, Hhat-inhibited, DGAT1/2-inhibited, or DGAT1/2 + Hhat -inhibited cells (Figure 13a,b), or between control and Hhat knockout cells which were either untreated or treated with both DGAT1 and 2 inhibitors (Figure 13c,d).

Figure 12. mRNA expression levels of DGAT1 and 2 in HepG2 cells

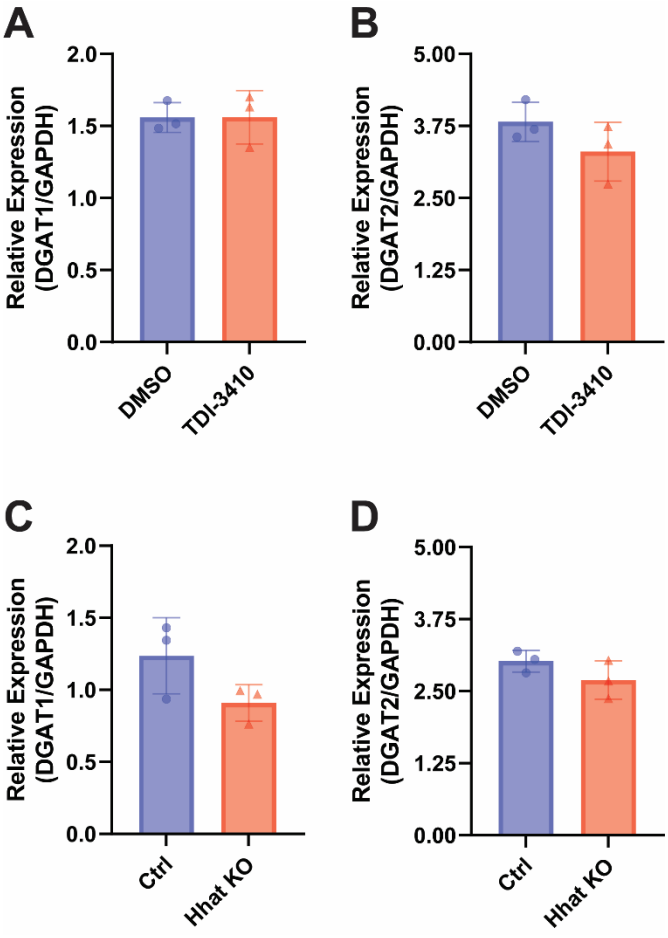

***A*,** DGAT1 mRNA was extracted from HepG2 cells treated with 200µM oleic acid following pre-treatment with DMSO or 2µM TDI-3410, and quantified by qPCR. Data were normalized to GAPDH expression and represent the average of three experiments (n=3) performed in at least triplicate ± SD. Data were analyzed by an unpaired, two-tailed T test. ***B*,** DGAT2 mRNA was analyzed as in *A*. ***C*,** DGAT1 mRNA was extracted from control or Hhat knockout HepG2 cells treated with 200µM oleic acid, and quantified by qPCR. Data were normalized to GAPDH expression and represent the average of three experiments (n=3) performed in at least triplicate ± SD. Data were analyzed by an unpaired, two-tailed T test. ***D*,** DGAT2 mRNA was analyzed as in *C*.

Figure 13. mRNA expression levels of ACAT1 and 2 in HepG2 cells

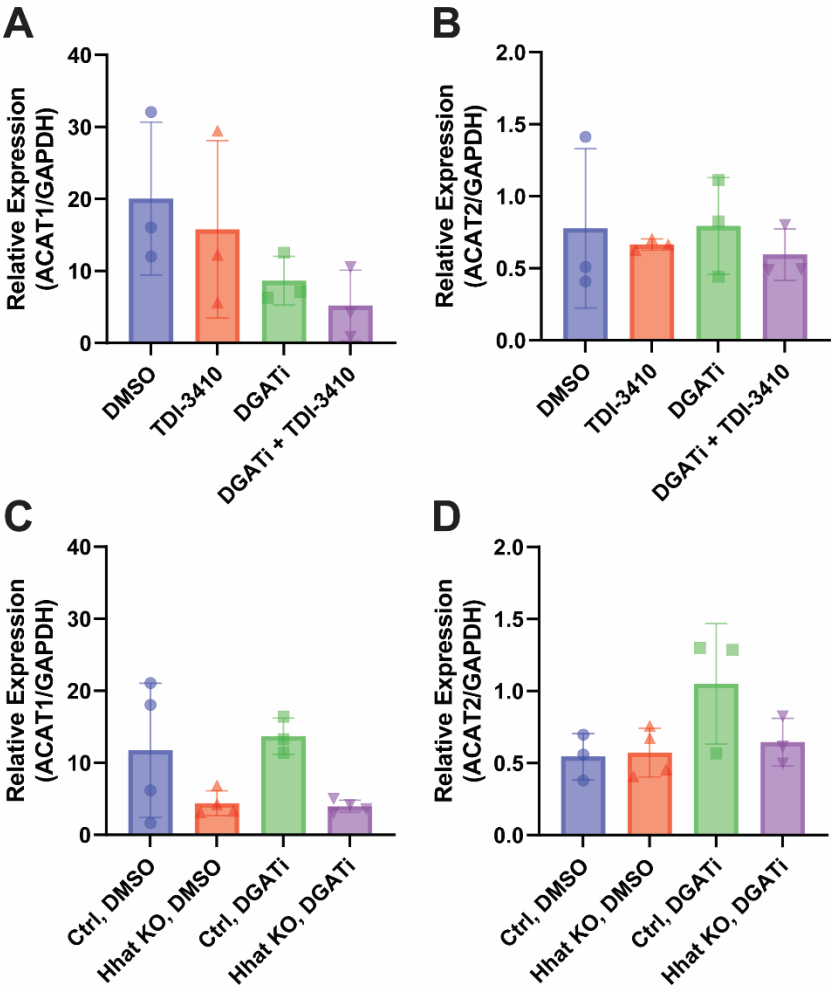

***A*,** ACAT1 mRNA was extracted from HepG2 cells treated with 200µM oleic acid following pre-treatment with DMSO, 7µM T863 + 3µM PF-06424439 (DGATi), 2µM TDI-3410, or 7µM T863 + 3µM PF-06424439 + 2µM TDI-3410, and quantified by qPCR. Data were normalized to GAPDH expression and represent the average of at least three experiments (n≥3) performed in at least duplicate ± SD. Data were analyzed by one-way ANOVA analysis with Tukey's multiple comparisons test. ***B*,** ACAT2 mRNA was analyzed as in *A*. ***C*,** ACAT1 mRNA was extracted from control or Hhat knockout HepG2 cells treated with 200µM oleic acid and DMSO or 7µM T863 + 3µM PF-06424439, and quantified by qPCR. Data were normalized to GAPDH expression and represent the

average of at least three experiments (n≥3) performed in at least duplicate ± SD. Data were analyzed by one-way ANOVA analysis with Tukey's multiple comparisons test. ***D*,** ACAT2 mRNA was analyzed as in *C*.

IV. Discussion

In this study, we came across an unexplained phenotype associated with DGAT1/2-inhibited HepG2 cells. Under these conditions, lipid droplet formation was restored with simultaneous inhibition or knockout of Hhat. These data suggest that Hhat and DGAT enzymes display interdependence, whereby DGAT-dependent lipid droplet formation is stimulated by depletion of functional Hhat. This phenotype could not be explained by increased levels of DGAT1/2 or ACAT1/2 expression, as determined by qPCR analysis. However, I observed considerable variation in the results between biological replicates among some of the ACAT qPCR analyses, and thus optimized or additional methods would be needed to confirm these findings. One such method would be to measure protein levels of ACAT enzymes in lysates from DGAT-inhibited vs. DMSO-treated Hhat knockout cells compared to those from control HepG2 cells. An additional approach would be to perform lipidomic analyses on cell lysates from the various conditions. Differences in lipid species abundance, specifically among cholesterol esters, DAG/TAG, and free fatty acids could help identify elements responsible for the compensation in lipid droplet formation observed in DGAT1/2-inhibited, Hhat knockout cells.

A central question is whether the rescue of lipid droplet formation in DGAT1/2-inhibited cells by Hhat knockout/inhibition is due to increased availability of fatty acyl-CoA substrates for the ACATs. In other words, does a lack of functional Hhat confer greater availability of the shared pool of fatty acyl-CoA substrates to other fatty acyltransferases such as the ACATs, thereby upregulating lipid droplet formation via increased cholesterol ester synthesis? To explore this possibility, the effect of inhibiting different MBOATs (e.g., Porcn or ACAT1 instead of or in addition to Hhat) on cellular lipid droplet formation can be analyzed. For example, if inhibition of Porcn similarly

rescues lipid droplet formation in DGAT1/2-inhibited cells, then a potential case for shared fatty acyl-CoA substrate use could be made. If this is so, a further question is whether the observed effects will be reproduced when fatty acids (converted to fatty acyl-CoAs inside the cell) other than oleic acid are added to cells.

Alternatively, the observed effects of Hhat knockout/inhibition in the DGAT-inhibited cells could be related to alteration of the Shh signaling pathway. (By the same token, it is also possible that potentially compromised Wnt signaling in Porcn-inhibited cells, an approach suggested above, could affect lipid droplet formation.) To determine whether changes in the Shh pathway are involved, rescue experiments could be performed in which SAG, a Smo agonist, is added to the DGAT1/2-inhibited, Hhat knockout/inhibited cells, and lipid droplet formation is monitored in these cells. If addition of SAG counters the increased lipid droplet formation conferred by Hhat knockout/inhibition in DGAT1/2 inhibited cells, a case could be made that Shh signaling regulates lipid droplet formation.

Overall, interdependence of fatty acyltransferases is an important issue because of its potential for clinical relevance. It is possible that pharmacological targeting of a particular fatty acyltransferase might impact the output of other fatty acyltransferases in cells. Such a scenario could result in undesired outcomes, namely, upregulation of cellular processes that are mediated by other fatty acyltransferases.

Chapter Five: Conclusions and future directions

1) Kinetic mechanism of other MBOATs

In this thesis work, I determined that Hhat catalyzes a random sequential reaction. Whether this mechanism is conserved among other MBOATs is an unanswered question, as the kinetic mechanism of other MBOATs has not been reported. DHHC acyltransferases have been shown to utilize an acyl-enzyme intermediate, with fatty acyl attachment to an internal cysteine as part of a two-step, ping-pong reaction mechanism (Jennings and Linder 2012). Both Hhat and other MBOATs lack a cysteine within the catalytic site, thus favoring a sequential mechanism not only for Hhat but for other MBOATs as well. However, whether substrate binding in a one-step, sequential mechanism for other MBOATs is ordered or random is not as predictable. Our results indicate that binding of the two Hhat substrates is independent, but differences in the structures of the substrate access routes/binding pockets among different MBOATs could confer different requirements for the sequence of substrate binding. This consideration is particularly relevant for lipid-modifying MBOATs, in which a different entry pathway for the recipient substrate (lateral within the membrane, Figure 4B) has been identified, compared to that in protein-modifying MBOATs (ER lumenal, Figure 4A). Thus, the sequence of substrate binding and product release in other MBOATs cannot be definitively assumed from that of Hhat, and should be validated experimentally on an individual basis.

To that end, future experiments could include purifying other MBOAT enzymes and optimizing the conditions (e.g., detergent, buffer, substrate concentrations) of the *in vitro* fluorescent assay I developed for use with these enzymes. Via custom synthesis, our laboratory acquired NBD-palmitoleoyl-CoA, the major reported substrate for Porcn, as well as biotinylated Wnt peptides that were previously used to measure the *in vitro* activity of Porcn with radioactive fatty acyl-CoA substrate analogs (Asciolla et al. 2017). Porcn has been successfully purified in active form (Lee et al. 2019), and thus performing kinetic analysis *in vitro* to determine the kinetic mechanism of Porcn is feasible.

For DGAT1, biotinylated DAG as well as biotinylated monoacylglycerol, which has also been reported to be a DGAT1 substrate (Yen et al. 2005), are commercially available. Preliminary experiments to optimize purification of DGAT1 (and DGAT2) as well as the *in vitro* NBD-acylation assay with these purified enzymes (using NBD-oleoyl-CoA and biotinylated DAG) were not successful. However, now that successful purification of DGAT1 in an active form has been reported (Wang et al. 2020), it should be possible to use this purification method to further optimize the assay.

To determine the kinetic mechanism of these purified MBOATs, I would employ the same kinetic analyses, titrating one substrate in the presence of various fixed (non-saturating) concentrations of the other. If a sequential reaction mechanism is identified, I would further probe the sequence of the reaction (random vs. ordered) with use of a dead-end competitive inhibitor (such as LGK974 for Porcn, which has shown to be compete with palmitoleoyl-CoA binding (Liu et al. 2022)) or an alternative (unlabeled) substrate, both of which have their own predicted Lineweaver-Burk plot patterns dependent upon the sequence of substrate binding (Segel 1975).

2) Substrate specificity of other MBOATs

As carried out for Hhat in this thesis work, our *in vitro* acylation assay presents a direct, straightforward means to perform further characterization of substrate specificity for other MBOATs. Fatty acyl-CoA substrate specificity of Porcn, for example, has been characterized *in vitro* and in cells, but comparison of important kinetic properties (such as affinity, turnover rate, and catalytic efficiency) of purified Porcn for/with different fatty acyl-CoA substrates has not yet been reported.

In our assay, the use of a biotinylated recipient substrate coupled with the use of a fluorescently labeled donor substrate enables competition analysis with either substrate. Hence, in a single assay, enzymatic preferences for various recipient substrates can be investigated. For example, biotinylated monoacylglycerol can be used in tandem with non-biotinylated DAG, or vice versa, for competition analysis with DGAT1 and a single NBD-labeled fatty acyl-CoA.

3) Fatty acyl-CoA distribution in cancer cells

Previous studies (Long et al. 2015; Pepinsky et al. 1998) found that fatty acyl attachment to Shh purified from cells varied based on cell context, and this thesis work determined that Hhat can utilize multiple fatty acyl-CoA substrates to fatty acylate Shh. These findings highlight the related possibility that fatty acyl attachment to Shh can depend upon fatty acyl-CoA content in particular cells. It is intriguing to contemplate whether cancer cells have a particular pattern of fatty acyl-CoA distribution (variety), which may ultimately impact fatty acyl attachment to Shh in these cells. To explore this

question, lipidomic analysis can be implemented to identify the endogenous fatty acyl-CoA species distribution present in various cancer cell lines. Similarities among different cell lines may indicate a shared mechanism of fatty acyl-CoA selection by cancerous cells. Another more specific approach is to purify Shh from these cells and identify the fatty acyl attachments by mass spectrometry, as performed in the aforementioned studies (Pepinsky et al. 1998; Taylor et al. 2001). As above, similarities in the fatty acyl attachment to Shh present in different cancer cell types may indicate a preference for certain fatty acyl-CoAs by cancerous cells. As noted earlier, the question of fatty acyl attachment to Shh (and Wnt or other proteins for that matter) is important because of the potential for varying cellular consequences (protein distribution, interactions with other proteins, etc.) conferred by the particular fatty acyl attachment. Whether cancer cells have a way of regulating fatty acyl-CoA selectivity to enhance their growth through various cellular pathways would be of great interest, and brings into question the role dietary modulation could play as a therapeutic approach.

4) Fatty acyl-CoA delivery to fatty acyltransferases

An important question for MBOAT function is: How are fatty acyl-CoAs shared and specifically selected for use by fatty acyltransferases? In cells, fatty acyl-CoAs are bound to membranes and fatty acyl-CoA binding proteins (ACBPs). These binding proteins are 10 kDa in size and bind medium and long -chain acyl-CoA esters with high affinity (Faergeman and Knudsen 1997). ACBPs protect fatty acyl-CoAs from hydrolysis by hydrolases (Rasmussen, Rosendal, and Knudsen 1993) and from having detergent-like effects on the cell membrane (Soupene and Kuypers 2015). It is curious to speculate whether ACBPs are responsible for directing substrate specificity of the various fatty

acyltransferases. To this end, two possible mechanisms can be imagined (Resh 2016). One possibility is that ACBP directly donates the fatty acyl-CoA substrate to the enzyme, potentially through an interaction between the enzyme and ACBP. Such a delivery method has been demonstrated *in vitro* for enzymes involved in β-oxidation and glycerolipid synthesis (Rasmussen et al. 1994). A second possibility is that ACBP interacts with a fatty acyltransferase in a way that sequesters and prevents other, less preferred fatty acyl-CoAs from binding within the enzyme. For example, association of NMT2 with ACBD6 has been shown *in vitro* to prevent palmitoyl-CoA from competitively binding and inhibiting the enzyme (Soupene et al. 2016). It is currently unknown whether either of these two mechanisms is employed by Hhat or other MBOATs.

To investigate this question, I looked for interaction between several fatty acyltransferases and ACBP1, the major ACBP in cells. I performed co-immunoprecipitation experiments using HEK293FT cells overexpressing an individual fatty acyltransferase (Hhat, DGAT1, DGAT2, and Porcn) and ACBP1. Experiments were also performed in which endogenous ACBP1 was co-immunoprecipitated with the overexpressed fatty acyltransferases. SURF4, an ER membrane-spanning cargo receptor protein that has no reported interaction with fatty acyl-CoAs or ACBP, was included as a negative control. No specific interaction between the tested fatty acyltransferases and ACBP1 was detected.

In addition, *in vitro* Hhat acylation assays were conducted in the absence and presence of purified ACBP1, both commercially purchased as well as WT and palmitoyl-CoA-binding-deficient mutant constructs which I purified myself. The goal was to determine whether an increase in Shh palmitoylation occurred as a result of ACBP1-mediated delivery of fatty acyl-CoA substrate to Hhat. Both palmitoyl-CoA and oleoyl-CoA were tested individually in the presence of ACBP1. These two fatty acyl-CoAs were

also tested in combination, in which one fatty acyl-CoA was NBD-labeled and the other was not, in case the presence of ACBP1 had an effect on competition between the two fatty acyl-CoAs. However, all scenarios resulted in a lack of a reproducible change in Hhat-mediated Shh fatty acylation specific to ACBP1.

These negative cell-based and *in vitro* findings indicated that ACBP1 does not interact with Hhat in a meaningful way. Nonetheless, it is possible that another ACBP family member interacts with Hhat to mediate substrate selectivity, either by direct delivery or by sequestration of certain substrates in the presence of others. To this end, it would be useful to include in future experiments other ACBPs (for co-immunoprecipitation experiments and *in vitro* assays) and/or fatty acyl-CoA substrates (alone and in combination in *in vitro* assays).

5) Exit path of the CoA byproduct following Hhat catalysis

Another unexplored area of Hhat enzymology is the location of the CoA byproduct following catalysis. CoA is an important molecule required for fatty acid metabolism, and its subcellular distribution could impact how and where it is utilized. As has been suggested for other MBOATs, structural studies of Hhat propose that the CoA byproduct from the fatty acylation reaction is released into the cytosol (Coupland et al. 2021; Jiang, Benz, and Long 2021), consistent with displacement of the CoA toward the cytosol in the Hhat enzyme-product complex compared to the enzyme-substrate complex (Jiang, Benz, and Long 2021). However, Hhat contains an opening to the ER as well (Figure 4A), where the fatty acylated Shh product is released, and thus it is possible that the CoA byproduct of the reaction could exit through this tunnel. Given the ability of palmitoyl-CoA to be transported through Hhat into the ER lumen as

demonstrated in biochemical experiments (Asciolla and Resh 2019), and the potential for the CoA molecule to adopt an elongated conformation that would enable its exit through the Hhat tunnel (Coupland et al. 2021), it is conceivable that the CoA byproduct could exit through the ER lumenal opening of Hhat, directly trailing the exiting fatty acylated product. While this exit pathway does not seem likely, given the structural evidence of CoA displacement toward the cytosol and subsequent sealing off of the cavity by Trp-335 as shown in the post-reaction structural snapshot of the enzyme, this question has never been experimentally resolved. Moreover, in lipid-modifying MBOATs, the CoA byproduct has a third opening through which it might exit, namely, a lateral gate within the ER lumen, identified in the structures of ACAT1 and DGAT1 (Figure 4B) (Qian et al. 2020; Sui et al. 2020; Long et al. 2020). How CoA would subsequently exit from the inner leaflet of the membrane is not clear. Nonetheless, as with Hhat, the exit pathway of the CoA molecule in other MBOATs has not been experimentally determined.

BIBLIOGRAPHY

Abdel-Salam, G. M. H., I. Mazen, M. Eid, N. Ewida, R. Shaheen, and F. S. Alkuraya. 2019. 'Biallelic novel missense HHAT variant causes syndromic microcephaly and cerebellar-vermis hypoplasia', *Am J Med Genet A*, 179: 1053-57.

Abe, Y., Y. Kita, and T. Niikura. 2008. 'Mammalian Gup1, a homolog of Saccharomyces cerevisiae glycerol uptake/transporter 1, acts as a negative regulator for N-terminal palmitoylation of Sonic hedgehog', *FEBS J*, 275: 318-31.

Agha, Z., Z. Iqbal, M. Azam, H. Ayub, L. E. Vissers, C. Gilissen, S. H. Ali, M. Riaz, J. A. Veltman, R. Pfundt, H. van Bokhoven, and R. Qamar. 2014. 'Exome sequencing identifies three novel candidate genes implicated in intellectual disability', *PLoS One*, 9: e112687.

Almeida, P. F. 2009. 'Thermodynamics of lipid interactions in complex bilayers', *Biochim Biophys Acta*, 1788: 72-85.

Amanai, K., and J. Jiang. 2001. 'Distinct roles of Central missing and Dispatched in sending the Hedgehog signal', *Development*, 128: 5119-27.

Andrei, S. A., E. W. Tate, and T. Lanyon-Hogg. 2022. 'Evaluating Hedgehog Acyltransferase Activity and Inhibition Using the Acylation-coupled Lipophilic Induction of Polarization (Acyl-cLIP) Assay', *Methods Mol Biol*, 2374: 13-26.

Antonny, B., S. Vanni, H. Shindou, and T. Ferreira. 2015. 'From zero to six double bonds: phospholipid unsaturation and organelle function', *Trends Cell Biol*, 25: 427-36.

Asciolla, J. J., M. M. Miele, R. C. Hendrickson, and M. D. Resh. 2017. 'An in vitro fatty acylation assay reveals a mechanism for Wnt recognition by the acyltransferase Porcupine', *J Biol Chem*, 292: 13507-13.

Asciolla, J. J., K. Rajanala, and M. D. Resh. 2019. 'In Vitro Analysis of Hedgehog Acyltransferase and Porcupine Fatty Acyltransferase Activities', *Methods Mol Biol*, 2009: 243-55.

Asciolla, J. J., and M. D. Resh. 2019. 'Hedgehog Acyltransferase Promotes Uptake of Palmitoyl-CoA across the Endoplasmic Reticulum Membrane', *Cell Rep*, 29: 4608-19 e4.

Azbazdar, Y., M. Karabicici, E. Erdal, and G. Ozhan. 2021. 'Regulation of Wnt Signaling Pathways at the Plasma Membrane and Their Misregulation in Cancer', *Front Cell Dev Biol*, 9: 631623.

Azbazdar, Y., O. Ozalp, E. Sezgin, S. Veerapathiran, A. L. Duncan, M. S. P. Sansom, C. Eggeling, T. Wohland, E. Karaca, and G. Ozhan. 2019. 'More Favorable Palmitic Acid Over Palmitoleic Acid Modification of Wnt3 Ensures Its Localization and Activity in Plasma Membrane Domains', *Front Cell Dev Biol*, 7: 281.

Baker, D. P., F. R. Taylor, and R. B. Pepinsky. 2007. 'Purifying the hedgehog protein and its variants', *Methods Mol Biol*, 397: 1-22.

Barrott, J. J., G. M. Cash, A. P. Smith, J. R. Barrow, and L. C. Murtaugh. 2011. 'Deletion of mouse Porcn blocks Wnt ligand secretion and reveals an ectodermal etiology of human focal dermal hypoplasia/Goltz syndrome', *Proc Natl Acad Sci U S A*, 108: 12752-7.

Bednarek, M. A., S. D. Feighner, S. S. Pong, K. K. McKee, D. L. Hreniuk, M. V. Silva, V. A. Warren, A. D. Howard, L. H. Van Der Ploeg, and J. V. Heck. 2000. 'Structure-function studies on the new growth hormone-releasing peptide, ghrelin: minimal sequence of ghrelin necessary for activation of growth hormone secretagogue receptor 1a', *J Med Chem*, 43: 4370-6.

Biechele, S., B. J. Cox, and J. Rossant. 2011. 'Porcupine homolog is required for canonical Wnt signaling and gastrulation in mouse embryos', *Dev Biol*, 355: 275-85.

Bischoff, M., A. C. Gradilla, I. Seijo, G. Andres, C. Rodriguez-Navas, L. Gonzalez-Mendez, and I. Guerrero. 2013. 'Cytonemes are required for the establishment of a normal Hedgehog morphogen gradient in Drosophila epithelia', *Nat Cell Biol*, 15: 1269-81.

Black, P. N., N. J. Faergeman, and C. C. DiRusso. 2000. 'Long-chain acyl-CoA-dependent regulation of gene expression in bacteria, yeast and mammals', *J Nutr*, 130: 305S-09S.

Blanc, M., F. David, L. Abrami, D. Migliozzi, F. Armand, J. Burgi, and F. G. van der Goot. 2015. 'SwissPalm: Protein Palmitoylation database', *F1000Res*, 4: 261.

Blanc, M., F. P. A. David, and F. G. van der Goot. 2019. 'SwissPalm 2: Protein S-Palmitoylation Database', *Methods Mol Biol*, 2009: 203-14.

Buglino, J. A., and M. D. Resh. 2008. 'Hhat is a palmitoylacyltransferase with specificity for N-palmitoylation of Sonic Hedgehog', *J Biol Chem*, 283: 22076-88.

Burke, R., D. Nellen, M. Bellotto, E. Hafen, K. A. Senti, B. J. Dickson, and K. Basler. 1999. 'Dispatched, a novel sterol-sensing domain protein dedicated to the release of cholesterol-modified hedgehog from signaling cells', *Cell*, 99: 803-15.

Cadena Del Castillo, C. E., J. T. Hannich, A. Kaech, H. Chiyoda, J. Brewer, M. Fukuyama, N. J. Faergeman, H. Riezman, and A. Spang. 2021. 'Patched regulates lipid homeostasis by controlling cellular cholesterol levels', *Nat Commun*, 12: 4898.

Callier, P., P. Calvel, A. Matevossian, P. Makrythanasis, P. Bernard, H. Kurosaka, A. Vannier, C. Thauvin-Robinet, C. Borel, S. Mazaud-Guittot, A. Rolland, C. Desdoits-Lethimonier, M. Guipponi, C. Zimmermann, I. Stevant, F. Kuhne, B. Conne, F. Santoni, S. Lambert, F. Huet, F. Mugneret, J. Jaruzelska, L. Faivre, D. Wilhelm, B. Jegou, P. A. Trainor, M. D. Resh, S. E. Antonarakis, and S. Nef. 2014. 'Loss of function mutation in the palmitoyl-transferase HHAT leads to syndromic 46,XY disorder of sex development by impeding Hedgehog protein palmitoylation and signaling', *PLoS Genet*, 10: e1004340.

Campana, M. B., F. J. Irudayanathan, T. R. Davis, K. R. McGovern-Gooch, R. Loftus, M. Ashkar, N. Escoffery, M. Navarro, M. A. Sieburg, S. Nangia, and J. L. Hougland. 2019. 'The ghrelin O-acyltransferase structure reveals a catalytic channel for transmembrane hormone acylation', *J Biol Chem*, 294: 14166-74.

Canto, P., D. Soderlund, E. Reyes, and J. P. Mendez. 2004. 'Mutations in the desert hedgehog (DHH) gene in patients with 46,XY complete pure gonadal dysgenesis', *J Clin Endocrinol Metab*, 89: 4480-3.

Chahal, K. K., M. Parle, and R. Abagyan. 2018. 'Hedgehog pathway and smoothened inhibitors in cancer therapies', *Anticancer Drugs*, 29: 387-401.

Chamoun, Z., R. K. Mann, D. Nellen, D. P. von Kessler, M. Bellotto, P. A. Beachy, and K. Basler. 2001. 'Skinny hedgehog, an acyltransferase required for palmitoylation and activity of the hedgehog signal', *Science*, 293: 2080-4.

Chang, C. C. Y., J. Sun, and T. Y. Chang. 2011. 'Membrane-bound O-acyltransferases (MBOATs)', *Front Biol*, 6: 177–82.

Chen, M. H., Y. J. Li, T. Kawakami, S. M. Xu, and P. T. Chuang. 2004. 'Palmitoylation is required for the production of a soluble multimeric Hedgehog protein complex and long-range signaling in vertebrates', *Genes Dev*, 18: 641-59.

Cleverdon, E. R., T. R. Davis, and J. L. Hougland. 2018. 'Functional group and stereochemical requirements for substrate binding by ghrelin O-acyltransferase revealed by unnatural amino acid incorporation', *Bioorg Chem*, 79: 98-106.

Constantinides, P. P., and J. M. Steim. 1985. 'Physical properties of fatty acyl-CoA. Critical micelle concentrations and micellar size and shape', *J Biol Chem*, 260: 7573-80.

Corbit, K. C., P. Aanstad, V. Singla, A. R. Norman, D. Y. Stainier, and J. F. Reiter. 2005. 'Vertebrate Smoothened functions at the primary cilium', *Nature*, 437: 1018-21.

Coupland, C. E., S. A. Andrei, T. B. Ansell, L. Carrique, P. Kumar, L. Sefer, R. A. Schwab, E. F. X. Byrne, E. Pardon, J. Steyaert, A. I. Magee, T. Lanyon-Hogg, M. S. P. Sansom, E. W. Tate, and C. Siebold. 2021. 'Structure, mechanism, and inhibition of Hedgehog acyltransferase', *Mol Cell*, 81: 5025-38 e10.

Creanga, A., T. D. Glenn, R. K. Mann, A. M. Saunders, W. S. Talbot, and P. A. Beachy. 2012. 'Scube/You activity mediates release of dually lipid-modified Hedgehog signal in soluble form', *Genes Dev*, 26: 1312-25.

Dai, Y., H. Tang, and S. Pang. 2021. 'The Crucial Roles of Phospholipids in Aging and Lifespan Regulation', *Front Physiol*, 12: 775648.

Darling, J. E., E. P. Prybolsky, M. Sieburg, and J. L. Hougland. 2013. 'A fluorescent peptide substrate facilitates investigation of ghrelin recognition and acylation by ghrelin O-acyltransferase', *Anal Biochem*, 437: 68-76.

Darling, J. E., F. Zhao, R. J. Loftus, L. M. Patton, R. A. Gibbs, and J. L. Hougland. 2015. 'Structure-activity analysis of human ghrelin O-acyltransferase reveals chemical determinants of ghrelin selectivity and acyl group recognition', *Biochemistry*, 54: 1100-10.

Davis, T. R., M. R. Pierce, S. X. Novak, and J. L. Hougland. 2021. 'Ghrelin octanoylation by ghrelin O-acyltransferase: protein acylation impacting metabolic and neuroendocrine signalling', *Open Biol*, 11: 210080.

Faergeman, N. J., and J. Knudsen. 1997. 'Role of long-chain fatty acyl-CoA esters in the regulation of metabolism and in cell signalling', *Biochem J*, 323 (Pt 1): 1-12.

Fujimoto, Y., J. Onoduka, K. J. Homma, S. Yamaguchi, M. Mori, Y. Higashi, M. Makita, T. Kinoshita, J. Noda, H. Itabe, and T. Takanoa. 2006. 'Long-chain fatty acids induce lipid droplet formation in a cultured human hepatocyte in a manner dependent of Acyl-CoA synthetase', *Biol Pharm Bull*, 29: 2174-80.

Galli, L. M., M. O. Anderson, J. Gabriel Fraley, L. Sanchez, R. Bueno, D. N. Hernandez, E. U. Maddox, V. R. Lingappa, and L. W. Burrus. 2021. 'Determination of the membrane topology of PORCN, an O-acyl transferase that modifies Wnt signalling proteins', *Open Biol*, 11: 200400.

Gao, B., J. Guo, C. She, A. Shu, M. Yang, Z. Tan, X. Yang, S. Guo, G. Feng, and L. He. 2001. 'Mutations in IHH, encoding Indian hedgehog, cause brachydactyly type A-1', *Nat Genet*, 28: 386-8.

Gao, X., and R. N. Hannoush. 2014. 'Single-cell imaging of Wnt palmitoylation by the acyltransferase porcupine', *Nat Chem Biol*, 10: 61-8.

Gonzalez Montoro, A., S. Chumpen Ramirez, and J. Valdez Taubas. 2015. 'The canonical DHHC motif is not absolutely required for the activity of the yeast S-acyltransferases Swf1 and Pfa4', *J Biol Chem*, 290: 22448-59.

Gottlieb, C. D., and M. E. Linder. 2017. 'Structure and function of DHHC protein S-acyltransferases', *Biochem Soc Trans*, 45: 923-8.

Gradilla, A. C., E. Gonzalez, I. Seijo, G. Andres, M. Bischoff, L. Gonzalez-Mendez, V. Sanchez, A. Callejo, C. Ibanez, M. Guerra, J. R. Ortigao-Farias, J. D. Sutherland, M. Gonzalez, R. Barrio, J. M. Falcon-Perez, and I. Guerrero. 2014. 'Exosomes as Hedgehog carriers in cytoneme-mediated transport and secretion', *Nat Commun*, 5: 5649.

Greaves, J., K. R. Munro, S. C. Davidson, M. Riviere, J. Wojno, T. K. Smith, N. C. Tomkinson, and L. H. Chamberlain. 2017. 'Molecular basis of fatty acid selectivity in the zDHHC family of S-acyltransferases revealed by click chemistry', *Proc Natl Acad Sci U S A*, 114: E1365-E74.

Greenspan, P., E. P. Mayer, and S. D. Fowler. 1985. 'Nile red: a selective fluorescent stain for intracellular lipid droplets', *J Cell Biol*, 100: 965-73.

Guan, C., Y. Niu, S. C. Chen, Y. Kang, J. X. Wu, K. Nishi, C. C. Y. Chang, T. Y. Chang, T. Luo, and L. Chen. 2020. 'Structural insights into the inhibition mechanism of human sterol O-acyltransferase 1 by a competitive inhibitor', *Nat Commun*, 11: 2478.

Gutierrez, J. A., P. J. Solenberg, D. R. Perkins, J. A. Willency, M. D. Knierman, Z. Jin, D. R. Witcher, S. Luo, J. E. Onyia, and J. E. Hale. 2008. 'Ghrelin octanoylation mediated by an orphan lipid transferase', *Proc Natl Acad Sci U S A*, 105: 6320-5.

Hall, E. T., E. R. Cleverdon, and S. K. Ogden. 2019. 'Dispatching Sonic Hedgehog: Molecular Mechanisms Controlling Deployment', *Trends Cell Biol*, 29: 385-95.

Hall, E. T., M. E. Dillard, D. P. Stewart, Y. Zhang, B. Wagner, R. M. Levine, S. M. Pruett-Miller, A. Sykes, J. Temirov, R. E. Cheney, M. Mori, C. G. Robinson, and S. K. Ogden. 2021. 'Cytoneme delivery of Sonic Hedgehog from ligand-producing cells requires Myosin 10 and a Dispatched-BOC/CDON co-receptor complex', *Elife*, 10.

Hama, K., Y. Fujiwara, S. Takashima, Y. Hayashi, A. Yamashita, N. Shimozawa, and K. Yokoyama. 2020. 'Hexacosenoyl-CoA is the most abundant very long-chain acyl-CoA in ATP binding cassette transporter D1-deficient cells', *J Lipid Res*, 61: 523-36.

Hardy, R. Y., and M. D. Resh. 2012. 'Identification of N-terminal residues of Sonic Hedgehog important for palmitoylation by Hedgehog acyltransferase', *J Biol Chem*, 287: 42881-9.

Harris, C. A., J. T. Haas, R. S. Streeper, S. J. Stone, M. Kumari, K. Yang, X. Han, N. Brownell, R. W. Gross, R. Zechner, and R. V. Farese, Jr. 2011. 'DGAT enzymes are required for triacylglycerol synthesis and lipid droplets in adipocytes', *J Lipid Res*, 52: 657-67.

Haynes, C. A., J. C. Allegood, K. Sims, E. W. Wang, M. C. Sullards, and A. H. Merrill, Jr. 2008. 'Quantitation of fatty acyl-coenzyme As in mammalian cells by liquid chromatography-electrospray ionization tandem mass spectrometry', *J Lipid Res*, 49: 1113-25.

Hishikawa, D., T. Hashidate, T. Shimizu, and H. Shindou. 2014. 'Diversity and function of membrane glycerophospholipids generated by the remodeling pathway in mammalian cells', *J Lipid Res*, 55: 799-807.

Hofmann, K. 2000. 'A superfamily of membrane-bound O-acyltransferases with implications for Wnt signaling', *Trends in Biochemical Sciences*, 25: 111-12.

Hosoda, H., M. Kojima, T. Mizushima, S. Shimizu, and K. Kangawa. 2003. 'Structural divergence of human ghrelin. Identification of multiple ghrelin-derived molecules produced by post-translational processing', *J Biol Chem*, 278: 64-70.

Huang, P., B. M. Wierbowski, T. Lian, C. Chan, S. Garcia-Linares, J. Jiang, and A. Salic. 2022. 'Structural basis for catalyzed assembly of the Sonic hedgehog-Patched1 signaling complex', *Dev Cell*, 57: 670-85 e8.

Ingham, P. W., and A. P. McMahon. 2001. 'Hedgehog signaling in animal development: paradigms and principles', *Genes Dev*, 15: 3059-87.

Iovine, V., M. Mori, A. Calcaterra, S. Berardozzi, and B. Botta. 2016. 'One Hundred Faces of Cyclopamine', *Curr Pharm Des*, 22: 1658-81.

Jennings, B. C., and M. E. Linder. 2012. 'DHHC protein S-acyltransferases use similar ping-pong kinetic mechanisms but display different acyl-CoA specificities', *J Biol Chem*, 287: 7236-45.

Jiang, H., X. Zhang, X. Chen, P. Aramsangtienchai, Z. Tong, and H. Lin. 2018. 'Protein Lipidation: Occurrence, Mechanisms, Biological Functions, and Enabling Technologies', *Chem Rev*, 118: 919-88.

Jiang, Y., T. L. Benz, and S. B. Long. 2021. 'Substrate and product complexes reveal mechanisms of Hedgehog acylation by HHAT', *Science*, 372: 1215-19.

Kawakami, Y., X. Wang, T. Shofuda, H. Sumimoto, J. Tupesis, E. Fitzgerald, and S. Rosenberg. 2001. 'Isolation of a new melanoma antigen, MART-2, containing a mutated epitope recognized by autologous tumor-infiltrating T lymphocytes', *J Immunol*, 166: 2871-7.

Kinnebrew, M., G. Luchetti, R. Sircar, S. Frigui, L. V. Viti, T. Naito, F. Beckert, Y. Saheki, C. Siebold, A. Radhakrishnan, and R. Rohatgi. 2021. 'Patched 1 reduces the accessibility of cholesterol in the outer leaflet of membranes', *Elife*, 10.

Kloska, A., M. Wesierska, M. Malinowska, M. Gabig-Ciminska, and J. Jakobkiewicz-Banecka. 2020. 'Lipophagy and Lipolysis Status in Lipid Storage and Lipid Metabolism Diseases', *Int J Mol Sci*, 21.

Kohtz, J. D., H. Y. Lee, N. Gaiano, J. Segal, E. Ng, T. Larson, D. P. Baker, E. A. Garber, K. P. Williams, and G. Fishell. 2001. 'N-terminal fatty-acylation of sonic hedgehog enhances the induction of rodent ventral forebrain neurons', *Development*, 128: 2351-63.

Kojima, M., H. Hosoda, Y. Date, M. Nakazato, H. Matsuo, and K. Kangawa. 1999. 'Ghrelin is a growth-hormone-releasing acylated peptide from stomach', *Nature*, 402: 656-60.

Komekado, H., H. Yamamoto, T. Chiba, and A. Kikuchi. 2007. 'Glycosylation and palmitoylation of Wnt-3a are coupled to produce an active form of Wnt-3a', *Genes Cells*, 12: 521-34.

Konitsiotis, A. D., S. C. Chang, B. Jovanovic, P. Ciepla, N. Masumoto, C. P. Palmer, E. W. Tate, J. R. Couchman, and A. I. Magee. 2014. 'Attenuation of hedgehog acyltransferase-catalyzed sonic Hedgehog palmitoylation causes reduced signaling, proliferation and invasiveness of human carcinoma cells', *PLoS One*, 9: e89899.

Konitsiotis, A. D., B. Jovanovic, P. Ciepla, M. Spitaler, T. Lanyon-Hogg, E. W. Tate, and A. I. Magee. 2015. 'Topological analysis of Hedgehog acyltransferase, a multipalmitoylated transmembrane protein', *J Biol Chem*, 290: 3293-307.

Kowatsch, C., R. E. Woolley, M. Kinnebrew, R. Rohatgi, and C. Siebold. 2019. 'Structures of vertebrate Patched and Smoothened reveal intimate links between cholesterol and Hedgehog signalling', *Curr Opin Struct Biol*, 57: 204-14.

Lanyon-Hogg, T., N. Masumoto, G. Bodakh, A. D. Konitsiotis, E. Thinon, U. R. Rodgers, R. J. Owens, A. I. Magee, and E. W. Tate. 2015. 'Click chemistry armed enzyme-linked immunosorbent assay to measure palmitoylation by hedgehog acyltransferase', *Anal Biochem*, 490: 66-72.

Lanyon-Hogg, T., N. V. Patel, M. Ritzefeld, K. J. Boxall, R. Burke, J. Blagg, A. I. Magee, and E. W. Tate. 2017. 'Microfluidic Mobility Shift Assay for Real-Time Analysis of Peptide N-Palmitoylation', *SLAS Discov*, 22: 418-24.

Lanyon-Hogg, T., M. Ritzefeld, L. Sefer, J. K. Bickel, A. F. Rudolf, N. Panyain, G. Bineva-Todd, C. A. Ocasio, N. O'Reilly, C. Siebold, A. I. Magee, and E. W. Tate. 2019. 'Acylation-coupled lipophilic induction of polarisation (Acyl-cLIP): a universal assay for lipid transferase and hydrolase enzymes', *Chem Sci*, 10: 8995-9000.

Lanyon-Hogg, T., M. Ritzefeld, L. Zhang, S. A. Andrei, B. Pogranyi, M. Mondal, L. Sefer, C. D. Johnston, C. E. Coupland, J. L. Greenfield, J. Newington, M. J. Fuchter, A. I. Magee, C. Siebold, and E. W. Tate. 2021. 'Photochemical Probe Identification of a Small-Molecule Inhibitor Binding Site in Hedgehog Acyltransferase (HHAT)*', *Angew Chem Int Ed Engl*, 60: 13542-47.

Lecarpentier, Y., O. Schussler, J. L. Hebert, and A. Vallee. 2019. 'Multiple Targets of the Canonical WNT/beta-Catenin Signaling in Cancers', *Front Oncol*, 9: 1248.

Lee, C. J., M. S. Rana, C. Bae, Y. Li, and A. Banerjee. 2019. 'In vitro reconstitution of Wnt acylation reveals structural determinants of substrate recognition by the acyltransferase human Porcupine', *J Biol Chem*, 294: 231-45.

Lee, J. D., P. Kraus, N. Gaiano, S. Nery, J. Kohtz, G. Fishell, C. A. Loomis, and J. E. Treisman. 2001. 'An acylatable residue of Hedgehog is differentially required in Drosophila and mouse limb development', *Dev Biol*, 233: 122-36.

Lee, J. D., and J. E. Treisman. 2001. 'Sightless has homology to transmembrane acyltransferases and is required to generate active Hedgehog protein', *Curr Biol*, 11: 1147-52.

Levental, I., D. Lingwood, M. Grzybek, U. Coskun, and K. Simons. 2010. 'Palmitoylation regulates raft affinity for the majority of integral raft proteins', *Proc Natl Acad Sci U S A*, 107: 22050-4.

Lewis, P. M., M. P. Dunn, J. A. McMahon, M. Logan, J. F. Martin, B. St-Jacques, and A. P. McMahon. 2001. 'Cholesterol modification of sonic hedgehog is required for long-range signaling activity and effective modulation of signaling by Ptc1', *Cell*, 105: 599-612.

Li, X., M. A. Ortiz, and L. Kotula. 2020. 'The physiological role of Wnt pathway in normal development and cancer', *Exp Biol Med (Maywood)*, 245: 411-26.

Li, Y., H. Zhang, Y. Litingtung, and C. Chiang. 2006. 'Cholesterol modification restricts the spread of Shh gradient in the limb bud', *Proc Natl Acad Sci U S A*, 103: 6548-53.

Liang, X., A. Nazarian, H. Erdjument-Bromage, W. Bornmann, P. Tempst, and M. D. Resh. 2001. 'Heterogeneous fatty acylation of Src family kinases with polyunsaturated fatty acids regulates raft localization and signal transduction', *J Biol Chem*, 276: 30987-94.

Lindwasser, O. W., and M. D. Resh. 2002. 'Myristoylation as a target for inhibiting HIV assembly: unsaturated fatty acids block viral budding', *Proc Natl Acad Sci U S A*, 99: 13037-42.

Liu, Y., X. Qi, L. Donnelly, N. Elghobashi-Meinhardt, T. Long, R. W. Zhou, Y. Sun, B. Wang, and X. Li. 2022. 'Mechanisms and inhibition of Porcupine-mediated Wnt acylation', *Nature*, 607: 816-22.

Long, J., R. Tokhunts, W. M. Old, S. Houel, J. Rodgriguez-Blanco, S. Singh, N. Schilling, J. Capobianco A, N. G. Ahn, and D. J. Robbins. 2015. 'Identification of a family of fatty-acid-speciated sonic hedgehog proteins, whose members display differential biological properties', *Cell Rep*, 10: 1280-87.

Long, T., Y. Sun, A. Hassan, X. Qi, and X. Li. 2020. 'Structure of nevanimibe-bound tetrameric human ACAT1', *Nature*, 581: 339-43.

Lucas, C., C. Ferreira, G. Cazzanelli, R. Franco-Duarte, and J. Tulha. 2016. 'Yeast Gup1(2) Proteins Are Homologues of the Hedgehog Morphogens Acyltransferases HHAT(L): Facts and Implications', *J Dev Biol*, 4.

Ma, D., Z. Wang, C. N. Merrikh, K. S. Lang, P. Lu, X. Li, H. Merrikh, Z. Rao, and W. Xu. 2018. 'Crystal structure of a membrane-bound O-acyltransferase', *Nature*, 562: 286-90.

Malgapo, M. I. P., and M. E. Linder. 2021. 'Substrate recruitment by zDHHC protein acyltransferases', *Open Biol*, 11: 210026.

Mann, R. K., and P. A. Beachy. 2004. 'Novel lipid modifications of secreted protein signals', *Annu Rev Biochem*, 73: 891-923.

Matevossian, A., and M. D. Resh. 2015a. 'Hedgehog Acyltransferase as a target in estrogen receptor positive, HER2 amplified, and tamoxifen resistant breast cancer cells', *Mol Cancer*, 14: 72.

———. 2015b. 'Membrane topology of hedgehog acyltransferase', *J Biol Chem*, 290: 2235-43.

McFie, P. J., S. L. Banman, S. Kary, and S. J. Stone. 2011. 'Murine diacylglycerol acyltransferase-2 (DGAT2) can catalyze triacylglycerol synthesis and promote lipid droplet formation independent of its localization to the endoplasmic reticulum', *J Biol Chem*, 286: 28235-46.

Mehta, S., S. Hingole, and V. Chaudhary. 2021. 'The Emerging Mechanisms of Wnt Secretion and Signaling in Development', *Front Cell Dev Biol*, 9: 714746.

Micchelli, C. A., I. The, E. Selva, V. Mogila, and N. Perrimon. 2002. 'Rasp, a putative transmembrane acyltransferase, is required for Hedgehog signaling', *Development*, 129: 843-51.

Miranda, M., L. M. Galli, M. Enriquez, L. A. Szabo, X. Gao, R. N. Hannoush, and L. W. Burrus. 2014. 'Identification of the WNT1 residues required for palmitoylation by Porcupine', *FEBS Lett*, 588: 4815-24.

Mitchell, D. A., G. Mitchell, Y. Ling, C. Budde, and R. J. Deschenes. 2010. 'Mutational analysis of Saccharomyces cerevisiae Erf2 reveals a two-step reaction mechanism for protein palmitoylation by DHHC enzymes', *J Biol Chem*, 285: 38104-14.

Miura, G. I., J. Buglino, D. Alvarado, M. A. Lemmon, M. D. Resh, and J. E. Treisman. 2006. 'Palmitoylation of the EGFR ligand Spitz by Rasp increases Spitz activity by restricting its diffusion', *Dev Cell*, 10: 167-76.

Muszbek, L., G. Haramura, J. E. Cluette-Brown, E. M. Van Cott, and M. Laposata. 1999. 'The pool of fatty acids covalently bound to platelet proteins by thioester linkages can be altered by exogenously supplied fatty acids', *Lipids*, 34 Suppl: S331-7.

Nakajima, S., M. Gotoh, K. Fukasawa, K. Murakami-Murofushi, and H. Kunugi. 2019. 'Oleic acid is a potent inducer for lipid droplet accumulation through its esterification to glycerol by diacylglycerol acyltransferase in primary cortical astrocytes', *Brain Res*, 1725: 146484.

Niewiadomski, P., S. M. Niedziolka, L. Markiewicz, T. Uspienski, B. Baran, and K. Chojnowska. 2019. 'Gli Proteins: Regulation in Development and Cancer', *Cells*, 8.

Nile, A. H., and R. N. Hannoush. 2019. 'Fatty acid recognition in the Frizzled receptor family', *J Biol Chem*, 294: 726-36.

Nile, A. H., S. Mukund, K. Stanger, W. Wang, and R. N. Hannoush. 2017. 'Unsaturated fatty acyl recognition by Frizzled receptors mediates dimerization upon Wnt ligand binding', *Proc Natl Acad Sci U S A*, 114: 4147-52.

Nishi, Y., H. Hiejima, H. Hosoda, H. Kaiya, K. Mori, Y. Fukue, T. Yanase, H. Nawata, K. Kangawa, and M. Kojima. 2005. 'Ingested medium-chain fatty acids are directly utilized for the acyl modification of ghrelin', *Endocrinology*, 146: 2255-64.

Niyaz, M., M. S. Khan, and S. Mudassar. 2019. 'Hedgehog Signaling: An Achilles' Heel in Cancer', *Transl Oncol*, 12: 1334-44.

Nygaard, R., J. Yu, J. Kim, D. R. Ross, G. Parisi, O. B. Clarke, D. M. Virshup, and F. Mancia. 2021. 'Structural Basis of WLS/Evi-Mediated Wnt Transport and Secretion', *Cell*, 184: 194-206 e14.

Ogiso, H., K. Nakamura, Y. Yatomi, T. Shimizu, and R. Taguchi. 2010. 'Liquid chromatography/mass spectrometry analysis revealing preferential occurrence of non-arachidonate-containing phosphatidylinositol bisphosphate species in nuclei and changes in their levels during cell cycle', *Rapid Commun Mass Spectrom*, 24: 436-42.

Ohgusu, H., K. Shirouzu, Y. Nakamura, Y. Nakashima, T. Ida, T. Sato, and M. Kojima. 2009. 'Ghrelin O-acyltransferase (GOAT) has a preference for n-hexanoyl-CoA over n-octanoyl-CoA as an acyl donor', *Biochem Biophys Res Commun*, 386: 153-8.

Onal, G., O. Kutlu, D. Gozuacik, and S. Dokmeci Emre. 2017. 'Lipid Droplets in Health and Disease', *Lipids Health Dis*, 16: 128.

Ozhan, G., E. Sezgin, D. Wehner, A. S. Pfister, S. J. Kuhl, B. Kagermeier-Schenk, M. Kuhl, P. Schwille, and G. Weidinger. 2013. 'Lypd6 enhances Wnt/beta-catenin signaling by promoting Lrp6 phosphorylation in raft plasma membrane domains', *Dev Cell*, 26: 331-45.

Palladino, A. A., J. Chen, S. Kallish, C. A. Stanley, and M. J. Bennett. 2012. 'Measurement of tissue acyl-CoAs using flow-injection tandem mass spectrometry: acyl-CoA profiles in short-chain fatty acid oxidation defects', *Mol Genet Metab*, 107: 679-83.

Panakova, D., H. Sprong, E. Marois, C. Thiele, and S. Eaton. 2005. 'Lipoprotein particles are required for Hedgehog and Wingless signalling', *Nature*, 435: 58-65.

Patel, S., A. Alam, R. Pant, and S. Chattopadhyay. 2019. 'Wnt Signaling and Its Significance Within the Tumor Microenvironment: Novel Therapeutic Insights', *Front Immunol*, 10: 2872.

Pepinsky, R. B., C. Zeng, D. Wen, P. Rayhorn, D. P. Baker, K. P. Williams, S. A. Bixler, C. M. Ambrose, E. A. Garber, K. Miatkowski, F. R. Taylor, E. A. Wang, and A. Galdes. 1998. 'Identification of a palmitic acid-modified form of human Sonic hedgehog', *J Biol Chem*, 273: 14037-45.

Perego, M., P. Glaser, A. Minutello, M. A. Strauch, K. Leopold, and W. Fischer. 1995. 'Incorporation of D-alanine into lipoteichoic acid and wall teichoic acid in Bacillus subtilis. Identification of genes and regulation', *J Biol Chem*, 270: 15598-606.

Petrova, E., A. Matevossian, and M. D. Resh. 2015. 'Hedgehog acyltransferase as a target in pancreatic ductal adenocarcinoma', *Oncogene*, 34: 263-8.

Petrova, E., J. Rios-Esteves, O. Ouerfelli, J. F. Glickman, and M. D. Resh. 2013. 'Inhibitors of Hedgehog acyltransferase block Sonic Hedgehog signaling', *Nat Chem Biol*, 9: 247-9.

Petrova, R., and A. L. Joyner. 2014. 'Roles for Hedgehog signaling in adult organ homeostasis and repair', *Development*, 141: 3445-57.

Pietrobono, S., S. Gagliardi, and B. Stecca. 2019. 'Non-canonical Hedgehog Signaling Pathway in Cancer: Activation of GLI Transcription Factors Beyond Smoothened', *Frontiers in Genetics*, 10.

Polakis, P. 2007. 'The many ways of Wnt in cancer', *Curr Opin Genet Dev*, 17: 45-51.

Polokoff, M. A., and R. M. Bell. 1978. 'Limited palmitoyl-CoA penetration into microsomal vesicles as evidenced by a highly latent ethanol acyltransferase activity', *J Biol Chem*, 253: 7173-8.

Qian, H., P. Cao, M. Hu, S. Gao, N. Yan, and X. Gong. 2019. 'Inhibition of tetrameric Patched1 by Sonic Hedgehog through an asymmetric paradigm', *Nat Commun*, 10: 2320.

Qian, H., X. Zhao, R. Yan, X. Yao, S. Gao, X. Sun, X. Du, H. Yang, C. C. L. Wong, and N. Yan. 2020. 'Structural basis for catalysis and substrate specificity of human ACAT1', *Nature*, 581: 333-38.

Raleigh, D. R., and J. F. Reiter. 2019. 'Misactivation of Hedgehog signaling causes inherited and sporadic cancers', *J Clin Invest*, 129: 465-75.

Rana, M. S., P. Kumar, C. J. Lee, R. Verardi, K. R. Rajashankar, and A. Banerjee. 2018. 'Fatty acyl recognition and transfer by an integral membrane S-acyltransferase', *Science*, 359.

Rana, M. S., C. J. Lee, and A. Banerjee. 2019. 'The molecular mechanism of DHHC protein acyltransferases', *Biochem Soc Trans*, 47: 157-67.

Rasmussen, J. T., N. J. Faergeman, K. Kristiansen, and J. Knudsen. 1994. 'Acyl-CoA-binding protein (ACBP) can mediate intermembrane acyl-CoA transport and donate acyl-CoA for beta-oxidation and glycerolipid synthesis', *Biochem J*, 299 (Pt 1): 165-70.

Rasmussen, J. T., J. Rosendal, and J. Knudsen. 1993. 'Interaction of acyl-CoA binding protein (ACBP) on processes for which acyl-CoA is a substrate, product or inhibitor', *Biochem J*, 292 (Pt 3): 907-13.

Resh, M. D. 2016. 'Fatty acylation of proteins: The long and the short of it', *Prog Lipid Res*, 63: 120-31.

———. 2021. 'Palmitoylation of Hedgehog proteins by Hedgehog acyltransferase: roles in signalling and disease', *Open Biol*, 11: 200414.
Resh, M. D., J. F. Glickman, E. Petrova, and O. Ouerfelli. 2016. "Treatment of pancreatic and related cancers with 5-acyl-6,7-dihydrothieno[3,2-c]pyridines." In. United States: Memorial Sloan Kettering Cancer Center, The Rockefeller University. U.S. Patent # 9.242,994 B2.
Rios-Esteves, J., B. Haugen, and M. D. Resh. 2014. 'Identification of key residues and regions important for porcupine-mediated Wnt acylation', *J Biol Chem*, 289: 17009-19.
Rios-Esteves, J., and M. D. Resh. 2013. 'Stearoyl CoA desaturase is required to produce active, lipid-modified Wnt proteins', *Cell Rep*, 4: 1072-81.
Rodgers, U. R., T. Lanyon-Hogg, N. Masumoto, M. Ritzefeld, R. Burke, J. Blagg, A. I. Magee, and E. W. Tate. 2016. 'Characterization of Hedgehog Acyltransferase Inhibitors Identifies a Small Molecule Probe for Hedgehog Signaling by Cancer Cells', *ACS Chem Biol*, 11: 3256-62.
Rodriguez-Blanco, J., N. S. Schilling, R. Tokhunts, C. Giambelli, J. Long, D. Liang Fei, S. Singh, K. E. Black, Z. Wang, F. Galimberti, P. A. Bejarano, S. Elliot, M. K. Glassberg, D. M. Nguyen, W. W. Lockwood, W. L. Lam, E. Dmitrovsky, A. J. Capobianco, and D. J. Robbins. 2013. 'The hedgehog processing pathway is required for NSCLC growth and survival', *Oncogene*, 32: 2335-45.
Roessler, E., E. Belloni, K. Gaudenz, P. Jay, P. Berta, S. W. Scherer, L. C. Tsui, and M. Muenke. 1996. 'Mutations in the human Sonic Hedgehog gene cause holoprosencephaly', *Nat Genet*, 14: 357-60.
Rojas, A., J. A. Del Campo, S. Clement, M. Lemasson, M. Garcia-Valdecasas, A. Gil-Gomez, I. Ranchal, B. Bartosch, J. D. Bautista, A. R. Rosenberg, F. Negro, and M. Romero-Gomez. 2016. 'Effect of Quercetin on Hepatitis C Virus Life Cycle: From Viral to Host Targets', *Sci Rep*, 6: 31777.
Rudolf, A. F., M. Kinnebrew, C. Kowatsch, T. B. Ansell, K. El Omari, B. Bishop, E. Pardon, R. A. Schwab, T. Malinauskas, M. Qian, R. Duman, D. F. Covey, J. Steyaert, A. Wagner, M. S. P. Sansom, R. Rohatgi, and C. Siebold. 2019. 'The morphogen Sonic hedgehog inhibits its receptor Patched by a pincer grasp mechanism', *Nat Chem Biol*, 15: 975-82.
Sanders, T. A., E. Llagostera, and M. Barna. 2013. 'Specialized filopodia direct long-range transport of SHH during vertebrate tissue patterning', *Nature*, 497: 628-32.
Sasai, N., M. Toriyama, and T. Kondo. 2019. 'Hedgehog Signal and Genetic Disorders', *Front Genet*, 10: 1103.
Segel, Irwin H. 1975. *Enzyme kinetics : behavior and analysis of rapid equilibrium and steady state enzyme systems* (Wiley: New York).
Sezgin, E., Y. Azbazdar, X. W. Ng, C. Teh, K. Simons, G. Weidinger, T. Wohland, C. Eggeling, and G. Ozhan. 2017. 'Binding of canonical Wnt ligands to their receptor complexes occurs in ordered plasma membrane environments', *FEBS J*, 284: 2513-26.
Shirakawa, R., S. Goto-Ito, K. Goto, S. Wakayama, H. Kubo, N. Sakata, D. A. Trinh, A. Yamagata, Y. Sato, H. Masumoto, J. Cheng, T. Fujimoto, S. Fukai, and H. Horiuchi. 2020. 'A SNARE geranylgeranyltransferase essential for the organization of the Golgi apparatus', *EMBO J*, 39: e104120.
Skoda, A. M., D. Simovic, V. Karin, V. Kardum, S. Vranic, and L. Serman. 2018. 'The role of the Hedgehog signaling pathway in cancer: A comprehensive review', *Bosn J Basic Med Sci*, 18: 8-20.

Smith, R. H., and G. L. Powell. 1986. 'The critical micelle concentration of some physiologically important fatty acyl-coenzyme A's as a function of chain length', *Arch Biochem Biophys*, 244: 357-60.

Smolich, B. D., J. A. McMahon, A. P. McMahon, and J. Papkoff. 1993. 'Wnt family proteins are secreted and associated with the cell surface', *Mol Biol Cell*, 4: 1267-75.

Soupene, E., J. Kao, D. H. Cheng, D. Wang, A. L. Greninger, G. M. Knudsen, J. L. DeRisi, and F. A. Kuypers. 2016. 'Association of NMT2 with the acyl-CoA carrier ACBD6 protects the N-myristoyltransferase reaction from palmitoyl-CoA', *J Lipid Res*, 57: 288-98.

Soupene, E., and F. A. Kuypers. 2015. 'Ligand binding to the ACBD6 protein regulates the acyl-CoA transferase reactions in membranes', *J Lipid Res*, 56: 1961-71.

Spector, A. A., and M. A. Yorek. 1985. 'Membrane lipid composition and cellular function', *J Lipid Res*, 26: 1015-35.

Speer, K. F., A. Sommer, B. Tajer, M. C. Mullins, P. S. Klein, and M. A. Lemmon. 2019. 'Non-acylated Wnts Can Promote Signaling', *Cell Rep*, 26: 875-83 e5.

Steinhauer, J., and J. E. Treisman. 2009. 'Lipid-modified morphogens: functions of fats', *Curr Opin Genet Dev*, 19: 308-14.

Stix, R., C. J. Lee, J. D. Faraldo-Gomez, and A. Banerjee. 2020. 'Structure and Mechanism of DHHC Protein Acyltransferases', *J Mol Biol*, 432: 4983-98.

Stone, S. J., H. M. Myers, S. M. Watkins, B. E. Brown, K. R. Feingold, P. M. Elias, and R. V. Farese, Jr. 2004. 'Lipopenia and skin barrier abnormalities in DGAT2-deficient mice', *J Biol Chem*, 279: 11767-76.

Sui, X., K. Wang, N. L. Gluchowski, S. D. Elliott, M. Liao, T. C. Walther, and R. V. Farese, Jr. 2020. 'Structure and catalytic mechanism of a human triacylglycerol-synthesis enzyme', *Nature*, 581: 323-28.

Takada, R., Y. Satomi, T. Kurata, N. Ueno, S. Norioka, H. Kondoh, T. Takao, and S. Takada. 2006. 'Monounsaturated fatty acid modification of Wnt protein: its role in Wnt secretion', *Dev Cell*, 11: 791-801.

Taylor, F. R., D. Wen, E. A. Garber, A. N. Carmillo, D. P. Baker, R. M. Arduini, K. P. Williams, P. H. Weinreb, P. Rayhorn, X. Hronowski, A. Whitty, E. S. Day, A. Boriack-Sjodin, R. I. Shapiro, A. Galdes, and R. B. Pepinsky. 2001. 'Enhanced potency of human Sonic hedgehog by hydrophobic modification', *Biochemistry*, 40: 4359-71.

Taylor, M. S., D. R. Dempsey, Y. Hwang, Z. Chen, N. Chu, J. D. Boeke, and P. A. Cole. 2015. 'Mechanistic analysis of ghrelin-O-acyltransferase using substrate analogs', *Bioorg Chem*, 62: 64-73.

Tukachinsky, H., R. P. Kuzmickas, C. Y. Jao, J. Liu, and A. Salic. 2012. 'Dispatched and scube mediate the efficient secretion of the cholesterol-modified hedgehog ligand', *Cell Rep*, 2: 308-20.

Tukachinsky, H., K. Petrov, M. Watanabe, and A. Salic. 2016. 'Mechanism of inhibition of the tumor suppressor Patched by Sonic Hedgehog', *Proc Natl Acad Sci U S A*, 113: E5866-E75.

Tuladhar, R., and L. Lum. 2015. 'Fatty acyl donor selectivity in membrane bound O-acyltransferases and communal cell fate decision-making', *Biochem Soc Trans*, 43: 235-9.

Tuladhar, R., N. Yarravarapu, Y. Ma, C. Zhang, J. Herbert, J. Kim, C. Chen, and L. Lum. 2019. 'Stereoselective fatty acylation is essential for the release of lipidated WNT proteins from the acyltransferase Porcupine (PORCN)', *J Biol Chem*, 294: 6273-82.

Valentine, W. J., K. Yanagida, H. Kawana, N. Kono, N. N. Noda, J. Aoki, and H. Shindou. 2022. 'Update and nomenclature proposal for mammalian lysophospholipid acyltransferases, which create membrane phospholipid diversity', *J Biol Chem*, 298: 101470.

van Rijn, J. M., M. van Hoesel, C. de Heus, A. H. M. van Vugt, J. Klumperman, E. E. S. Nieuwenhuis, R. H. J. Houwen, and S. Middendorp. 2019. 'DGAT2 partially compensates for lipid-induced ER stress in human DGAT1-deficient intestinal stem cells', *J Lipid Res*, 60: 1787-800.

Verardi, R., J. S. Kim, R. Ghirlando, and A. Banerjee. 2017. 'Structural Basis for Substrate Recognition by the Ankyrin Repeat Domain of Human DHHC17 Palmitoyltransferase', *Structure*, 25: 1337-47 e6.

Wang, L., H. Qian, Y. Nian, Y. Han, Z. Ren, H. Zhang, L. Hu, B. V. V. Prasad, A. Laganowsky, N. Yan, and M. Zhou. 2020. 'Structure and mechanism of human diacylglycerol O-acyltransferase 1', *Nature*, 581: 329-32.

Webb, Y., L. Hermida-Matsumoto, and M. D. Resh. 2000. 'Inhibition of protein palmitoylation, raft localization, and T cell signaling by 2-bromopalmitate and polyunsaturated fatty acids', *J Biol Chem*, 275: 261-70.

Wierbowski, B. M., K. Petrov, L. Aravena, G. Gu, Y. Xu, and A. Salic. 2020. 'Hedgehog Pathway Activation Requires Coreceptor-Catalyzed, Lipid-Dependent Relay of the Sonic Hedgehog Ligand', *Dev Cell*, 55: 450-67 e8.

Woldegiorgis, G., T. Spennetta, B. E. Corkey, J. R. Williamson, and E. Shrago. 1985. 'Extraction of tissue long-chain acyl-CoA esters and measurement by reverse-phase high-performance liquid chromatography', *Anal Biochem*, 150: 8-12.

Wu, F., Y. Zhang, B. Sun, A. P. McMahon, and Y. Wang. 2017. 'Hedgehog Signaling: From Basic Biology to Cancer Therapy', *Cell Chem Biol*, 24: 252-80.

Yang, J., M. S. Brown, G. Liang, N. V. Grishin, and J. L. Goldstein. 2008. 'Identification of the acyltransferase that octanoylates ghrelin, an appetite-stimulating peptide hormone', *Cell*, 132: 387-96.

Yang, J., T. J. Zhao, J. L. Goldstein, and M. S. Brown. 2008. 'Inhibition of ghrelin O-acyltransferase (GOAT) by octanoylated pentapeptides', *Proc Natl Acad Sci U S A*, 105: 10750-5.

Yen, C. L., M. Monetti, B. J. Burri, and R. V. Farese, Jr. 2005. 'The triacylglycerol synthesis enzyme DGAT1 also catalyzes the synthesis of diacylglycerols, waxes, and retinyl esters', *J Lipid Res*, 46: 1502-11.

Yen, C. L., S. J. Stone, S. Koliwad, C. Harris, and R. V. Farese, Jr. 2008. 'Thematic review series: glycerolipids. DGAT enzymes and triacylglycerol biosynthesis', *J Lipid Res*, 49: 2283-301.

Yin, Y., Y. Li, and W. Zhang. 2014. 'The growth hormone secretagogue receptor: its intracellular signaling and regulation', *Int J Mol Sci*, 15: 4837-55.

Yu, J., P. J. Liao, W. Xu, J. R. Jones, D. B. Everman, H. Flanagan-Steet, T. H. Keller, and D. M. Virshup. 2021. 'Structural model of human PORCN illuminates disease-associated variants and drug-binding sites', *J Cell Sci*, 134.

Yu, L., C. Zhou, J. Fan, J. Shanklin, and C. Xu. 2021. 'Mechanisms and functions of membrane lipid remodeling in plants', *Plant J*, 107: 37-53.

Zhai, L., D. Chaturvedi, and S. Cumberledge. 2004. 'Drosophila wnt-1 undergoes a hydrophobic modification and is targeted to lipid rafts, a process that requires porcupine', *J Biol Chem*, 279: 33220-7.

Zhang, J., J. Nie, H. Sun, J. Li, J. P. Andersen, and Y. Shi. 2022. 'De novo labeling and trafficking of individual lipid species in live cells', *Mol Metab*, 61: 101511.

Zhang, Q., D. Yao, B. Rao, L. Jian, Y. Chen, K. Hu, Y. Xia, S. Li, Y. Shen, A. Qin, J. Zhao, L. Zhou, M. Lei, X. C. Jiang, and Y. Cao. 2021. 'The structural basis for the phospholipid remodeling by lysophosphatidylcholine acyltransferase 3', *Nat Commun*, 12: 6869.

Zhang, S. Q., H. Peng, L. Y. Song, X. M. Li, H. Y. Jiang, K. T. Yao, and T. Zhao. 2005. '[Detection of KIAA1173 gene expression in nasopharyngeal carcinoma tissues and cell lines on tissue microarray]', *Ai Zheng*, 24: 1322-6.

Zhu, A. J., L. Zheng, K. Suyama, and M. P. Scott. 2003. 'Altered localization of Drosophila Smoothened protein activates Hedgehog signal transduction', *Genes Dev*, 17: 1240-52.

Zhu, X., Y. Cao, K. Voogd, and D. F. Steiner. 2006. 'On the processing of proghrelin to ghrelin', *J Biol Chem*, 281: 38867-70.